


Spring 2013

The effect of network transitions on spontaneous activity and synchrony in developing neural networks

Jude P. J. Savarraj

Follow this and additional works at: <https://digitalcommons.latech.edu/dissertations>

 Part of the [Biomedical Engineering and Bioengineering Commons](#), [Nanoscience and Nanotechnology Commons](#), and the [Oncology Commons](#)

**THE EFFECT OF NETWORK TRANSITIONS ON
SPONTANEOUS ACTIVITY AND SYNCHRONY
IN DEVELOPING NEURAL NETWORKS**

by

Jude PJ Savarraj, B.E., M.S.

A Dissertation Presented in Partial Fulfillment
of the Requirements for the Degree
Doctor of Philosophy

COLLEGE OF ENGINEERING AND SCIENCE
LOUISIANA TECH UNIVERSITY

May 2013

UMI Number: 3573604

All rights reserved

INFORMATION TO ALL USERS

The quality of this reproduction is dependent upon the quality of the copy submitted.

In the unlikely event that the author did not send a complete manuscript and there are missing pages, these will be noted. Also, if material had to be removed, a note will indicate the deletion.



UMI 3573604

Published by ProQuest LLC 2013. Copyright in the Dissertation held by the Author.

Microform Edition © ProQuest LLC.

All rights reserved. This work is protected against unauthorized copying under Title 17, United States Code.



ProQuest LLC
789 East Eisenhower Parkway
P.O. Box 1346
Ann Arbor, MI 48106-1346

LOUISIANA TECH UNIVERSITY

THE GRADUATE SCHOOL

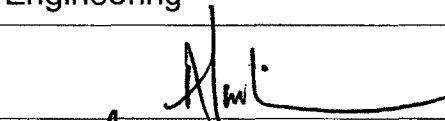
December 17, 2012

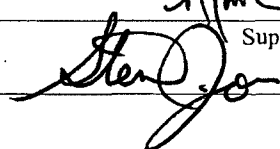
Date

We hereby recommend that the dissertation prepared under our supervision
by Jude Praveen Jeganath Savarraj, M.S.

entitled The Effect of Network Transitions on Spontaneous Activities and Synchrony
in Developing Neural Networks

be accepted in partial fulfillment of the requirements for the Degree of
Doctor of Philosophy in Biomedical Engineering




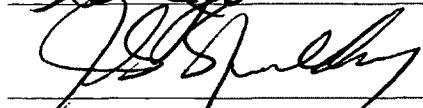
Supervisor of Dissertation Research



Head of Department

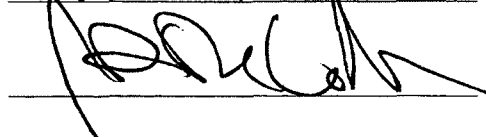
Department

Recommendation concurred in:










Advisory Committee

Approved: 

Director of Graduate Studies

Approved: 

Dean of the Graduate School



Dean of the College

ABSTRACT

Connectivity patterns of developing neural circuits and the effects of its dynamics on network behavior, particularly the emergence of spontaneous activity and synchrony, are not clear. We attempt to quantify anatomical connectivity patterns of rat cortical cultures during different stages of development. By culturing the networks on dishes embedded with micro electrode arrays, we simultaneously record electrical activity from multiple regions of the developing network and monitor its electrical behavior, particularly its tendency to fire spontaneously and to synchronize under certain conditions. We investigate possible correlations between changes in the network connectivity patterns and spontaneous electrical activity and synchrony. Cocultures showed a higher degree of synchrony than primary cultures. Networks with cancer cells, besides failing to synchronize, produced seizure-like events. We expect these results to elucidate the effect of connectivity on network behavior and hence to provide insight into the effects of various disease states on network properties. Such information could be used to diagnose such states.

APPROVAL FOR SCHOLARLY DISSEMINATION

The author grants to the Prescott Memorial Library of Louisiana Tech University the right to reproduce, by appropriate methods, upon request, any or all portions of this Dissertation. It is understood that "proper request" consists of the agreement, on the part of the requesting party, that said reproduction is for his personal use and that subsequent reproduction will not occur without written approval of the author of this Dissertation. Further, any portions of the Dissertation used in books, papers, and other works must be appropriately referenced to this Dissertation.

Finally, the author of this Dissertation reserves the right to publish freely, in the literature, at any time, any or all portions of this Dissertation.

Author



Date

April 26th, 2013

DEDICATION

This dissertation is dedicated to my dear parents Mr. Jeganathan Savarraj and Mrs. Agnes Savarraj for the constant support and love through the times.

TABLE OF CONTENTS

ABSTRACT.....	iii
DEDICATION.....	v
LIST OF TABLES.....	x
LIST OF FIGURES.....	xi
ACKNOWLEDGMENTS.....	xvi
CHAPTER 1 INTRODUCTION.....	1
1.1 Research Hypothesis.....	1
1.1.1 Central Hypothesis.....	1
1.1.2 Research Aims.....	1
1.2 Overview.....	3
CHAPTER 2 BACKGROUND.....	5
2.1 General Overview of the Nervous System.....	5
2.1.1 Glutamate Uptake and Glial Cells.....	7
2.1.2 Glial Dysfunction and Tumor-Related Abnormal Activity.....	8
2.1.3 Traditional Paradigms.....	8
2.1.4 Reductionism.....	10
2.2 Synchronicity.....	12
2.2.1 Synchrony in Neural Systems.....	13
2.2.2 Importance of Synchronization.....	15
2.2.3 Diseases Caused by Disrupted and Abnormal Synchronization.....	16
2.2.4 Need for Studies of Synchrony in Neural Systems.....	18

2.3	Brain Connectivity	19
2.3.1	Connectome	19
2.3.2	Network Theory and Small-World Networks.....	23
2.4	Approach.....	25
CHAPTER 3 MATERIALS AND METHODS		29
3.1	Overview.....	29
3.2	Culture Methods and MEA Setup.....	30
3.2.1	Neural Extraction and Plating Protocols.....	31
3.2.2	Solutions and Reagents for Cell Culture.....	32
3.2.3	AraC Treatment	33
3.2.4	C6/lacZ7 (CRL-2303) Cells.....	34
3.3	Graph Abstraction.....	34
3.3.1	Morphological Generalizations.....	35
3.3.2	Graph Methods.....	37
3.3.2.1	Parameters that Quantify Network Connections	37
3.3.2.2	Example Network Types	40
3.4	Measures of Synchrony	43
3.4.1	Correlation Coefficient:	43
3.4.2	Cross-Correlation:.....	44
3.4.3	Coherence:	46
CHAPTER 4 RESULTS		48
4.1	Introduction.....	48
4.2	Network Analysis	49
4.2.1	Tendency to Clump and form Small Clusters.....	50
4.2.1.1	Node Evolution.....	53

4.2.1.2	Cluster Connectivity	57
4.2.2	Small-World Analysis.....	58
4.2.2.1	Clustering Coefficient and Characteristic Path Length	58
4.3	Functional Results (Spontaneous Activity and Spectrum)	61
4.3.1	Functions for Different Cell Density	61
4.3.2	Emergence of Spontaneous Activity.....	62
4.3.2.1	Basal Activity in Cocultures.....	63
4.3.2.2	Basal Activity in Cancer Dishes.....	68
4.3.2.3	Effect of Glutamate on Basal Activity	70
4.4	Frequency Spectrum and Synchrony Analysis	71
4.4.1	Power Spectrum Analysis.....	72
4.4.2	Correlated Activity Analysis.....	77
4.4.3	Cross-Correlation Analysis.....	82
4.4.4	Coherence Analysis	88
4.4.4.1	CRL-2303	88
4.4.4.2	Cancer (Large SLE).....	88
CHAPTER 5 DISCUSSION.....		91
5.1	Progression of Cell Culture Development.....	94
5.1.1	Initial Formation of Connections	94
5.1.2	Emergence of Small Clusters and Local Activity.....	94
5.1.3	Inter-Cluster Connectivity Development.....	96
5.2	Disruption of Synchrony in Primary Cultures	98
5.3	Seizure-like Events (SLEs) in CRL-2303 treated Dishes.....	99
CHAPTER 6 FUTURE WORK		104
CHAPTER 7 CONCLUSION.....		107

BIBLIOGRAPHY 108

LIST OF TABLES

Table 1: Locke's solution recipe.....	33
Table 2: Clustering coefficient values for different models	59
Table 3: Characteristic path length values for different models.....	60

LIST OF FIGURES

Figure 2-1: Schematic of a simple neuron with dendrites and axon extensions.....	6
Figure 2-2: Neurotransmitter activity at a synaptic cleft.....	7
Figure 2-3: Field of study layout.....	10
Figure 2-4: Synchronicity illustration between two sets of signals. The set of signals to the left are in phase synchrony with each other and the set on the right is out of phase.....	13
Figure 2-5: The <i>C. elegans</i> wiring diagram (Varshney <i>et al</i> , 2011).....	20
Figure 2-6: (a) Illustration of information processing from the peripheral systems, the spinal cord, and the brain (by Cajal). (b) A summary of connections in the cortical areas that are generalized (Sporns, 2011).....	21
Figure 2-7: Basic approach of representing human brain as modular networks. This diagram is a macroscopic connectivity representation of the brain. Each ‘module’ or node is a specific region and may correspond to millions of neurons and connections within themselves (Sporns, 2011).....	22
Figure 2-8: Small-world networks have neither the regularity of ring lattice networks, nor the randomness of Erdős-Renyi networks (Watts and Strogatz, 1998).....	23
Figure 2-9: Research approach.....	26
Figure 3-1: A Microelectrode array dish with embedded electrode grid.....	30
Figure 3-2: Example of a simple graph.....	35
Figure 3-3: The incomplete graph (left) has ($n=5$, $e=5$) has a connection density of 50% as a simple graph with $n=5$ can have at most 10 edges.....	37
Figure 3-4: Nodes a and b have overlapping connections to e, d, and f. The amount of overlap is the ratio between the overlapping connections to the total number of connections. The connections between a and b are ignored, if they exist.....	38

Figure 3-5: Examples of cluster indices for simple networks.....	40
Figure 3-6: An illustration of a ring lattice graph (n=50, k=4). This graph has high clustering coefficient but low characteristic path length.	41
Figure 3-7: The Erdős- Renyi model generated for different probability values (0.001, 0.01, and 0.1, from left to right respectively) for a node size of 50. When the probability changes from 0.01 to 0.1, the graph is typically completely connected. When 'p' has a value $p > \ln(n)/n$, the graph is mostly connected (i.e., all edges have at least one node).....	42
Figure 3-8: A small-world network showing high local connectivity and low characteristic path length. Most real-world examples follow this pattern of connectivity.	43
Figure 3-9: Illustration of negatively-correlated, uncorrelated, and positively-correlated data.....	44
Figure 3-10: Cross-correlation relation between two signals. Cross-correlation is a function of time lag and is an indication of which signal precedes another. A zero time lag is an indication that signals are synchronous.	45
Figure 3-11: An illustration of coherence between two signals. The two random signals have a 5 Hz sinusoid, a 40 Hz sinusoid, and an arbitrary frequency imposed upon them. The coherence function exaggerates the common frequency between the two signals.	47
Figure 4-1: Coculture network on DIV 4. Neurons tend to clump together to form tight local clusters.	50
Figure 4-2: An intricate network of neurons and glial cells around the recording area of the MEA (DIV 7). The entire grid (8 X 8) is presented on the top. A small subsection of the center recording electrodes is enlarged. Neurons are identified by their neurite extensions. Glial cells lack neuritis and are relatively darker and rounder in contrast to neurons.	52
Figure 4-3: Graphical representation of connectivity evolution of an evolving network. By DIV 4, small locally-connected clusters of neurons were observed.	53
Figure 4-4: Graphical representation of culture networks from DIV 6 to DIV 9. Clusters increased in node size by absorbing unconnected neurons in the vicinity. Clusters that began to form earlier during development had the tendency to grow larger than others. By DIV 8 and DIV 9, some areas within the network are unoccupied by neurons but mostly filled with edges. Networks were drawn using the graph analysis and visualization software <i>Pajek</i> (Batagelj <i>et al</i> , 2003).....	54

Figure 4-5: Representation of a small sub-section in the electrode grid and the tracing of clusters of neurons. Individual connections between neurons are not shown (but are assumed to have high local connectivity with each other). High inter-cluster connectivity is observed.	56
Figure 4-6: Graphical representation of a coculture network (DIV 8 and DIV 9). By DIV 8, clusters develop. The neurons in a cluster together are represented as a compressed 'node.' In DIV 8, clusters are minimally connected to form an almost connected network. During DIV 8, the connectivity between the clusters increases, reducing the network's cluster characteristic path length.....	57
Figure 4-7: The clustering coefficient of the network is compared with different network models during different days <i>in vitro</i> . Neural cultures networks have a much higher local CC in comparison to other models CC of the clusters were much lower.....	58
Figure 4-8: The characteristic path length of the network is compared with different network models during different days <i>in vitro</i> . Neural culture networks have a much lower value. CC of the clusters was comparable to that of random networks.....	59
Figure 4-9: Node connectivity distributions of different networks compared with a mature neural culture.	61
Figure 4-10: Emergence of spontaneous electrical activity after a few days of network development.....	62
Figure 4-11: Raster activity of events at different days <i>in vitro</i>	64
Figure 4-12: Changes in number of events for cocultures and AraC-treated plates.....	65
Figure 4-13: Inter-event interval (IEI) histogram during different stages for development. Event intervals are irregular during the earlier phase of development and progressively become shorter.	66
Figure 4-14: Dishes treated with AraC show similar IEI profiles to those of normal cocultures.	67
Figure 4-15: The first return map of IEI intervals of coculture and AraC plated dishes during different days <i>in vitro</i> . AraC-plated cultures tend to become more periodic (marked by a cluster of points, DIV 9) compared to cocultures....	68
Figure 4-16: Basal event rate evolution for cocultures and CRL-2303 treated plates. Plates treated with CRL-2303 cells showed lower event rates than regular cocultures.....	69

Figure 4-17: (a) A series of spikes in cocultures. (b) Cancer affected cells showed large burst events followed by long quiet periods (c) Magnified ‘spike’ event (d) a small section of the cancer SLE (e) CR-2303 plated networks exhibited significant higher basal burst amplitude ($p < 0.01$ for DIV 7, DIV 8 and DIV 9) compared to cocultures.....	70
Figure 4-18: Effect of glutamate on coculture network activity. Glutamate enhances spiking activity, but the IBI profile is identical to regular cocultures.	71
Figure 4-19: PSD of basal activity during initial stages of development.	72
Figure 4-20: Emergence of activity in the delta band (DIV 8 and DIV 9).....	73
Figure 4-21: Emergence of activity for AraC-treated networks.	74
Figure 4-22: Application of glutamate results in an increase in the δ , θ , and α frequency bands. This was evaluated to compare with hyper-excitatory behavior in cancer cultures.	75
Figure 4-23: Frequency spectrum of CRL-2303-treated networks.....	76
Figure 4-24: The frequency spectrum of both SLE-type events and regular events in cancer networks is shown.	76
Figure 4-25: Emergence of correlated activity in electrode regions.....	77
Figure 4-26: Synchronization map (DIV 8 and DIV 9).....	78
Figure 4-27: Correlation activity in cultures treated with AraC.....	79
Figure 4-28: Correlated activity profile for different types of bursts in CRL-2303 plated dishes.....	80
Figure 4-29: Correlation coefficient calculated for all active electrodes for same DIV in CRL-2303- plated and regular cocultures. Cocultures not only synchronized but remained in a state of synchrony for longer periods.	81
Figure 4-30: Synchrony profile for all three types. AraC-treated networks showed the least amount of synchrony. Cancerous networks showed intermediate synchrony.....	82
Figure 4-31: Time lags were calculated for one event (recorded in four electrodes).....	83
Figure 4-32: Time lags were calculated for another event across the same electrodes. ...	84
Figure 4-33: Time lags for a short SLE computed for a different pair of electrodes (E1-E4).....	85

Figure 4-34: Time lags for a short SLE computed for different pair of electrodes (E5-E8).....	85
Figure 4-35: Time lags for a longer SLE computed for different pair of electrodes (E1-E4).....	86
Figure 4-36: Time lags for a short SLE computed for different pair of electrodes (E5-E8).....	87
Figure 4-37: Time lags for three different time stamps in the same recording, from the same pair of electrodes. Both negative lag and zero lag were observed.....	87
Figure 4-38: Frequency overlap in the δ range was observed with almost all pairs of electrodes	88
Figure 4-39: Frequency overlap in the late delta and early theta bands were observed with almost all pairs of electrodes. β -dips were also observed in large SLE events.	89
Figure 4-40: Frequency overlap in the late delta and early theta were observed with almost all pairs of electrodes. β -dips were also observed in large SLE events.	89
Figure 4-41: Frequency overlap in β bands were also observed in shorter SLE events (E1-E12).....	90
Figure 4-42: Frequency overlap in β bands in shorter SLE events (E7-E12).....	90
Figure 5-1: Abstract representation of network transition of the same network in consecutive days. While the network is completely connected, small increments in cluster connectivity could result in significant changes in network functionality.	97

ACKNOWLEDGMENTS

I thank my advisor Dr. Alan Chiu for his constant encouragement, support and financial assistance through the course of this work. I thank members of my advisory committee, particularly Dr. Mark Decoster for his expertise, technical support and help without which the work would not have been possible. I thank Dr. Kinsey Ryan Cotton for her patient assistance and help for the cell culture experiments. I thank my lab mates, particularly Dr. Daniel Moller for his time and assistance for different aspects of this work. I would like to thank Dr. Steve Jones for providing the template and assisting with the proof-reading of this dissertation. I thank Dr. James Spaulding for his assistance throughout the duration of this work.

CHAPTER 1

INTRODUCTION

1.1 Research Hypothesis

1.1.1 Central Hypothesis

The objective of this research is to identify and mathematically quantify transitions of specific network parameters of a developing biological neural network that correlates with the onset of spontaneous activity and synchronized bursting in different regions of the network. The effect of certain disease states on the evolution of the network and its function is evaluated and quantified.

We hypothesize that, *increase in cluster index of a developing neural network correlates with spontaneous activity and synchrony of neural activity. Neural networks without glial cells will exhibit poor synchronized activity, and those with cancer cells will exhibit abnormal electrical activity.*

1.1.2 Research Aims

To address the above hypothesis, the research is divided into two main categories: structural and functional analysis. For structural analysis, first, the optimal level of neurons in a biological model of a network of neurons is empirically determined. Microscopic techniques and graphical algorithms are used to quantify and analyze network parameters. For functional analysis, multielectrode recording techniques are

used to measure electrical activity from different sites of the network. Possible correlations between structure and function of the network are then determined. Thus, the following four aims are undertaken.

Aim #1- Estimate the minimum neuron plating density necessary to establish a healthy neural network that will exhibit the electrical properties under study.

Brain tissues of newborn rats are explanted and prepared for plating in dishes. Different plating densities of neurons (5k, 10k, 50k, 100k, 200k, and 500k neurons per dish) are tried, and neurite proliferation in the network is monitored by imaging the network in frequent intervals. The cell-plating density is established as the minimum number of neurons for which the network can produce spontaneous extracellular voltage activity and synchronization over time.

Aim #2 – Establish a mathematical framework to represent neural network dynamics as quantifiable terms, and use graph algorithms to extract network parameters.

Multiple high-resolution microscopic images of different network regions are taken over regular time intervals. The images are combined to create a montage. Neurons and connections between them are identified and traced, and the resulting network is represented in a mathematical framework. Graph algorithms are applied to these mathematical data to extract subtle information, such as cluster index and characteristic path length of the network.

Aim #3 - Record extracellular voltage potential from multiple network sites via embedded microelectrodes and use signal processing tools to analyze the data.

Neurons are plated on micro electrode dishes that have electrodes embedded in them that can record extracellular voltage fluctuations. Signals are then amplified, filtered, processed and analyzed.

Aim #4 – In certain samples, the glial cell population is decreased, and cancer cells are added. The subsequent changes in network dynamics and functionality are compared with the normal state.

To assess the electrical profile under diseases conditions, the proliferation of glial cells is curbed in pre-mitotic stage by the addition of Cytosine arabinoside (AraC). Tumor growth is induced in the network by plating the network with cancerous cell lines. Electrical activity at different stages of disease proliferation is measured.

1.2 Overview

The remainder of this dissertation is arranged as follows: Chapter 2 presents background, motivation, literature review, and the need for this study. The need is presented from fundamental and clinical research perspectives. A review on the importance of spontaneous oscillations and synchronization rhythms both *in vivo* and *in vitro*, and the justification for employing the biological model to be used is presented. Current methods in brain network analysis, including their advantages and limitations, are presented and contrasted with our methods. The justifications for network abstractions and reductions employed in our methods are presented. The relationship between this study and existing knowledge in neuroscience is described. Ways through which other disciplines could contribute to network-level neuroscience, and vice-versa, are discussed. Chapter 3 presents methods, including the neural culture techniques, the microelectrode recording hardware setup, the signal processing tools, and the applied

synchrony measures. Microscopic methods, reductionist approaches and justifications used in identification and network tracing process of neurons and connections are described. Reasoning behind chosen measures and algorithms used to analyze networks are described. Chapter 4 presents the general network analysis results and compares the statistical distributions of anatomical connectivity in normal (disease-free) networks to those of abnormal networks. The second half of this chapter presents the results from the signal processing techniques and measures of synchrony. Electrical activities obtained from normal and pathological states are compared, and changes are traced over time. Chapter 5 discusses the results and presents explanations for the observed trends. Specific network transitions and correlations to changes in function are explained. The relevance of the above mentioned results to the broader framework of the research gap is also discussed. Chapter 6 discusses potential future work. Chapter 7 is conclusion.

CHAPTER 2

BACKGROUND

This chapter presents the research problem and its motivation. The basics of information processing in neural systems and conventional approaches in network analysis are reviewed. We attempt to justify the scale in which we study the problem. The importance of synchronous oscillations in *in vivo* and *in vitro* systems and pathological conditions that arise from their disruptions are reviewed.

2.1 General Overview of the Nervous System

The brain is the center of the nervous system. It is composed of primarily two types of cells, neurons and glia. A mammalian brain contains billions of neurons, and each neuron can have thousands of electrochemical and electrical connections. Neurons are mainly responsible for the information processing capacity of the brain. A neuron receives and transmits information via dendrites and axons, respectively. A schematic of a simple neural cell and its processes is shown in Figure 2-1.

The opening of ion channels allows ions to flow between the extracellular medium and the cell interior. The ion flow, in turn, increases or decreases the neuron's electrical potential. Electrical potential accumulating in the cell from many neighboring neurons adds up in the axon hillock

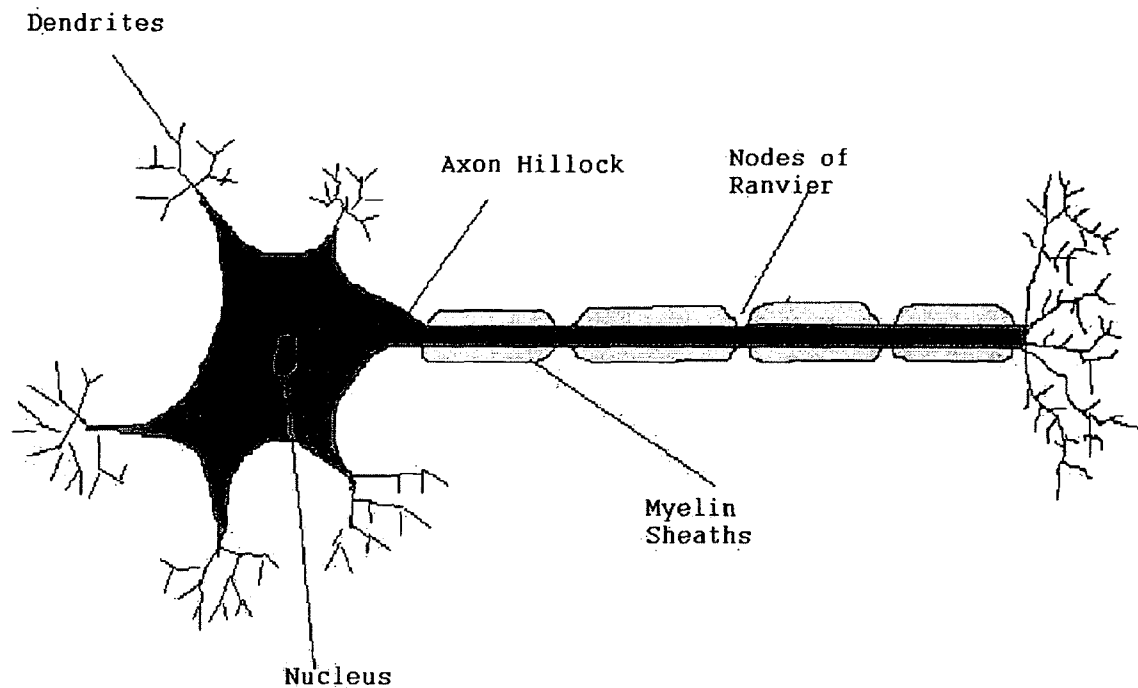


Figure 2-1: Schematic of a simple neuron with dendrites and axon extensions.

. If the summation of electrical impulses exceeds a threshold voltage, the neuron fires with an all-or-none phenomenon called the action potential that propagates via its axons to dendrites of the neurons it connects with. The propagation of an action potential across long distances in the organism's body is facilitated by myelin sheaths along the axon. When the action potential reaches the end of the axon, voltage-gated Ca^{2+} channels are activated resulting in an influx of calcium ions into the cell from extracellular space. These calcium ions bind with intracellular vesicles that contain neurotransmitters. By the process of exocytosis, the vesicles release neurotransmitters into the synaptic cleft as show in Figure 2-2. The neurotransmitter release, in turn, increases or decreases the potential of the post-synaptic cell, depending upon the type of neurotransmitters released.

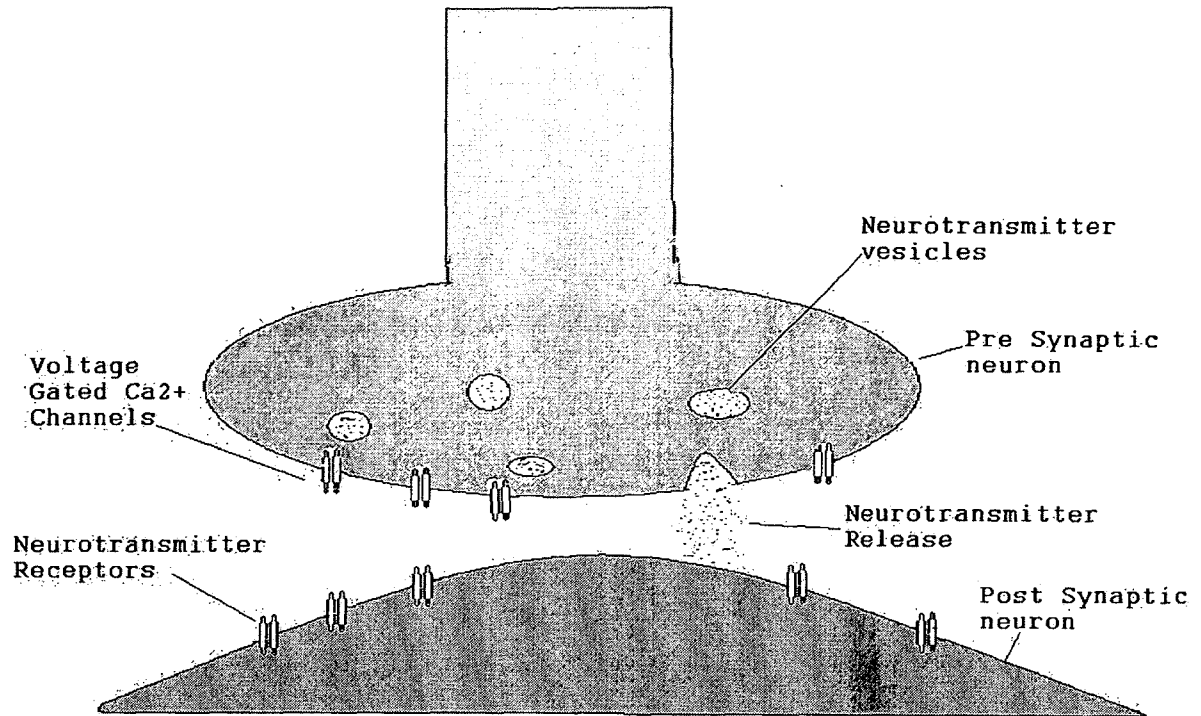


Figure 2-2: Neurotransmitter activity at a synaptic cleft.

Through this mechanism, most nervous systems receive, transmit, and process information and determine the organism's behavior. Neurons differ from one another in size, function and morphology.

2.1.1 Glutamate Uptake and Glial Cells

Glutamate, an excitatory neurotransmitter, is the predominant mediator of excitatory activity in the mammalian nervous system (Fonnum, 1984). It also plays a role in development of neural systems (McDonald and Johnston, 1990) and in intracellular signaling. Glutamate released from a presynaptic terminal activates postsynaptic glutamate receptors, leading to a positive current influx. The glutamate in the synaptic cleft must be removed as quickly as possible because high amounts of glutamate in the extracellular medium are a noise source that decreases the signal-to-noise ratio. Also,

high concentrations of extracellular glutamate are excitotoxic, and energy requirements are decreased when the glutamate is recycled. Removal is primarily accomplished by transporter proteins in glial cells. Glutamate transporters GLT and GLAST remove glutamate from the synaptic cleft and convert it into glutamine through a process called the glutamate-glutamine cycle (Bak *et al*, 2006). Glutamine is absorbed by surrounding neurons and is converted into glutamate to replenish its neurotransmitter resources. A detailed overview on glutamate uptake is presented here (Danbolt, 2001).

2.1.2 Glial Dysfunction and Tumor-Related Abnormal Activity

Glial cells perform multiple functions on the nervous system in addition to glutamate removal. They communicate with neurons bidirectionally through tripartite synapses and play an active role in synaptic function and information processing in the nervous system. Gliomas are tumors that originate from glial cells in the brain and spinal cord. Most of the patients with glioma (60-80%) experience some sort of seizure during the course of the disease (Lynam *et al*, 2007). Intracranial implantation of C6 glioma cells in rat neocortex resulted in epileptiform discharges in them (Köhling *et al*, 2006). Prolonged elevation of glutamate in the extracellular medium has been implicated in cortical hyperexcitability, including seizures and a number of neurological disorders (Wang and Qin, 2010).

2.1.3 Traditional Paradigms

Physiologists and behaviorists have studied the nervous system for several centuries. The perspectives that researchers take while studying the brain (or for that matter, any other natural phenomena that can be studied experimentally) have largely depended upon the availability of tools and instruments during that epoch. For instance,

the invention of microscope during the 17th century enabled scientists to look deeper into tissue, formulate better hypothesis and design better experiments. For much of scientific history, we have been restricted to study the brain mostly at the organism and behavior level. Psychologists, traditionally and currently, rely on subjective recounts of an individual's thoughts and behaviors to understand, diagnose and treat problems. The advent of tools to study and manipulate electricity during the late 19th century and the discovery that nervous tissue can be stimulated by electric current enabled electrophysiologists to design experiments to study the nervous system at the systems and peripheral level, notably the experiments of Luigi Galvani and Alessandro Volta. Staining techniques developed by Golgi, detailed works by Ramon Cajal, and his subsequent discovery that neurons communicate with each other through electrochemical junctions called synapses marked the next paradigm shift in neuroscience. The different levels at which neuroscience research is conducted are shown in Figure 2-3. The advancements in 20th century neuroscience are attributed to concurrent advances in electronics. The discovery of electroencephalograph (EEG) waves by Hans Berger led researchers to postulate that large numbers of neurons must be synchronizing and acting in unison. Similarly, advancements in cellular electrophysiology and clamp experiments, which culminated into the works of Hodgkin and Huxley, increased our understanding of the brain at the cellular level.

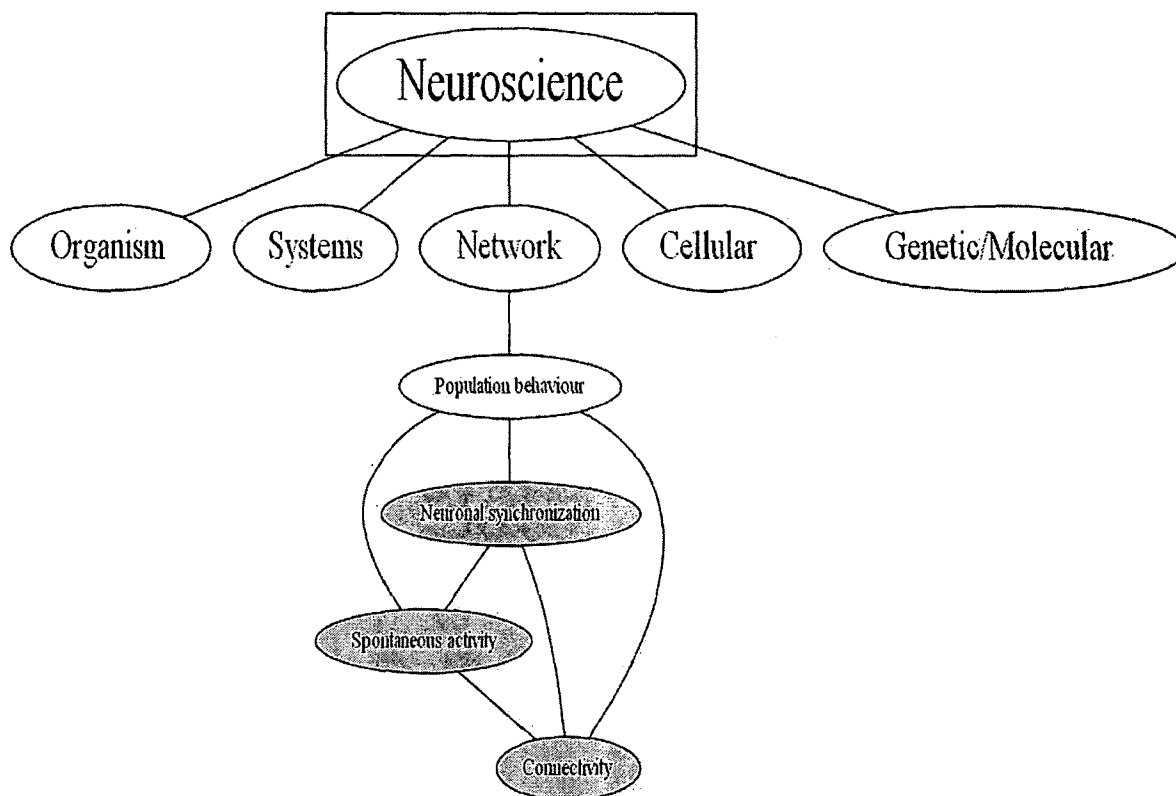


Figure 2-3: Field of study layout.

2.1.4 Reductionism

Currently, two main approaches are used in neuroscience research. The first is a mesoscopic approach that de-emphasizes the individual components of the system by treating the system as a whole. Electroencephalography (EEG), functional magnetic resonance imaging, and other imaging methods fall in this category. The other perspective is the microscopic view or the reductionist approach that tends to explain the neural function at the molecular level. Network neuroscience deals with the behavior of a small population of neurons or micro-circuits. For instance, we understand the role of individual pacemaker cells in the sino atrial-node, but we do not understand the precise

mechanisms through which these cells communicate and maintain synchronous bursting through the lifetime of the organism. We have little understanding on how these pacemaker cells, working as a network, show spontaneous and synchronized activity. In other words, the synchronized firing of the cells cannot be explained from merely the biophysical properties of the cells and the various chemical transmitters that affect them. Its explanation requires insight into how they act as a network to produce such ‘emergent’ behaviors. Several such networks, called Central Pattern Generators (CPGs), are present in both the invertebrate and the vertebrate systems (Hooper, 2000). CPGs are usually a population of excitable cells that produce rhythmic behavior within an organism’s system so as to perform a function. A lack of progress in the neural-network levels has largely been due to technological limitations that are being addressed very recently. The advances in microelectrode arrays (MEAs) as a consequence of micromanufacturing techniques (Gross *et al*, 1977) have helped us to collect electrical data at a precision that was not possible before. MEAs (arrays, in which the electrodes were few micrometers in diameter) can record neural activity from many neurons at the same time. Signal and spike sorting algorithms enable classification and separation of spikes from single neurons. Since these MEAs are patterned over glass, the transparent properties of the substrate allow network dynamics to be simultaneously recorded both optically and electrically over time. The recording dishes can be stored in the incubator for long periods of time, and it is possible to maintain them for a few weeks to months (depending upon the protocol). This setup has enabled us to observe fine changes in network level and the corresponding changes in the functional level at the same time.

Such experimental approaches will offer fundamental insight on how neurons form networks for information processing and problem solving.

2.2 Synchronicity

Synchronization is defined as simultaneous behavior. Consider a dynamical system with multiple elements in it. Let each element be defined by V_n number of variables in which at least one oscillates periodically in a fixed time interval. If the phase difference (ϕ) between at least one of this oscillation variable is zero, then the system is in perfect *in-phase synchrony* with respect to that variable. However, while quantifying synchronous behavior, especially in the brain, degrees of synchronicity are preferred. Figure 2-4 illustrates phase synchrony between two sets of signals. The phase lag between the signals is denoted by ϕ . When the signals are completely in phase, there is no lag between them, and the phase lag is zero. When the signals are not in phase synchrony, the lag is not zero, and the signals are out of phase.

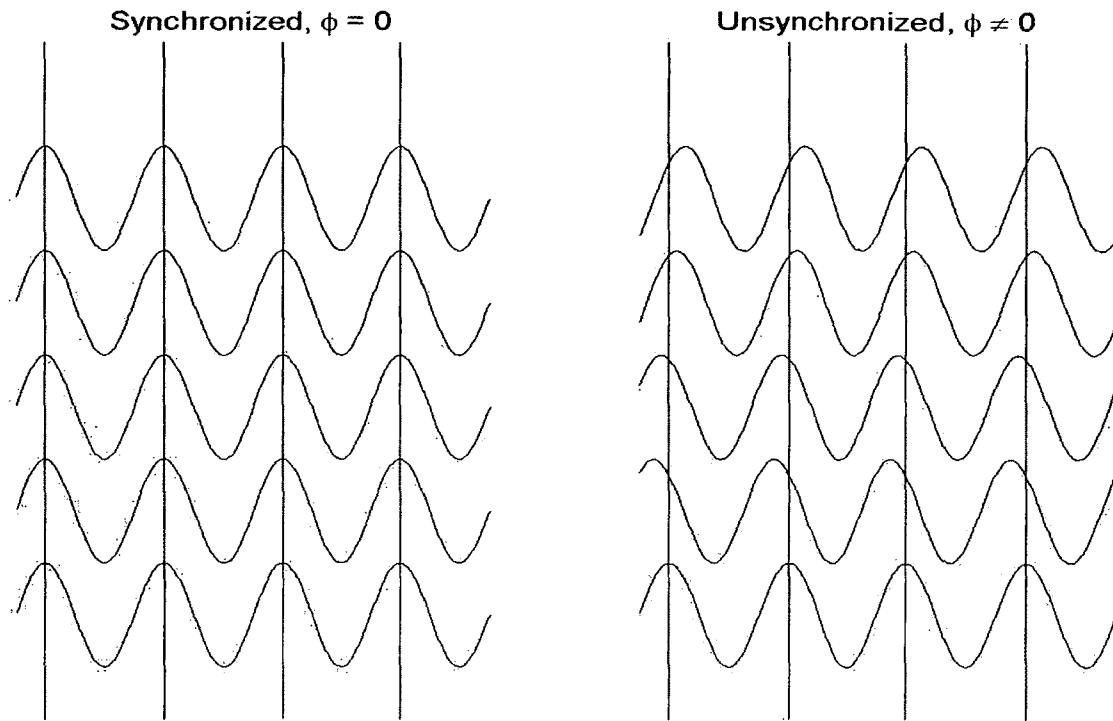


Figure 2-4: Synchronicity illustration between two sets of signals. The set of signals to the left are in phase synchrony with each other and the set on the right is out of phase.

Synchronized behavior in nature can be observed in both inanimate physical systems and biological systems. System synchronization can either be spontaneous or directed. In directed synchronization, distinct external information or stimuli (discrete or continuous) is required to move the system and maintain the elements in more synchronized states. When a system moves into and maintains synchronization without external intervention, it is said to have spontaneously synchronized. Many examples of each type of synchrony exist in the natural and the physical world.

2.2.1 Synchrony in Neural Systems

Synchrony between two coupled oscillators was first reported by Christian Huygens in 1665, where he observed two coupled pendulums spontaneously synchronized. Since then, synchronous behavior has been observed in diverse systems,

including pacemaker cells, fireflies, fish swarms, and laser beams (Strogatz and Stewart, 1993). Synchronous processes are also found in the Human body (Glass, 2001).

Oscillatory and synchronized behavior is ubiquitous across the nervous systems of different species. The first documented reports of synchronized behavior in the human brain are from the experiments of German psychiatrist Hans Berger (Tudor, 2005).

Berger discovered EEG, an important breakthrough as a diagnostic tool for normal brain activity and disorders. He also noticed different frequency bands in his recordings which are now classified as delta (~0-4 Hz), theta (~4-8 Hz), alpha (~8-12 Hz), beta (~12-30) and gamma (~25-100) oscillations. It was later understood that these recordings, often obtained by placing scalp electrodes and amplifying the signal, are the spatial summation of the electrical activity of perhaps millions of neurons underneath the skull (Llinas, 1988). Since these discoveries, synchronous behavior has been observed through the nervous systems and at various levels. On the macroscopic level, they have been observed in the thalamo cortical network (Llinas, 1988) and on the microscopic level and in computational modeling studies (Hooper, 2000; Kiehn and Butt, 2003).

Synchronous behavior has also been reported at the mesoscopic, or network level. At the network level, a group of interconnected neurons (usually ranging from a few hundred to thousands) which are coupled via complex interconnections, exhibit synchronous rhythmic behavior. The most studied among the smaller networks that produce rhythmic behaviors are the central pattern generators (CPG). They are a small network of neurons, found mostly in the spinal cord, that produce rhythmic behavior even though they have no sensory feedback (Hooper, 2000; Kiehn and Butt, 2003). Rhythmic

oscillations have also been observed in cortical networks, especially in the hippocampus region (Buzsáki, 2002).

2.2.2 Importance of Synchronization

Functional correlates of synchronized oscillations are usually investigated after discovery. These oscillations may underlie many cognitive processes and functions. They may also play an important role in the formation and the retrieval of memory. Phase-synchronized oscillations may facilitate neural communication and improve both working memory and long-term memory in the medial temporal lobe (Fell and Axmacher, 2011). Oscillations around the theta band were reported on investigations of episodic memory (Stam, 2005; Klimesh *et al*, 1997). Stam *et al* also reported alpha and theta rhythms during memory performance. Cyclic oscillations were also reported during various stages of sleep, though their functions remain unknown (Dement and Kleitman, 1957). Even spontaneous synchronicity is observed in resting states of the brain that is attributed to smaller networks (Cabral *et al*, 2011). Long range EEG correlations were correlated to certain memory functions (Weiss *et al*, 1998). Cortical synchronization may play an important role in information processing and learning (Singer, 1993). Conscious processing, arousal, attention, and integration have been correlated with gamma range frequencies (Engel and Singer, 2001). Oscillations were also reported in experiments involving other complex functions and cognitive processes, such as recognition of faces and facial expressions (Başar and Güntekin, 2008).

Endogenous oscillations also shape neural circuitry during earlier stages of neural development in different parts of the nervous system. For the formation of neural circuitry in a system, differentiation, cell type determination, and pathway formation are

largely governed by genetically specified cues and are activity independent. Later, circuitry is refined by stimuli from the various senses, also termed as activity dependent. Neural systems also have endogenous oscillations that are independent of external stimuli and that shape the formation of these circuits. Endogenous oscillations are vital for the formation of visual pathways (Penn and Shatz, 1999). Synchrony of oscillations in the gamma band is important in the development of cortical circuits (Uhlhaas *et al*, 2010). Synchronized activity has been observed even prior to the formation of synapses in embryonic cells (Spitzer, 1995). These oscillations are attributed to transient elevations of Ca^{2+} ions and they contribute to network development (Holliday and Spitzer, 1990). Oscillations have also been observed in developing hippocampal circuits (Ben-Ari, 2001). The CA1 region of the hippocampus showed endogenous oscillations during the earlier stages of development (Garaschuk *et al*, 1998).

2.2.3 Diseases Caused by Disrupted and Abnormal Synchronization

Disrupted synchronous oscillations, caused by multiple pathological and disease states, affects the functionality of the nervous system at many levels. Epilepsy is a classic example of abnormal hyper-synchrony (Fisher *et al*, 2005). Epileptic seizures affect over 50 million people worldwide (World Health Organization) and the mechanisms underlying abnormal synchrony of neurons during seizure episodes are not clearly understood. Abnormal neurochemical changes can cause seizures. Both gamma-Aminobutyric acid (GABA) and glutamate neurotransmitter systems have complex production, release and uptake mechanisms. Any pathological changes to these or other neurotransmitter systems could result in the occurrence of seizure episodes (Day *et al*, 2012). Disruptions to GABA and glutamate transport mechanisms, biochemical

modification of receptors, gene expression, changes in extracellular concentrations of ions, modulation transmission by glial cells and abnormal network organization are other causes for seizure activity (Bromfield *et al*, 2006).

In contrast, diminished synchronization can be caused by inhibitory neurons. EEG traces of patients with schizophrenia showed failures in synchronization in the gamma band (Spencer *et al*, 2003). The responses to stimuli of these patients in the gamma band were reduced in the left hemisphere and increased in the right hemisphere compared to normal individuals. Overall, their activity in the gamma range was lower (Haig *et al*, 2000). Alzheimer's disease (AD), which is common among people aged over 65, is a neurodegenerative disease affecting over 24 million people worldwide. EEG recordings of people with AD indicate a difference in the delta oscillatory range (Yener *et al*, 2007). Children with ADHD showed strong gamma phase-locked oscillations for stimuli selectively sent to the right brain suggesting that gamma oscillations may play a role in sensory-motor integration in such children (Yordanova *et al*, 2001). In another study on ADHD patients, task-related gamma-band responses in the parieto-occipital area were enhanced (Lenz *et al*, 2008). Bipolar disorder (BD) is also reflected in abnormal EEG bands (Levinson *et al*, 2007). Deficits in cortical inhibitory networks related to GABA transmission are correlated with BD (Levinson *et al*, 2007). In another experiment, the EEGs of people with BD showed reduced power in responses for different frequencies of stimulation (McDonnell and Abbott, 2009). For complete review of brain disorders related to disruptions, see (Başar and Güntekin, 2008) and (Uhlhaas and Singer, 2006).

2.2.4 Need for Studies of Synchrony in Neural Systems

To understand brain behavior during resting and active states and during pathological conditions, one must examine synchronized oscillations underlying those states. Although the regions of the brain where such behaviors are exhibited have been identified, the biophysical mechanisms and the complex network interactions through which a network of neurons collaborate are not clearly understood. Studying only individual neurons does not explain the emergence of much complex network behavior. Therefore a network-level study approach is required to understand this phenomena (Kwok *et al*, 2007). If structure is related to function, then the structural components of the neural system that enables the network to have synchronized states needs to be identified. Glial cells play an important role in the network organization and synchronization. The ability of glial cells to regulate glutamate release and uptake could play a role in neurons synchronization (Angulo *et al*, 2004). But the extent to which glial cells could affect the self-organization of a network and the levels of synchronization is not known. The following issues related to spontaneous oscillations and synchronized behaviors (and general excitability) are addressed; the role glial cells play in the development and in sustaining of spontaneous oscillations and synchronized activity in developing networks, and the role of diseases, particularly the development of brain tumor cells, and how they influence the general excitability and spontaneous activity of the network.

2.3 Brain Connectivity

2.3.1 Connectome

To understand the behavior of any system as a function of its components, we need to understand the architecture of the system. A system can be made of any set of components, and these components could be connected to one another in many possible combinations. Different combinations of connectivity lead to different architectures and thereby different system properties. For instance, graphite and diamond are allotropes of the same element, carbon. Both are entirely made of carbon atoms, but they exhibit completely different properties like hardness, brittleness and melting point. To understand the properties of graphite, we should understand not only the properties of carbon atoms but also the way the components are connected (lattice structure). This principle can be extended to neurological systems as well. The main information processing components in the nervous systems are neurons. Much is known about individual neurons and their biophysical properties, mainly from patch clamp recordings. In theory, behavior and function are a result of information exchange and interactions at the network level. A complete map of any neural system is termed as a connectome. A connectome of any neural system can be defined as a complete map of its neural connections. It would incorporate information on the types of neurons a system has, the dendrites and synapses of each neuron, the direction in which the neurons are connected with one another, and the synaptic weight of such connectivity (if possible, but not necessary). A complete understanding of the network properties is imperative to understand the functioning of any nervous system, including the human brain. The connectome is the neurological analogy of the genome. Hypothetically, with the

connectome information and sufficient computational resources, it should be possible to completely model the system under study. So far, the only species for which this map has been laid out is *Caenorhabditis elegans* also known as *C. elegans* (White *et al*, 1986).

C. elegans is a transparent hermaphrodite nematode about 1 mm in length. Its nervous system consists of 302 neurons and 56 glial cells. The neurons fall under 18 different classes. There are about 7000 synapse junctions (5000 chemical synapses, 2000 neuromuscular junctions and a few GAP junctions). The role of each neuron, its afferents, and its efferent are known. Substantial information is also available on its genome. A picture of its neural architecture shown in Figure 2-5 illustrates that even a simple organism can have an extremely complex neural architecture.

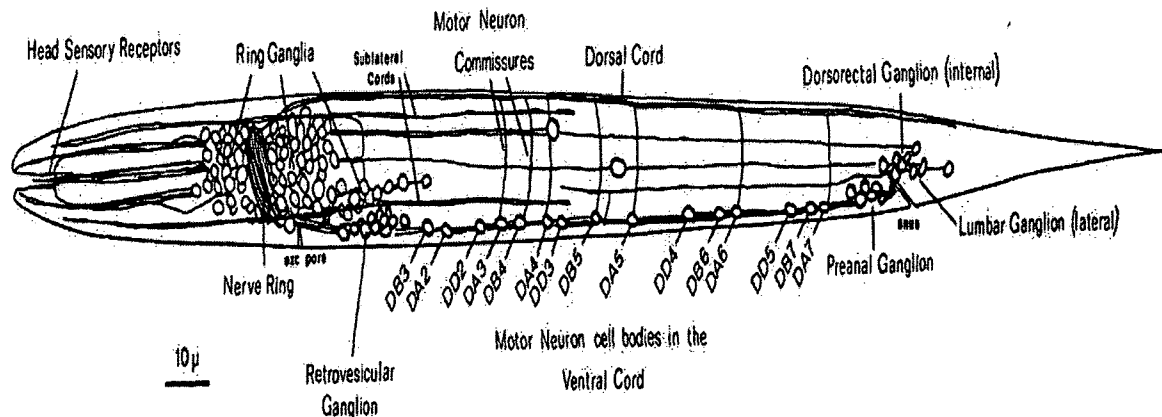


Figure 2-5: The *C. elegans* wiring diagram (Varshney *et al*, 2011).

In the human nervous systems, the study of circuitry has been limited to smaller circuits. Spinal circuits and reflexive circuits have been studied extensively mainly because of their simplicity. An illustration of a small spinal circuit and a more complex cortical circuit is shown in Figure 2-6. The brain, however, is more complicated. The human brain has 100 billion cells with an average of 10,000 synapses for each neuron. A

comprehensive connectome of the human brain would constitute 10^{15} pieces of information (i.e., 10^4 connections for each neuron for 10^9 neurons). Were we to include the strength of the synapses and the directionality of the connection, the amount of information to represent would be more. An endeavor of this magnitude is beyond contemporary technological tools. However, some reductionist approaches allow one to obtain the connectomes of sub-regions at a mesoscopic level. Figure 2-7 is a macroscopic connectivity representation of the brain. Each ‘module’ or node is a specific region and may correspond to millions of neurons and connections within itself (Sporns, 2011).

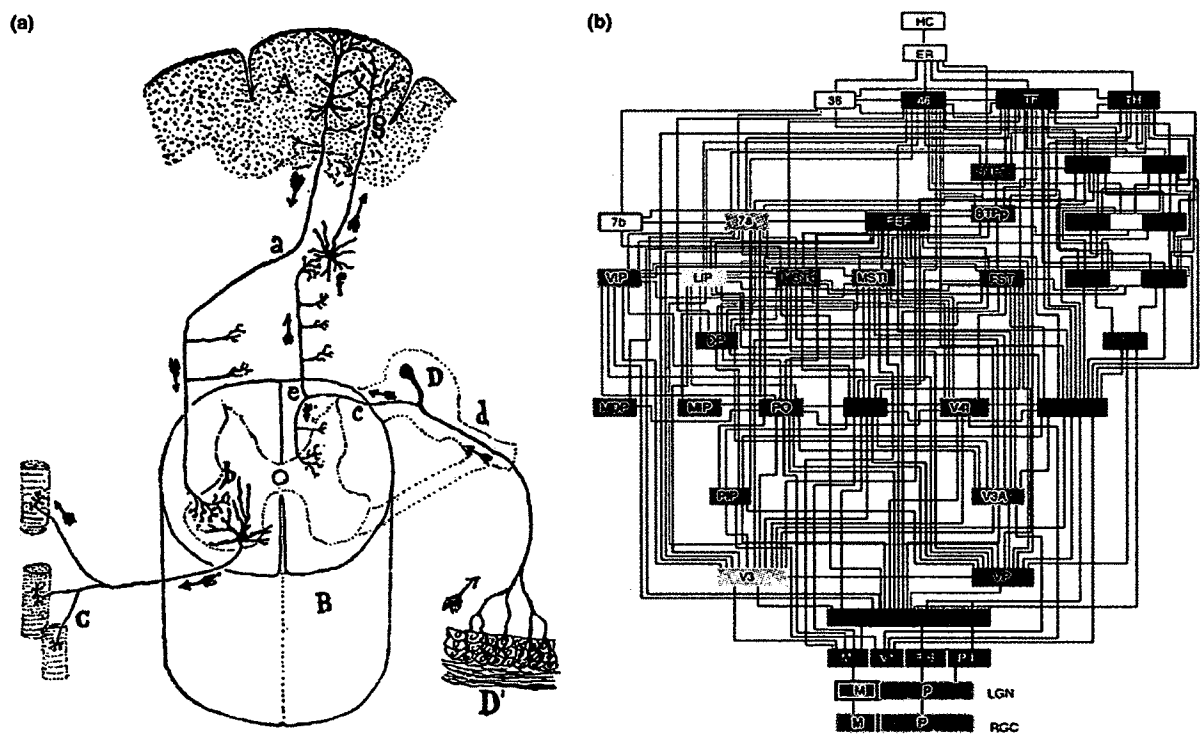


Figure 2-6: (a) Illustration of information processing from the peripheral systems, the spinal cord, and the brain (by Cajal). (b) A summary of connections in the cortical areas that are generalized (Sporns, 2011).

Mesoscale reductionist approaches (Sporns, 2011) produce low-resolution connectomes by only accounting for connections between brain sub-regions. For

instance, statistical connectivity information of the cortex, allows us to map approximate connectivity patterns that exist between them.

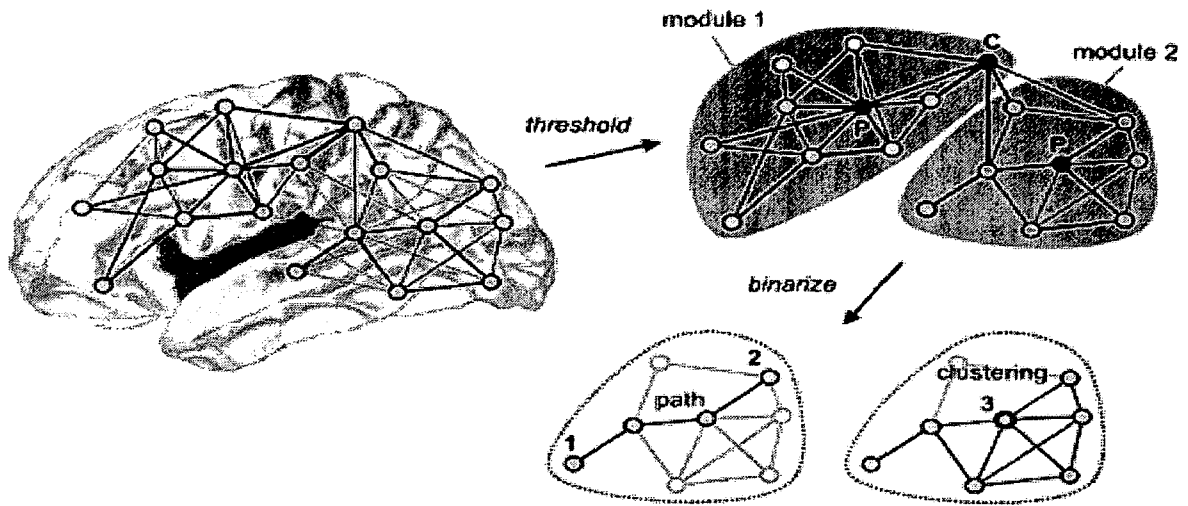


Figure 2-7: Basic approach of representing human brain as modular networks. This diagram is a macroscopic connectivity representation of the brain. Each 'module' or node is a specific region and may correspond to millions of neurons and connections within themselves (Sporns, 2011).

Another type of connectome that is usually studied is the functional connectome.

Close proximity between two nodes does not necessarily implicate a functional connectivity between these two nodes. A functional connectome is a network representing units that are connected functionally (Sporns, 2011). Due to the high specificity of functions of single neurons, there have been criticisms over these mesoscopic reductionist methods. Even single neurons in the hippocampus are said to encode spatial information and exhibit unique responses to different stimuli (O'Keefe and Dostrovsky, 1971). Single neurons in the primate visual cortex encode information (Tovée *et al*, 1993).

2.3.2 Network Theory and Small-World Networks

Networks are ubiquitous in nature (Watts and Strogatz 1998). A wide variety of natural systems (involving networks) have been modeled and studied using graph theoretical approaches. The internet, intercellular signaling pathway networks, ecological networks, citation networks, movie actors network, phone call networks, power networks, neural networks, biological networks, and coupled oscillator models are among the wide range of self-organizing networks that have been studied mathematically (*The Geometry of Biological Time*, 2001). Networks have typically modeled as either completely regular or random. Regular networks usually have a pattern in their structure and random network are completely stochastic in nature (Figure 2-8).

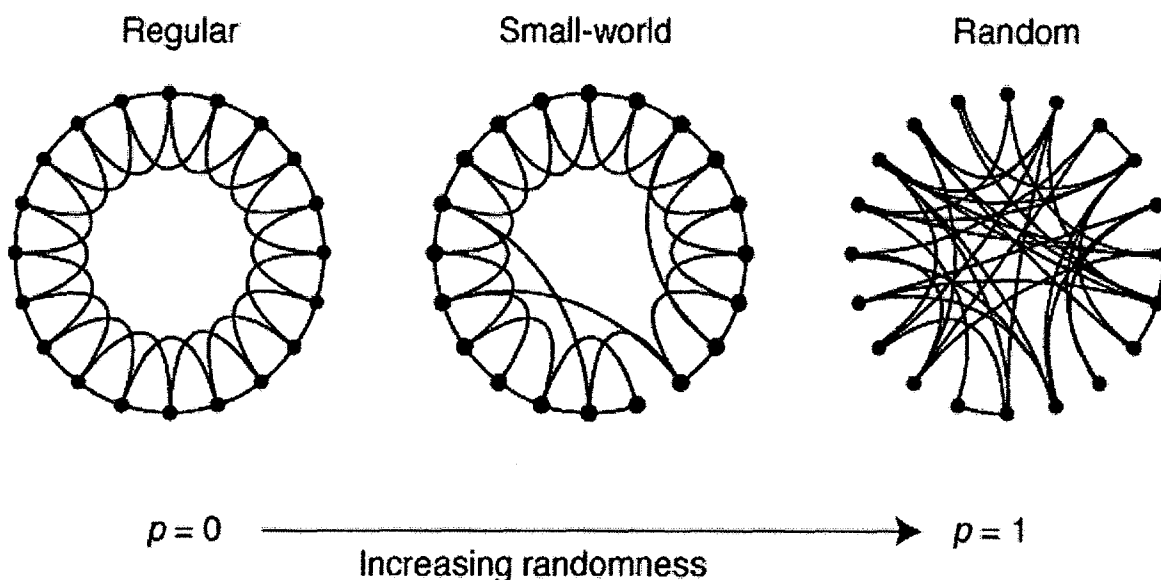


Figure 2-8: Small-world networks have neither the regularity of ring lattice networks, nor the randomness of Erdős-Renyi networks (Watts and Strogatz, 1998).

The lattice structure of an element is a repetitive pattern of the same basic structure and is classified as a regular network. More complicated networks are

traditionally classified as random networks. Erdős and Renyi were pioneers in developing this model (Erdős and Rényi, 1960). In their model, no specific arrangement was used for the “links” of the graphs. The links usually follow a statistical distribution. Recently, new data on large-scale networks, occurring in nature and social systems, suggest that these networks are neither completely structured nor random. They fall in between these two classes and have been termed as small-world networks (Watts and Strogatz, 1998). A regular network has a high level of local interaction (clustering coefficient) with its neighbors, and the number of links required to reach a distant node is high. In a completely random network, usually, local interactions are lower; however, the number of links needed to reach distant nodes (path length) is small compared to that of a regular network. A small-world network lies in between the two. It has a high level of local interactions between the nodes (quantified as clustering coefficient) and low characteristic path length. After this phenomena was discovered, several networks that were earlier classified as random networks have been re-classified as small-world networks, including the connectome of *C. elegans* (Varshney *et al*, 2011).

Small-world networks have also been identified in brain regions. Both the anatomical and functional connectivity networks could fall under the small-world category (Sporns *et al*, 2004). Small-world networks may also play a role in neural synchrony (Yu *et al*, 2008) and formation of memory (Bohland and Minai, 2001). Their disruption has been implicated in certain diseases, like epilepsy (Kramer and Cash, 2012) and Alzheimer’s (Sanz-Arigita *et al*, 2010). In this study, we investigate where such networks can emerge during the self-organization of neurons and whether they are

relevant to the emergence of synchronous behaviors. We will also investigate the effect of disease on the small-world topology.

At the network level, the following questions are addressed: (Q3) Can a neural culture be classified as a small-world network? What transitions take place in network architecture in a developing network that result in the emergence and the sustaining of spontaneous activity and synchronized oscillations in the network? (Q4) How do certain disease states, such as lack of glial cells or the growth of cancer cells, affect network properties?

2.4 Approach

The first task in addressing the questions described in the previous sections (Q1, Q2, Q3, and Q4) is to develop a biological neuron network model that can be morphologically and electrically observed over the course of development. Our objective is to use network analysis tools to study the morphology and to combine multisite recordings with signal processing techniques to determine any relationships that exist between these two as shown in Figure 2-9.

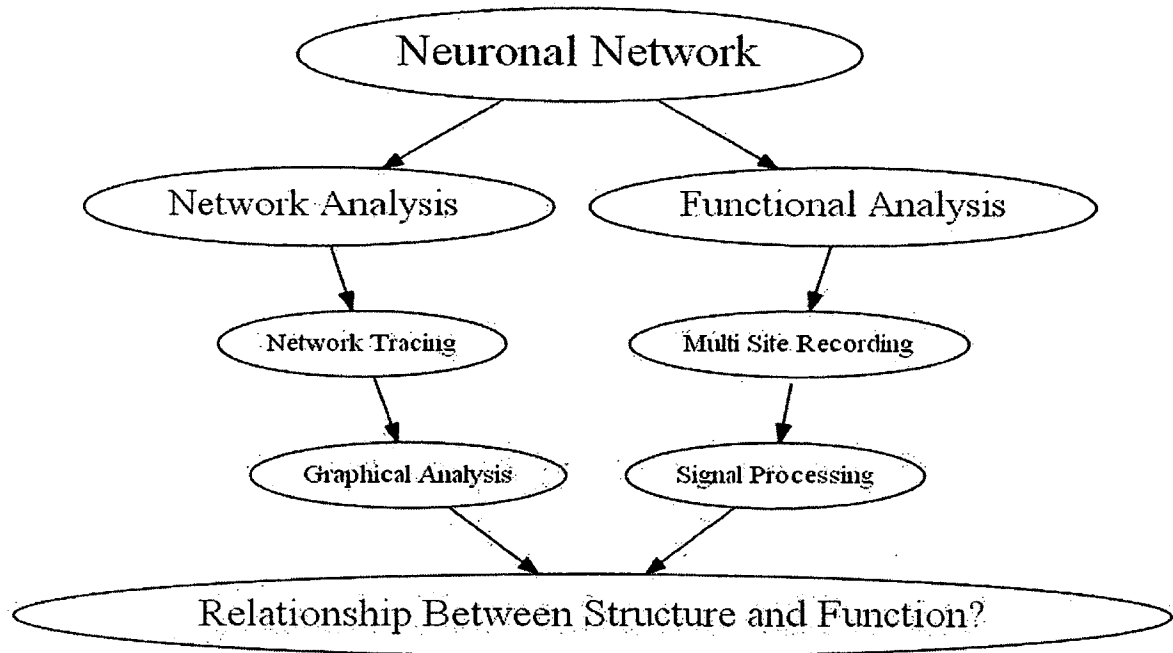


Figure 2-9: Research approach

Ideally, the network model could be developed in an *in vivo* model, where the organism is in its natural environment. However, such a setup is not practical. To overcome this difficulty, traditionally, neurons have been explanted from growing brains of rat fetuses, dissociated, and attached to surfaces to which they adhere and form networks. It has been reported that a set of dissociated neurons can self-organize into an electrically active network (Segev *et al*, 2003). Many such random networks have also been reported to develop spontaneous activity and synchronized oscillations (Chiappalone *et al*, 2006). The approach is limited because this network is outside its natural biological environment. The neurons are also removed at a critical stage in their development phase, which is disrupted by the explant procedure (Potter *et al*, 2003). Another limitation is that these neurons are deprived of any sensory stimuli that they normally receive from other sensory organs (such as visual, auditory, and olfactory systems). Sensory stimuli modify the network throughout the lifespan of the organism.

However, such models can produce valuable results depending on the phenomena under study. Since spontaneous activity and self-organized synchronization has been observed in culture networks, one can argue that these phenomena are an intrinsic property of a set of neurons since they do not depend on external stimuli or on the conditions, *ex vivo* or *in vivo*, in which they develop (Habets *et al*, 1987). It is possible that in the development of the network, neural changes pertaining to learning and memory could be universal properties and independent of conditions and hence can be studied *ex vivo* (Marom and Shahaf, 2002). Also, experimental protocols that could be performed in *ex vivo* studies have some advantages over *in vivo* setups. The development of microelectrode arrays (MEA) allows recording extracellular electrical potential from multiple sites of the network at a much higher resolution (Thomas Jr. *et al*, 1972). These arrays are glass dishes with microelectrodes embedded underneath that are in contact with neurons that are plated over the glass dish. It is also possible, with appropriate techniques, to monitor the activity of single neurons in a network (Gross *et al*, 1977). The ability to record (and to stimulate) from multiple sites (up to 64 electrodes) offers the prospect of monitoring and manipulating the system from a network level (Pine, 1980). Focal electrical stimulation, pharmacological manipulation, and manipulation of the network architecture are possible in this setup (Chiappalone *et al*, 2006). Certain disease models have also been established using MEAs (Liu *et al*, 2009). These studies may offer fundamental insight in the development, diagnosis, and treatment of such diseases.

Since these cultures could also be established in substrates that are transparent to light, it is easy to monitor the architecture of network evolution *in vitro*. Even disease states, such as epilepsy, can theoretically be represented via network connectivity

(Srinivas *et al*, 2007). In our study, after plating the dissociated neurons on these substrates and periodic imaging of a subset sample of the network (which we believe retains some of the universal properties that the network holds), an *ex vivo* model that retains some key properties of *in vivo* models and that can be structurally and electrically monitored is established. After imaging, using certain reductionist approaches and assumptions, we extract the information into an abstract graph theoretical framework. After establishing this framework, we use several graph algorithms which analyze these networks by searching through and extracting connectivity parameters that is not easily observable (Bullmore and Sporns, 2009). By this procedure, we can monitor changes in the connectivity parameters of the network as it develops and matures. We can also identify these parameters in disease states (cancer and diseases attacking glia cells) and compare them with that of normal cultures. Since these parameters are usually numbers, we could possible quantify abnormal networks effectively. By recording multisite electrical activity and finding correlations between different sites of the network, it may be possible to associate the dynamics of network parameters when the network transitions into oscillatory and synchronous modes. Similarly, we can see how various diseases states affect network excitability, spontaneous oscillations, and synchronizations and perhaps offer novel diagnostic techniques for clinical use.

CHAPTER 3

MATERIALS AND METHODS

3.1 Overview

This section describes the materials, methods, and protocols used in this study. In Section 3.2, the configuration of the special microelectrode dish and the arrangement of electrodes within it are presented. The hardware setup up for recording, filtering amplifying, sampling, and digitizing the signals are presented next. The experimental protocol for cell explant and plating, the criterion for choosing optimal plating density, and the rationale for choosing the disease model (AraC and CRL-2303 treatment) are discussed. In Section 3.3, the network tracing procedure and the assumptions for mathematical abstractions of the network are discussed. The rationale for choosing appropriate network descriptive parameters (such as cluster index and characteristic path length) and their definitions are presented. Other standard models that are traditionally used to model networks are presented. Three standard models are discussed. A regular lattice network, the random network and the small-world network model are presented. These models are later compared with our mathematically abstracted neural networks. Lastly, in Section 3.4, various signal processing measures used to quantify neural synchrony are discussed.

3.2 Culture Methods and MEA Setup

Each MEA is an 8 x 8 grid of electrodes embedded in a glass substrate that can record extracellular electrical potential from as many as 64 sites (Multi Channel Systems_ MCS, Reutlingen, Germany). The diameter of each electrode is around 30 μm and the spacing between electrodes is 200 μm . Each electrode is made of titanium nitride with an impedance of 30-50 $\text{K}\Omega$. A schematic of the dish is shown in Figure 3-1.

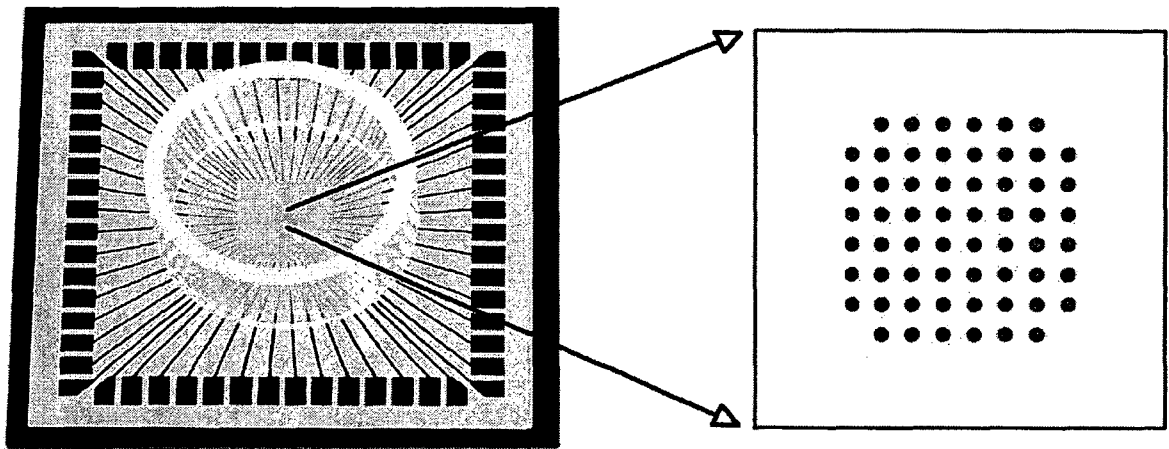


Figure 3-1: A microelectrode array dish with embedded electrode grid

The recording area is surrounded by a ring within which the cells are plated and the culture is added. Each electrode from the recording area is mapped to a contact pad at the edges of the dish. Even though there are sixty four electrodes from which signals can be recorded, our hardware only has the capacity to record from fifteen channels at a given time. One channel is always grounded. The electrical signals from the dish are transferred to the recording stages via these contact pads. In the recording stage, the signals are first pre-filtered and amplified. The gain of the amplifier and the sampling frequency of the recordings can be chosen manually via the software. An analog-to-digital converter is

used to digitize the signals. The MC_RACK software (Reutlingen, MCS systems) is used to display and analyze data.

3.2.1 Neural Extraction and Plating Protocols

Whole brains were obtained from neonatal day 1 Sprague Dawley rats. In this protocol, the rats are killed by cervical dislocation. After decapitation, the skull is removed with micro scissors and the brain is placed in an 8-10 ml basal media. The protocol was approved by the Institutional Animal Care and Use Committee (IACUC). The meninges and blood vessels were removed with a small tip forceps. The brainstem was removed and discarded. A 50 ml tube containing basal media is used to store the tissue while the other brains were extracted. The 50 ml tube is maintained at 4 °C through the procedure. After the brains from all the pups were removed, the brain tissues were removed by aspirating with 10 ml pipette and pipette aid. The tissue is blown into a 15 ml tube. Another 8 ml of complete media is added and titrated for about 15 times. The supernatant will contain most of the neural cells. The supernatant is removed and put into a 15 ml tube in ice.

The standard MEAs (8X8 grid) were used. Prior to the day of the experiment, the dishes were rinsed with deionized water and soaked in 70% ethanol for 20 minutes. The alcohol was then pipetted out and the dishes (put inside Petri dishes) were kept in a sterile hood with the lid slightly open. Dishes were exposed to UV light overnight to make them completely sterile. During the morning of the experiment, the dishes were pretreated with Poly-L-lysine (PLL) for an hour. Later, the PLL was pipetted out, and the dish was washed with PBS buffer solution. The dishes were then allowed to dry completely in a BSL II hood.

After a hemocytometer was used to count the cells, the appropriate amount of neurons (in our case, 200 k/dish) was transferred into the MEA dish. Special concentric rings with perforated Teflon sheets were used to cover the MEA well. The dishes were incubated and all recordings were performed at 37 °C.

3.2.2 Solutions and Reagents for Cell Culture

To prepare 250 ml of Neural Culture Media (NCM), the following reagents were used:

- (a) Fetal Bovine Serum (FBS)-25 ml
- (b) Horse Serum (HS)-25 ml
- (c) Glucose solution in sterile water (deionized) -120 mg/mL[1.25 ml]
- (d) Glutamine in sterile water (deionized)-20 mg/mL[1.25 ml]
- (e) Penicillin-Streptomycin solution -[1.25 ml]
- (f) Ham's F12-K media – [98 ml]
- (g) Basal Media Eagle's (BME)-98.25 ml

In a sterile environment (BSL II hood), the BME is transferred into a filtration unit. FBS, if frozen, is thawed, and HS is added to the filtration unit. Glucose solution, glutamine solution, PS and F12-K are added successively. The lid is put back on the filtration unit and the vacuum is started. The supply filter is then connected. All the liquid is drawn through and the upper twist portion of the filtration unit is removed. The sterile cap, from a separate bag is placed on the media flask. The media is then labeled, dated, and put in an initial flask. To distinguish hyper excitatory activity from seizure-like events, cultures were stimulated with glutamate. Locke's solution (Table 1) is used as the vehicle for the glutamate solution.

Table 1: Locke's Solution Recipe

Component	M.W	Amount Used	Final Concentration
NaCl	58.44	2250.0 mg	154 mM
KCl	74.55	104.4	5.6 mM
NaHCO ₃	84.01	75.6 mg	3.6 mM
CaCl ₂ ·2H ₂ O	147	84.5 mg	2.3 mM
MgCl ₂ ·6H ₂ O	203	61.0 mg	1.2 mM
Glucose	180.2	252.3 mg	5.6 mM
Hepes	pH 7.4	1.25 ml of IM stock	5 mM
Water (purified)	pH 7.4	248.75 ml	

The components are dissolved in purified water and about 100 ml of purified water is added to the filtration unit. Water is added to the dissolved components and 1.25 ml of 1 M stock Hepes. After the cap is put on, the vacuum is turned on. The liquid is allowed to pass through the filter and vacuum is turned off before bubbles form. The top of the vacuum is twisted and a sterile cap is put onto the container of media.

3.2.3 AraC Treatment

To compare the electrical activity of normal cocultures (cultures that include a mix of neurons and glial cells) with a replated culture (a culture primary composed of neurons and less glial cells), the cultures are treated with AraC. AraC is a cytosine and an antimetabolic agent that interferes with DNA synthesis of the cell resulting in its death (Svensson and Aldskogius, 1993). It is used mainly in the treatment of cancer because it can selectively destroy tumor cells (Rudnick *et al*, 1979). AraC has been reported to be highly effective in limiting the proliferation of normal glial cells (Nunez 2008). AraC is

added to the culture during the S-phase during the synthesis of DNA. Usually, about 10^{-5} M of AraC is added 2-3 days after the dissociation for maximal efficacy.

3.2.4 C6/lacZ7 (CRL-2303) Cells

The C6/LacZ7 cell line (purchased from ATCC) is an aggressive glioma tumor cell line (Benda *et al*, 1968). It is well suited for experimental study models of glioblastoma growth and spread (Grobbs *et al*, 2002). These cell line express a lacZ reporter gene and they have the ability to stain blue which is important to distinguish them from other cells and hence useful in quantitative model and analysis of tumor cells. Rat C6 glioma cells transplanted into rat neocortex resulted in hyperexcitability in regions around the tumor (Köhling *et al*, 2006).

In this study, normal healthy cultures and CRL-2303 induced tumors were compared. The functionality of the networks are quantified electrically by the magnitude of activity, firing rates, frequency components, cross-correlation, and coherence measures. The analysis will help to distinguish healthy and diseased models via their electrical profile and would contribute to the understanding and diagnosis of such diseases under clinical conditions.

3.3 Graph Abstraction

A graph is formulated as $G = (V, E)$, where V represents all the nodes or vertices and E represents all the edges, with each edge associated with at most two nodes. The vertex set V of the graph in Figure 3-2 is $V=\{a,b,c,d,e,f,g,h\}$, and the edge set is given by $E=\{e1,e2,e3,e4,e5,e6,e7,e8,e9\}$. A simple graph is a graph without self-connections and multiple edges. Here we have approximated our data as a simple graph.

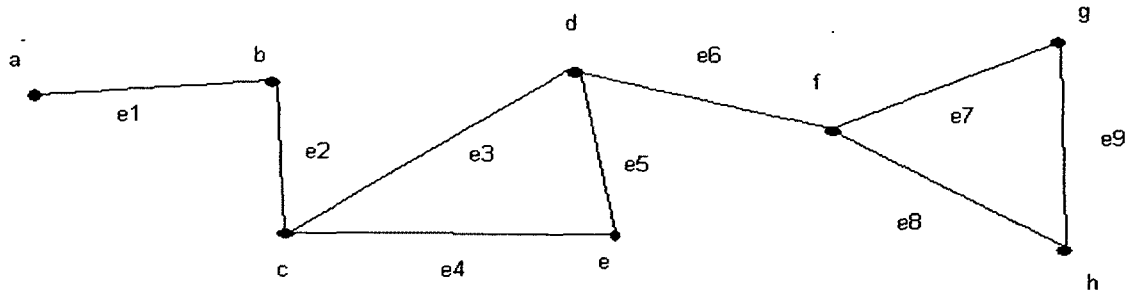


Figure 3-2: Example of a simple graph

3.3.1 Morphological Generalizations

The neural network is represented mathematically for our analysis. Multiple algorithms and procedures have been developed to extract from network subtle information that is otherwise difficult to spot. For this process, the following generalizations are proposed.

Neurons are abstracted as nodes of a graph, and the connections (neuritis) between them are as edges. Only neurons are considered and glial cells are not considered as nodes.

- i) *Edges are abstracted as unidirectional and unweighted.* Ideally, the communication between two neurons has three distinct pieces of information(s). They are direction, type (inhibitory or excitatory) and strength of the communication(s). However, due to technological constraints it is extremely difficult to obtain such information the scale (size) of the networks under study. Therefore, we have reduced connections between two neurons as a unidirectional and unweighted edge. *Multiple edges are ignored.* Sometimes, one neuron can communicate with another neuron through a number of communication pathways (multiple). Our reductionist approach assumes multiple

connections as redundant and all multiple connections are clubbed as one unweighted edge.

- ii) *Self-innervations are ignored.* We also observed that certain neurons extend neuritis (connections) to it causing a self-innervating loop. Such types of neurons are called as autapses. We have ignored such connections.
- iii) *Large groups of neurons are termed as clusters.* After the first week of development, neurons migrate and form closely knit clusters. The neural density is extremely high in some regions and low in others. Since it is not possible to visualize individual connections in these clusters, we have assumed that they have high connectivity ($p = 1$). This assumption is made because a typical brain *in vivo* has a large number of connections between neurons.
- iv) *Nodes are assumed to be of equal weight* irrespective of size, shape and type. All nodes are unweighted and have the same property. In reality, however, a network contains many types of neurons and interneurons. While, ideally, addition of the differences among neurons to the model would improve accuracy, we believe it is not necessary as we focus mainly on the networks connections and not its components.

With the following assumptions, it is possible to represent any neural network as a simple graph (G). Further, each graph can be represented via an adjacency matrix, $A(G)$ upon which other algorithms can be used to extract specific information. $A(G)$ is a symmetric matrix which is described as follows: Let $N_1, N_2, N_3, \dots, N_n$ represent the n nodes of the graph G . The edges of the graph are given by $S_{ij} = 1$ (i, j), if and only if there exists an edge between i and j . $S_{ij} = 0$, otherwise. All diagonal elements are zero as self-innervations are omitted.

3.3.2 Graph Methods

3.3.2.1 Parameters that Quantify Network Connections

Average connection density (K_{den}) is the ratio between the number of connections in a graph to the total number of possible connections in the graph (i.e., the number of connections that would be if were a complete network where every node is connected to every other node, as in Figure 3-3).

$$K_{den} = \frac{\text{No of edges in the graph}}{(n^2-n)/2}$$

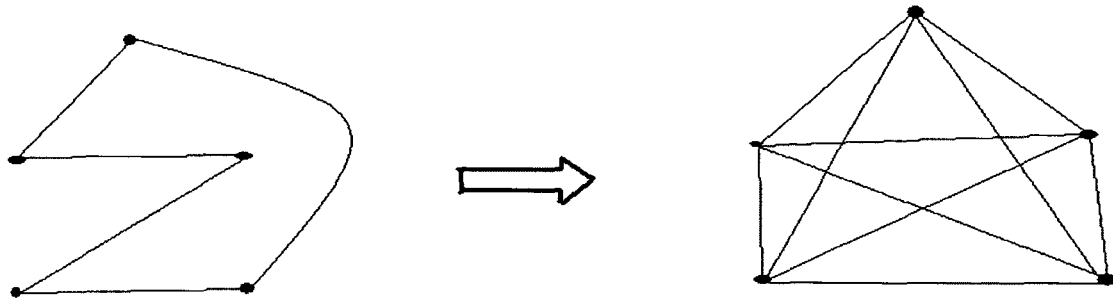


Figure 3-3: The incomplete graph (left) has ($n=5$, $e=5$) has a connection density of 50% as a simple graph with $n=5$ can have at most 10 edges.

Average connection density is a measure of the sparseness of a network. The higher the connection density, the higher is the connectedness of a network and vice versa. Higher connection density also implies that the network has more redundant connections and hence more robust. Biological networks and neural networks are very redundant and ample extra wiring is provided in case of loss of connectivity due to disease or injury.

The degree of any node is the sum of the edges that are linked to that node. The degree of node d is 3 since three edges, e_3 , e_5 , and e_6 , are linked to that node as shown in

Figure 3-2. The average degree of a network is the ratio between the sum of degrees of all the nodes and the number of nodes. It is given by,

$$D_{avg} = \frac{\sum_{i=1}^n D_i}{n}.$$

The degree of a node may imply the importance the node plays within the realm of the network. If a node has a high degree, it is more likely to participate in receiving, sending, or processing information. Nodes with higher degrees could be more important than nodes with lower ones. The function of a network may be altered more when a node with a higher degree is removed or damaged compared to a node with fewer degrees.

The connectivity matching index (CMI) between two neurons is the amount of connectional overlap between them, excluding the connection between each other. It is a symmetric quality. $M(G)$ is a matrix that contains entries of CMI between all neurons in the network. A high CMI between two neurons indicates similar anatomical connectivity and similar functional roles. The CMI between two nodes is illustrated in Figure 3-4. The red lines are overlapping connections and the black lines are non-overlapping ones.

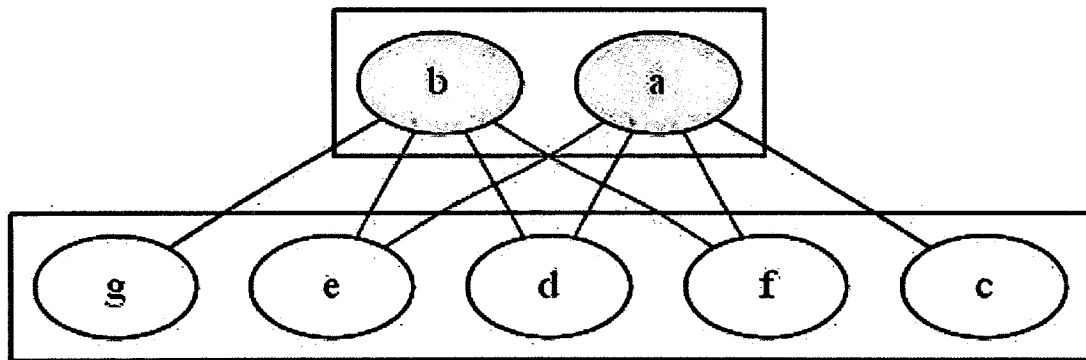


Figure 3-4: Nodes *a* and *b* have overlapping connections to *e*, *d*, and *f*. The amount of overlap is the ratio between the overlapping connections to the total number of connections. The connections between *a* and *b* are ignored, if they exist.

If there exists at least one path between two nodes i and j , then the reachability between the nodes is $r_{ij} = 1$. If there exist no path, then $r_{ij} = 0$. Reachability represents how much the graph is connected. The reachability matrix $R(G)$ is a record of reachability between all the nodes (Harary 1969). Reachability is the most basic measure of structural and functional connectivity in a network. If any element in the $R(G)$ matrix is zero, then it could indicate brain injury or disease. $R(G)$ can be used as a preliminary measure of the vulnerability of a network after damage, but it does not indicate the extent of the damage.

If there are edges and its associated vertices between any two nodes i and j , then there exists a path between these two nodes. Path length (λ_{ij}) between two nodes, i and j , is the number of edges it takes to transverse from node i to node j .

The distance matrix $D(G)$ is a record of the shortest path lengths between all the nodes to each other. If two nodes have no path between them, then they are *infinitely* apart and the distance between them is ∞ . The breadth-first algorithm is used to find the distances between various nodes. The *distance* we talk about here not physical distance, but synaptic distances. For instance, a neuron might be 20 μm apart from another neuron yet not be connected to it via synapses. Similarly, one can say that the neurons of the motor cortex are ‘closer’ to other bioexcitable cells (like muscle cells) in the leg than to other auditory neurons that are physically nearby. Thus, it is reasonable to claim that ‘graphical distance’ is a more relevant measure of distance than metric distance.

The cluster index of a node is a measure of connection density its neighbors. If a node i has N neighbors, then the CI of i is the ratio of the number of connections that

exist between them to the total number of possible connections (i.e., if it were a complete network).

Mathematically, the cluster index of any node i is defined as,

$$C_i = \frac{2|\{e_{ij}\}|}{(K_i-1)K_i} : v_j, v_k \in N_i, e_{jk} \in E,$$

where, i is the node for which the coefficient is calculated. Examples of cluster indices are shown in Figure 3-5. When the neighbors of a node are completely connected with one another, then the cluster index of that node is highest. When the neighbors are not connected to other neighbors, then the cluster index is zero. The CI is a measure of how well the neighbors of a node are connected with each other.

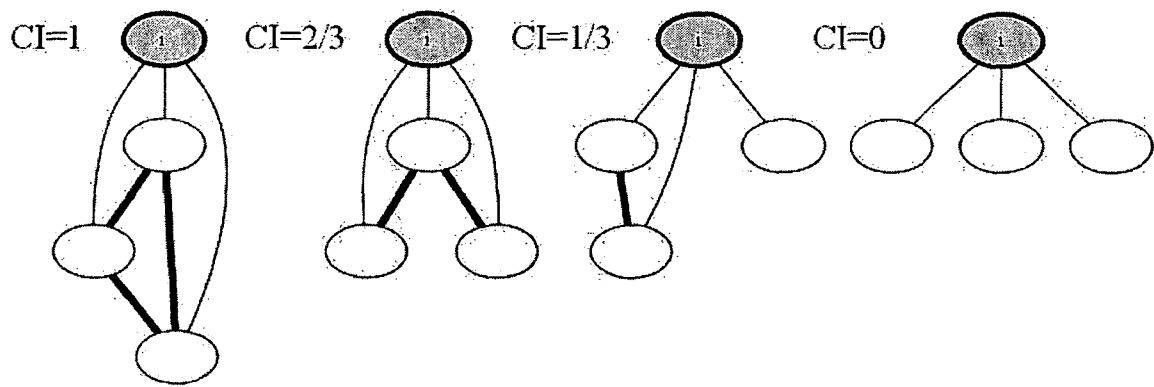


Figure 3-5: Examples of cluster indices for simple networks.

The algorithms to compute the cluster indices and characteristic path lengths are described elsewhere (Sporns 2003).

3.3.2.2 Example Network Types

Ring Lattice Network Model $G(n,k)$:

A ring lattice graph is one of the simplest regular graphs (Figure 3-6). Regular graphs have precise patterns to the way the nodes are connected to each other. They are

described by $G(n, k)$, where n is the number of nodes and k is the exact number edges a node is permitted to have. These graphs are well connected locally, but the overall connectivity is low because of its higher characteristic path length.

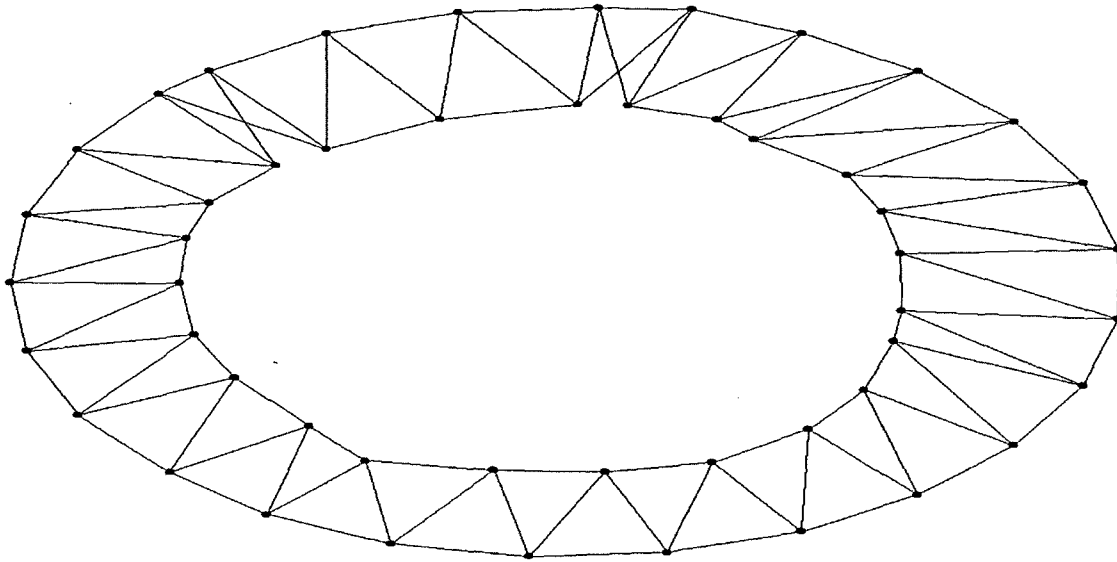


Figure 3-6: An illustration of a ring lattice graph ($n=50, k=4$). This graph has high clustering coefficient but low characteristic path length.

Erdős –Renyi Network model:

The Erdős-Renyi model was proposed by Paul-Erdős and Alfred Renyi as for modeling and generating random graphs of specified nodes and connection probabilities (Figure 3-7). The probability of an edge in the graph is independent of other edges and the number of nodes. It is usually denoted by $G(n, p)$ model, where G is the graph, n is the number of nodes, and p is the connection that an edge exists between any two vertices. The expected value on the number of edges in the network is $E(v) = \binom{n}{2}p$.

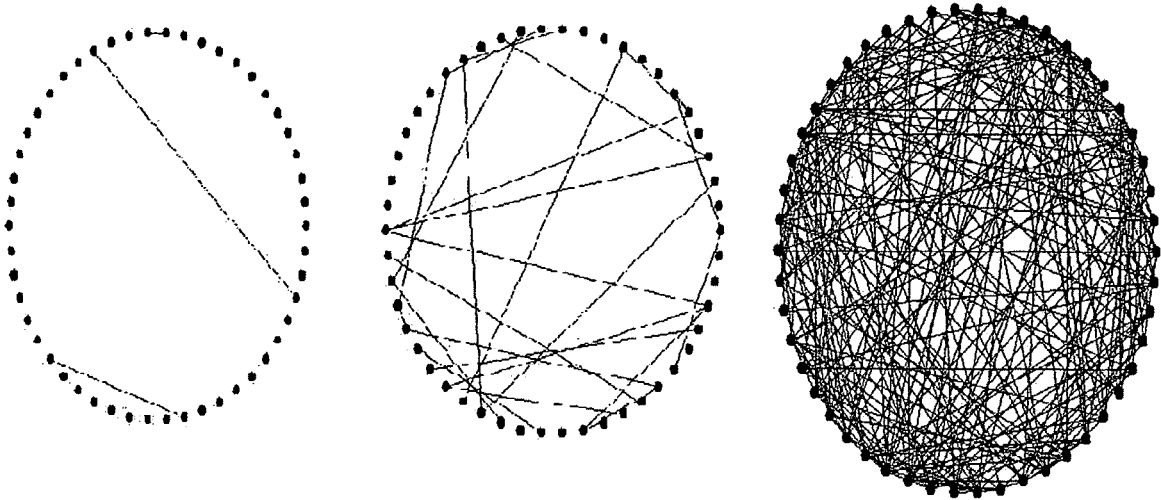


Figure 3-7: The Erdős- Renyi model generated for different probability values (0.001, 0.01, and 0.1, from left to right respectively) for a node size of 50. When the probability changes from 0.01 to 0.1, the graph is typically completely connected. When 'p' has a value $p > \ln(n)/n$, the graph is mostly connected (i.e., all edges have at least one node).

The characteristic path time of a full connected random graph is low (i.e., if this graph was a model of a real world network, we can ascertain that the number of paths for information to travel from one node to another is relatively quick in comparison to a regular graph). However, the clustering coefficient of these models are low as we assume that even neighboring nodes are connected to each other at the same probability as other member in the graph. Many real-world networks have high local clustering coefficient and this model may not be appropriate to model those networks.

Small-World Network Model:

A small-world network has high local clustering (link ring lattice graphs) and low characteristic path length (as Erdős-Renyi graph models). Most real world networks appear to have small-world connectivity and are modeled using this paradigm (Figure 3-8).

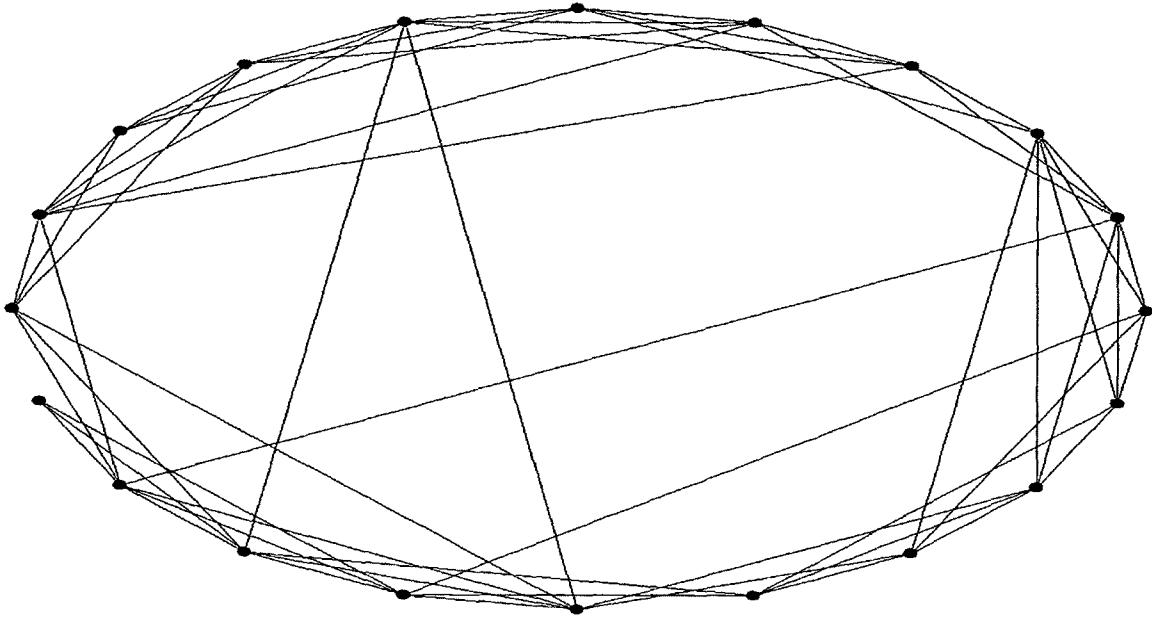


Figure 3-8: A small-world network showing high local connectivity and low characteristic path length. Most real-world examples follow this pattern of connectivity.

3.4 Measures of Synchrony

3.4.1 Correlation Coefficient:

The correlation coefficient between any two random variables X and Y is defined as the ratio of the products of their variance to the products of their standard deviations.

It is a measure of correlation between two variables.

Mathematically, it is written as

$$\rho_{x,y} = \frac{cov(X,Y)}{\sigma_X \sigma_Y} = \frac{E[(X - \mu_X)(Y - \mu_Y)]}{\sigma_X \sigma_Y},$$

where σ_X and σ_Y are the standard deviations of X and Y respectively and $cov(X,Y)$ is the covariance of X and Y . The correlation coefficient for pairs of data that are inversely correlated, uncorrelated, and positively correlated, respectively, is illustrated in Figure 3-9.

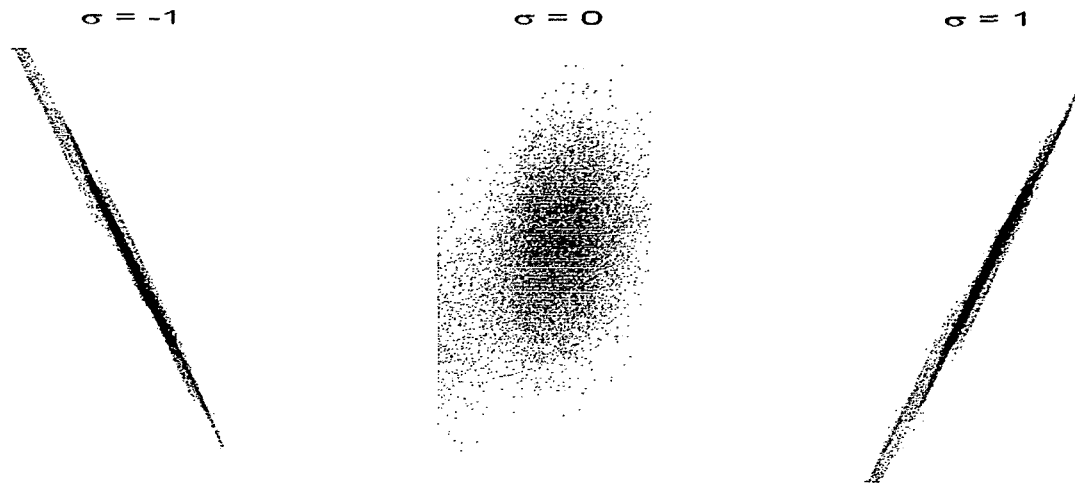


Figure 3-9: Illustration of negatively-correlated, uncorrelated, and positively-correlated data.

The value of correlation coefficient can range from -1 to $+1$. If $\rho_{x,y} = 1$, then, the two signals are identical (positively-correlated). If $\rho_{x,y} = 0$, then there is no linear correlation between the two variables. If $\rho_{x,y} = -1$, then the two signals are similar and negatively correlated.

3.4.2 Cross-Correlation:

The cross-correlation between any two signals is a measure of similarity between two signals as a function of a time lag applied to one of the two signals. Alternatively, it is a measure of how much distance (in terms of time) a signal b has to slide for it to have a maximum correlation with another signal a .

Mathematically, for any two functions, cross-correlation is defined as:

$$(f * g)(t) = \int_{-\infty}^{\infty} f^*(\tau) g(t + \tau) d\tau,$$

where, f and g are continuous functions. The right hand side of the equation is a convolution of the two signals with a time lag τ applied to one of the signals.

For discrete signals, cross-correlation can be defined as,

$$(f * g)[n] = \sum_{-\infty}^{+\infty} f[m] g[n + m].$$

This form is similar to the previous formula, but instead of a continuous time lag τ we have a discrete sample interval m . An illustration of cross-correlation function of two simultaneous signals is shown in Figure 3-10.

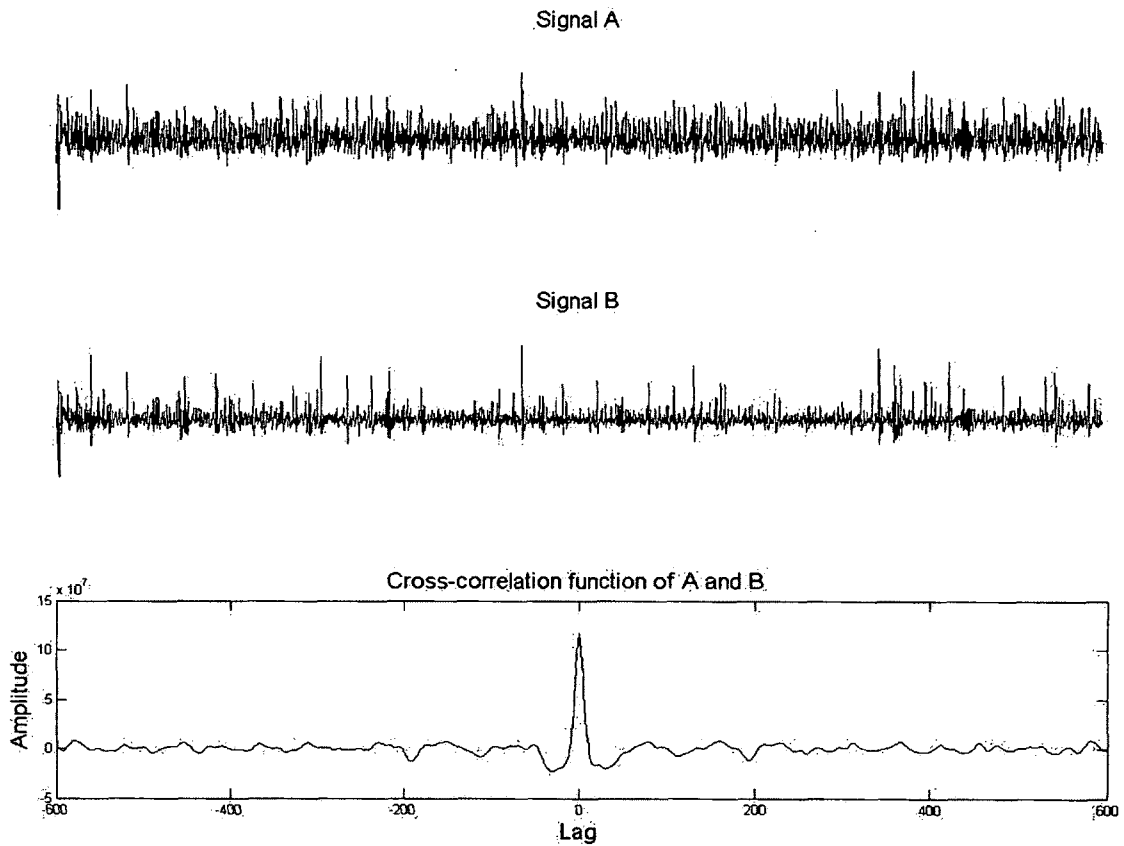


Figure 3-10: Cross-correlation relation between two signals. Cross-correlation is a function of time lag and is an indication of which signal precedes another. A zero time lag is an indication that signals are synchronous.

The cross-correlation function is obtained by sliding a signal B across A to find the lag at which there are maximally-correlated. In cell culture recordings, there is a difference between moving waves of electrical activity and oscillations. Waves of activity

(like calcium waves) originate at one part of the culture and travel through the network. Such wavelike behaviors have also been reported in large neural network simulations. When waves travel through the network, two electrodes may have similar neural activity. But if the activity is not simultaneous, the oscillations are not considered to be globally synchronous. Therefore, by calculating the cross-correlation function between electrodes showing highly-correlated activity, we can estimate the time lag between the two signals. If the lag time is less than the time taken for the signal to propagate through the network (depending upon the conduction speed of the axons/neural tissue in-between the two electrodes), then we can deduce that the simultaneous activity is not causal.

3.4.3 Coherence:

Coherence is measure of similarity between the frequency spectra of two signals. It is used to estimate the amount of overlap in the frequency domain (as opposed to the time domain). It is mathematically defined as:

$$C_{xy}(\omega) = \frac{P_{xy}(\omega)}{\sqrt{P_{xx}(\omega) P_{yy}(\omega)}},$$

where, $P_{xx}(\omega)$ and $P_{yy}(\omega)$ are the power spectrums of the two signals for different frequencies ω . $P_{xy}(\omega)$ is the cross-power spectrum for the two signals. The power spectrum or the energy spectral density is the energy of the signal as a function of its frequency. Mathematically,

$$P_{xx}(\omega) = \frac{1}{2\pi} \left| \int_{-\infty}^{\infty} f(t) e^{-i\omega t} dt \right|^2 = \frac{1}{2\pi} F(\omega) F^*(\omega),$$

and for discrete time signals,

$$P_{xx}(\omega) = \frac{dt^2}{2\pi} \left| \sum_{n=-\infty}^{\infty} f_n e^{-i\omega n} \right|^2 = \frac{dt^2}{2\pi} F_d(\omega) F^*(\omega),$$

where, $F_d(\omega)$ and $F^*(\omega)$ are the discrete Fourier transform and its complex conjugate respectively. The coherence function of two signals with arbitrary frequencies superimposed in them is shown in Figure 3-11.

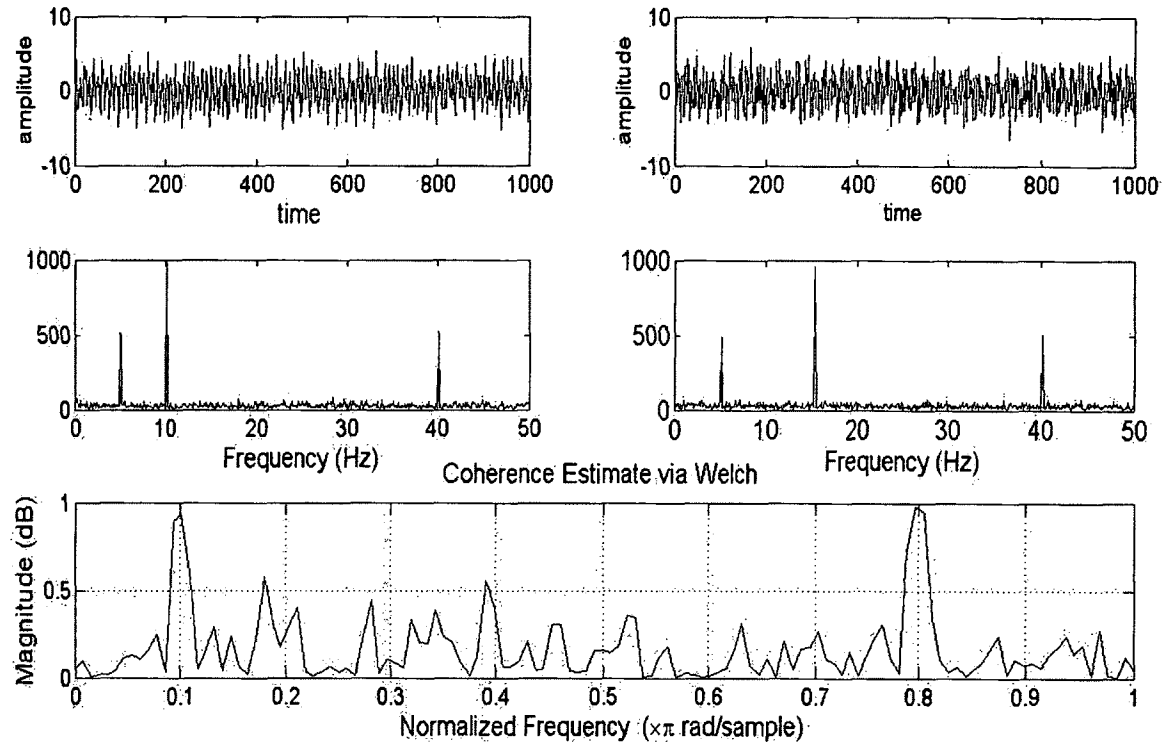


Figure 3-11: An illustration of coherence between two signals. The two random signals have a 5 Hz sinusoid, a 40 Hz sinusoid, and an arbitrary frequency imposed upon them. The coherence function exaggerates the common frequency between the two signals.

The coherence function can be used to identify correlations within specific frequency bands in the signals. The time signal contains frequencies from different bands, namely delta ($\sim 0-4$ Hz), theta ($\sim 4-8$ Hz), alpha ($\sim 8-12$ Hz), beta ($\sim 12-30$ Hz) and gamma ($\sim 25-100$ Hz). After these frequency bands have been identified, it is often of interest to identify which bands of frequencies overlap in the two signals.

CHAPTER 4

RESULTS

4.1 Introduction

The results are organized in two sections. In Section 4.2, the network properties of the neural culture are discussed. Some qualitative properties of the culture are described, and then quantitative analysis of the network is provided. An attempt is made to classify ‘neural culture networks, by comparing them with other graphical models that have been described in literature. We attempt to offer explanations for emergence of spontaneous activity and synchronicity in the network as a function of network properties.

The functional analysis of the network is discussed in Section 4.3. In the first part, basal activity of cultures is reported. The emergence of spontaneous activity and synchrony and the strength and spread of synchrony during different days *in vitro* (DIV) is presented. The role of glial cells in supporting synchronous oscillations is studied. Burst height, inter-burst interval distributions and other parameters are compared between the two networks. In the second part of this section, we study a disease model using this setup. The effect of cancer cells on the spontaneous oscillations and degree of synchrony in cocultures is evaluated quantitatively.

4.2 Network Analysis

In this subsection, we present results on the characterization of the biological neural network, the quantification of network properties, and the changes in network properties during different days *in vitro*. Neurons are allowed to self-organize into functional networks without application of any external electrical or chemical cues. Multiple images of small contiguous sections of the culture are captured. After these images are merged, the connections between different components of the network are traced and are mathematically represented as a graph. Each graph has an adjacency matrix (a matrix of zeros and ones) which contains the connectivity pattern of the sub-network. Graph algorithms are then used to extract subtle information from the matrix. The dynamics of the network as a function of time is presented. The network is then compared to various other model networks of similar size. A ring lattice model, a small-world network model (Watts-Stogatz model), and a random network (Erdős- Renyi model) are used as comparison models. The characteristic path length and the clustering coefficient of the network are computed over time, notably when the network produces spontaneous oscillations and produces global oscillations.

Immediately after the dishes are plated with the cells, they are stored in an incubator at 37 °C. They are not disturbed during the first 48 hours after plating as the mechanical stresses may cause them to detach. Neurons begin to form local networks (with other neurons in the immediate vicinity) on DIV 3. Locally, neurons are often highly connected with each other as shown in Figure 4-1.



Figure 4-1: Coculture network on DIV 4. Neurons tend to clump together to form tight local clusters.

Neurons are differentiated from glial cells by their size, shape and neurite processes that emerge from them. They also differ in their contrast, with glial cells appearing to be much darker than neurons.

4.2.1 Tendency to Clump and form Small Clusters

The recording region was imaged at different positions and the figures were merged to form a montage of the entire electrode region. In Figure 4-2 (top) the entire recording area of the MEA is shown. For the network analysis, a small electrically active sub-section of the network is selected as shown in Figure 4-2 (bottom).

During the first few days of culture, neurons begin to develop neurites that extends to neighboring cells. During this phase of development, cells (neurons and glial) are distributed more evenly through the MEA showing no preferential attachment to any other cell or area. Neurite growth increases rapidly, and the intercellular spaces are proliferated with neuritis. Up to the third day *in vitro*, there was almost no electrical activity, but once neurons began to connect with neighboring neurons, spontaneous neural activity of low

frequency was observed. During the next phase of development, neurons began to cluster (not clump) together. It appears that these neurons are clumped, but upon closer inspection, they are separated by a small distance. Initially during the clustering phase, the number of neurons in each cluster is low and the number of clusters is higher, but later, clusters tend to group together.

Neurons that are not connected usually perish by apoptosis. During development, an effective strategy is to have more neurons than needed and later prune unconnected or improperly connected neurons and thus preserving only functionally useful pathways. Neurons require signally molecules (trophic factors) from neighboring cells to stay alive. Therefore, neurons that don't connect fail to receive any trophic factors from neighboring neurons which leads to its apoptotic death. Blockage of apoptotic death at this stage can lead to severe malfunction and deformities in the organism's brain.

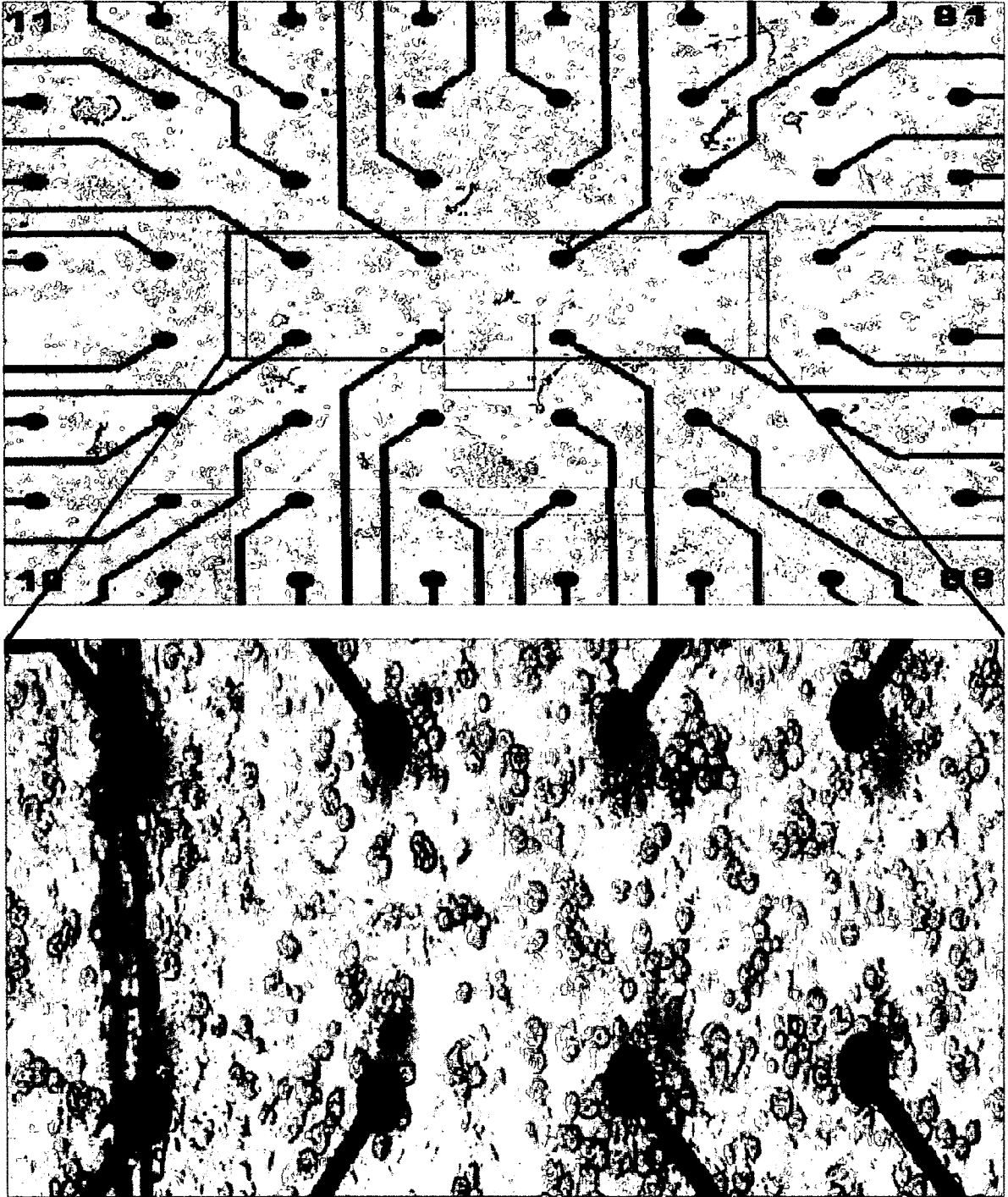


Figure 4-2: An intricate network of neurons and glial cells around the recording area of the MEA (DIV 7). The entire grid (8 X 8) is presented on the top. A small subsection of the center recording electrodes is enlarged. Neurons are identified by their neurite extensions. Glial cells lack neuritis and are relatively darker and rounder in contrast to neurons.

4.2.1.1 Node Evolution

A representation of the evolving network, based on the morphological characterization assumptions described, is presented in Figure 4-3 and Figure 4-4.

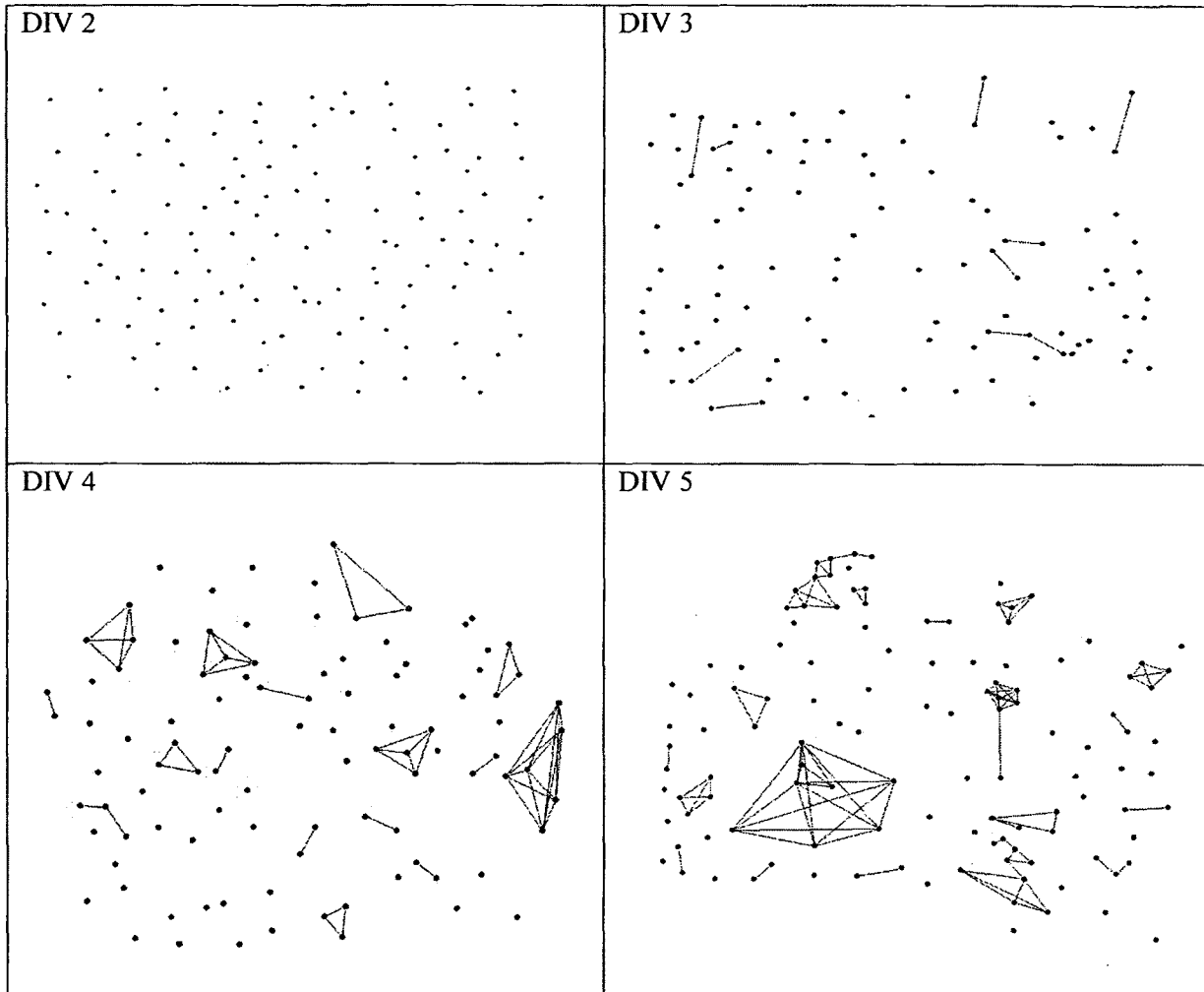


Figure 4-3: Graphical representation of connectivity evolution of an evolving network. By DIV 4, small locally-connected clusters of neurons were observed.

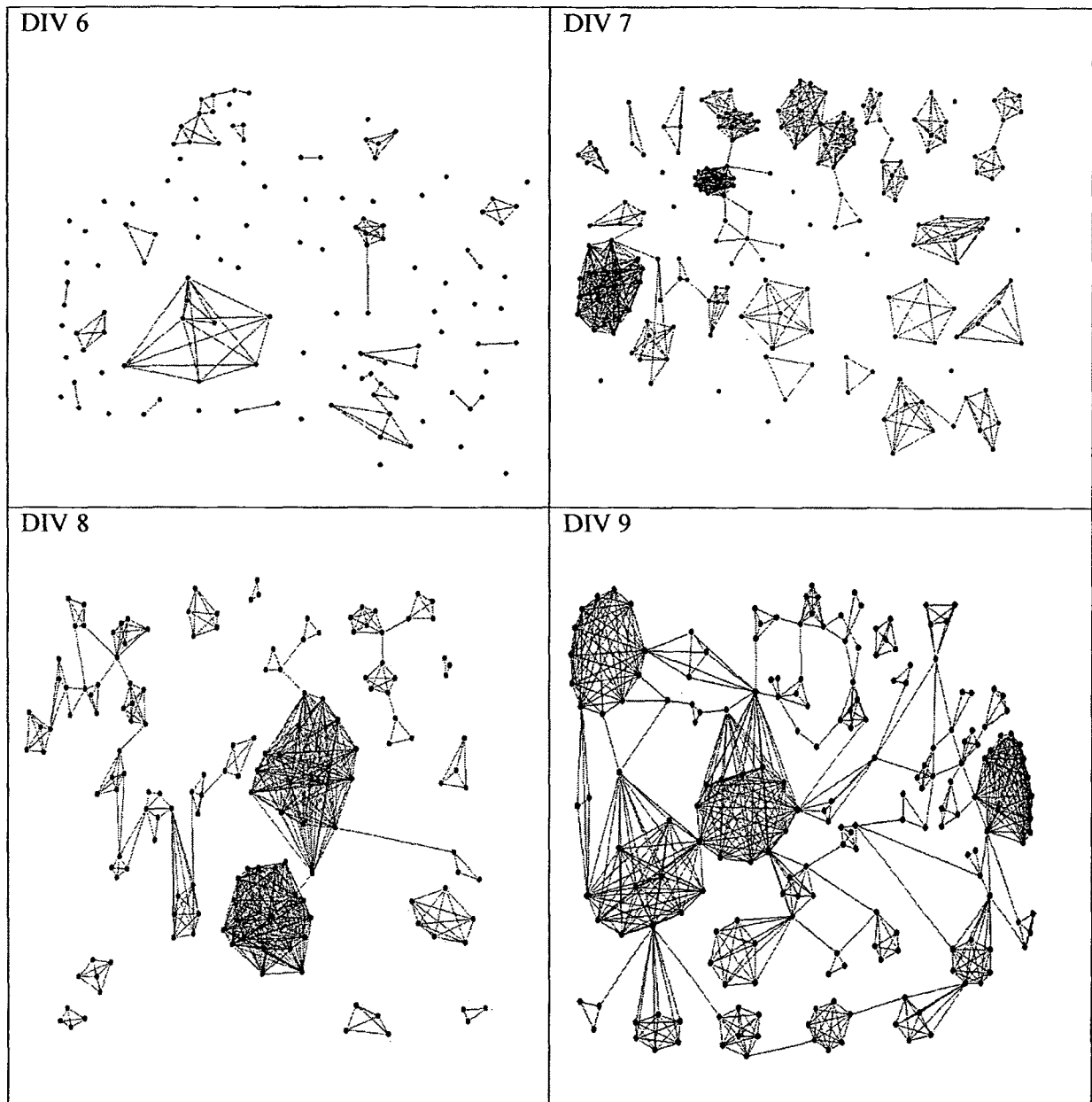


Figure 4-4: Graphical representation of culture networks from DIV 6 to DIV 9. Clusters increased in node size by absorbing unconnected neurons in the vicinity. Clusters that began to form earlier during development had the tendency to grow larger than others. By DIV 8 and DIV 9, some areas within the network are unoccupied by neurons but mostly filled with edges. Networks were drawn using the graph analysis and visualization software *Pajek* (Batagelj *et al*, 2003).

When clusters began to self-emerge in the network, empty patches were present (i.e., areas without any cells). These spaces were later found to be filled with neurites. Clusters of different sizes begin to appear during this phase of development. By DIV 7 highly connected large clusters were noticed as shown in Figure 4-5. However, these clusters are not well connected with each other during this phase. The grouping of clusters also coincided with high (but uncorrelated) activity between the different electrodes. Cluster size ranging from three to hundreds of neurons was observed. It is likely that clusters that began to form earlier were generally larger than those that formed later. The enhanced growth of earlier clusters may be caused by a preferential attachment of unconnected neurons to larger clusters than smaller ones i.e., the probability of a neuron attaching to a cluster is proportional to the size of the cluster and inversely proportional to the distance. By DIV 8 and DIV 9, clusters are almost completely formed and different functional phenomena were observed. During various stages, the morphological assumptions described earlier were used to estimate the number of neurons and neurites within the recording vicinity. These data were combined with appropriate probabilistic values and used to generate standard models of graphs (from regular to highly random graphs). The culture group was then compared with the standard models.

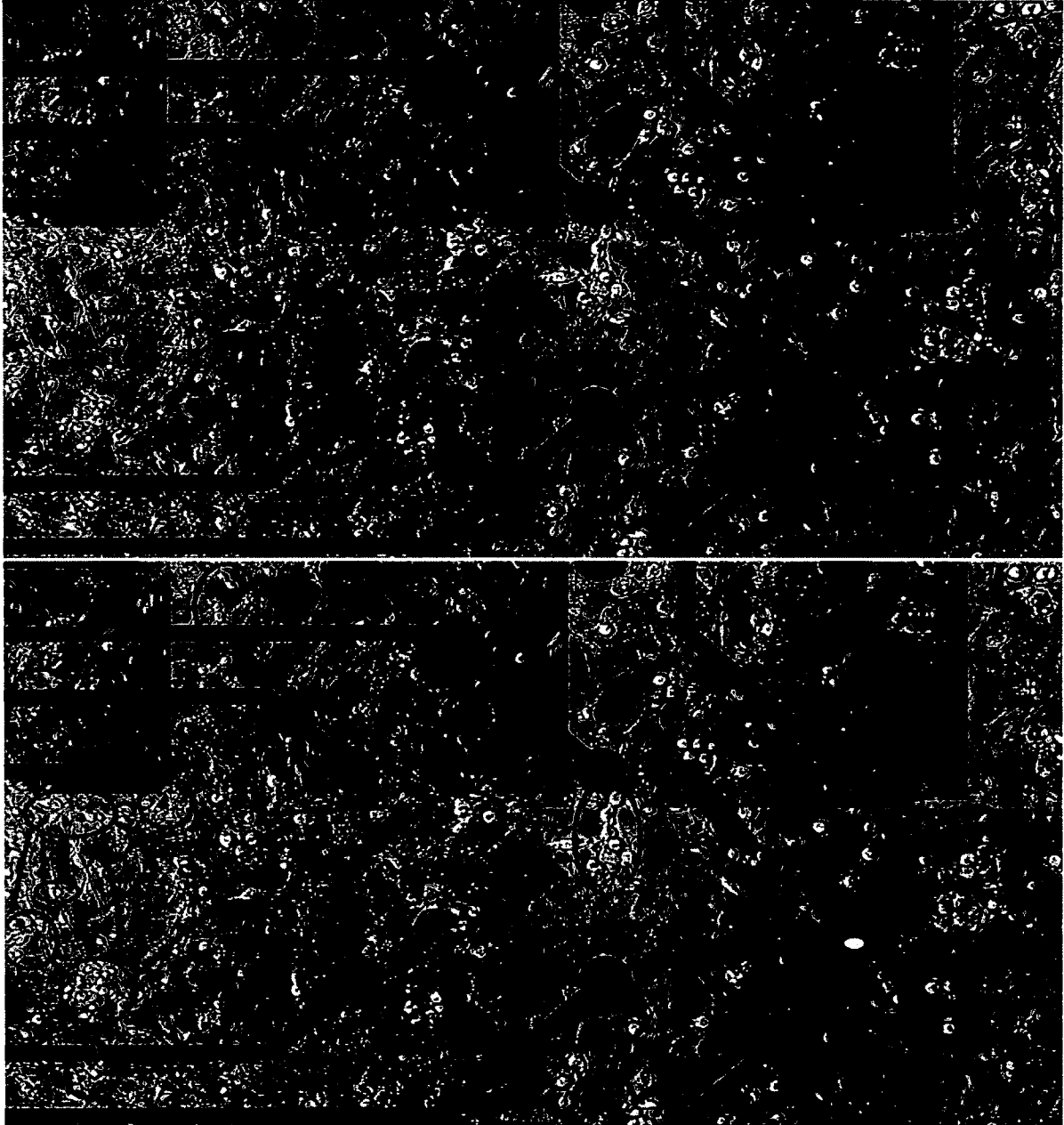
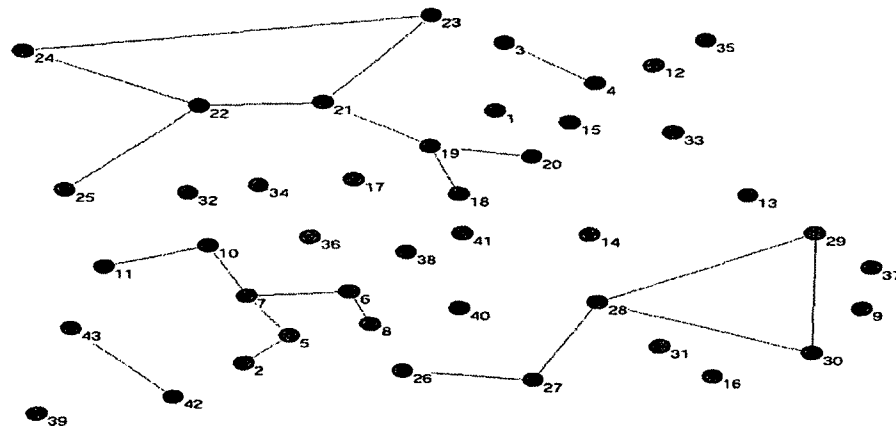


Figure 4-5: Representation of a small sub-section in the electrode grid and the tracing of clusters of neurons. Individual connections between neurons are not shown (but are assumed to have high local connectivity with each other). High inter-cluster connectivity is observed.

4.2.1.2 Cluster Connectivity

To study cluster connectivity, groups of neurons that were close to one another were considered as cluster nodes and the connections between them were mapped as shown in Figure 4-6.

DIV 8



DIV 9

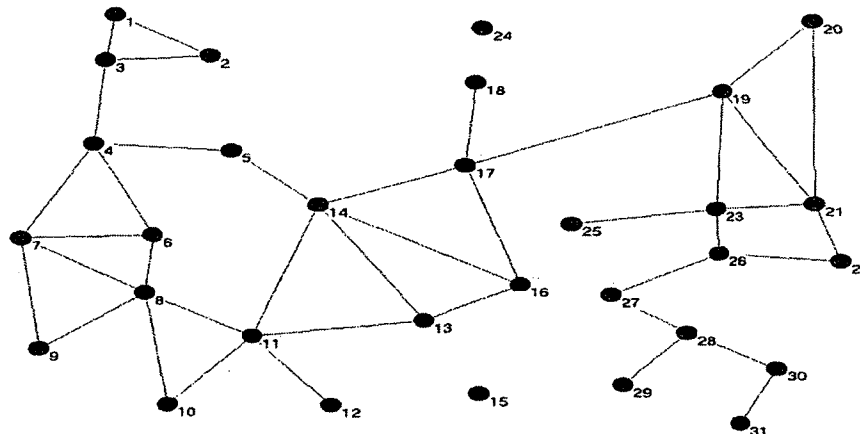


Figure 4-6: Graphical representation of a coculture network (DIV 8 and DIV 9). By DIV 8, clusters develop. The neurons in a cluster together are represented as a compressed 'node.' In DIV 8, clusters are minimally connected to form an almost connected network. During DIV 8, the connectivity between the clusters increases, reducing the network's cluster characteristic path length.

4.2.2 Small-World Analysis

The cluster abstraction was also mathematically analyzed and compared with that of standard models.

4.2.2.1 Clustering Coefficient and Characteristic Path Length

Based on experimental data, the clustering coefficients for the three standard models (Lattice, Random and Watts-Strogatz) were computed and plotted for different DIVs as shown in Figure 4-7.

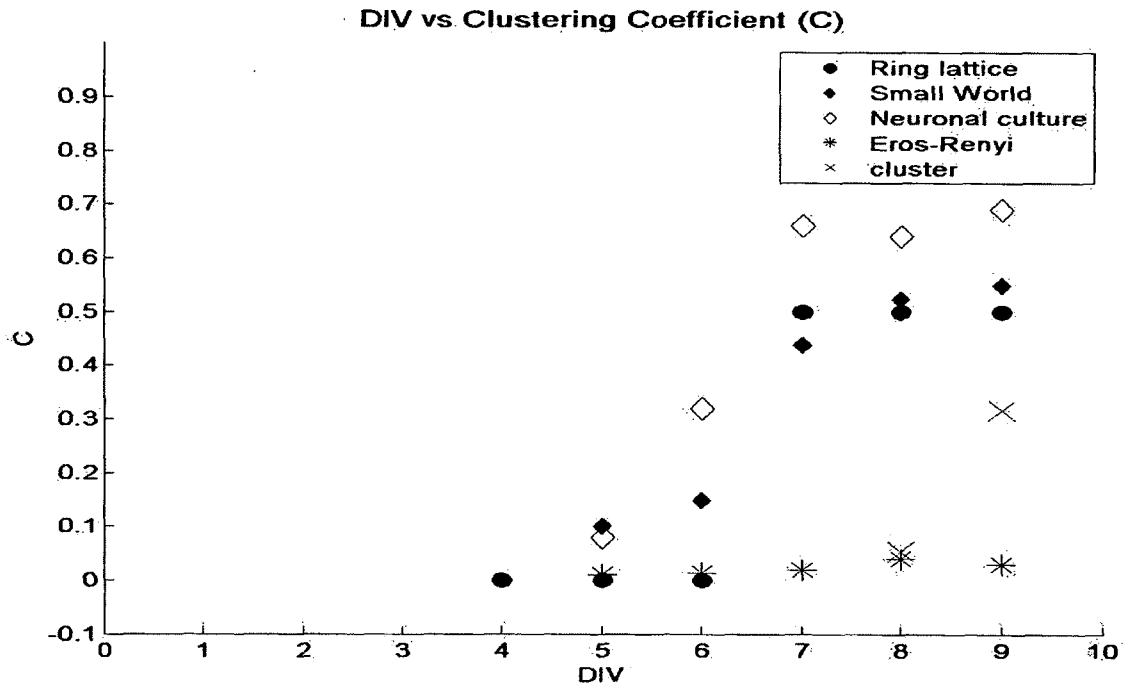


Figure 4-7: The clustering coefficient of the network is compared with different network models during different days *in vitro*. Neuronal cultures networks have a much higher local CC in comparison to other models CC of the clusters were much lower.

Clustering coefficients for the culture and the cluster nodes were plotted. Both had a high CCs that were similar to those of small world networks. The numerical values are tabulated in Table 2.

Table 2: Clustering Coefficient Values for Different Models

DIV	$G(n, e)$		Ring Lattice	Small-world	Co-culture	Erdős-Renyi	Cluster
4	100	100	0	NA	NA	NA	NA
5	230	420	0	0.1	0.08	0.01	NA
6	151	135	0	0.14	0.32	0.014	NA
7	199	723	0.5	0.4	0.66	0.02	NA
8	159	557	0.5	0.5	0.64	0.04	0.0542
9	208	672	0.5	0.54	0.69	0.03	0.3163

Based on experimental data, the characteristic path lengths for different models were computed and plotted for different DIVs (Figure 4-8).

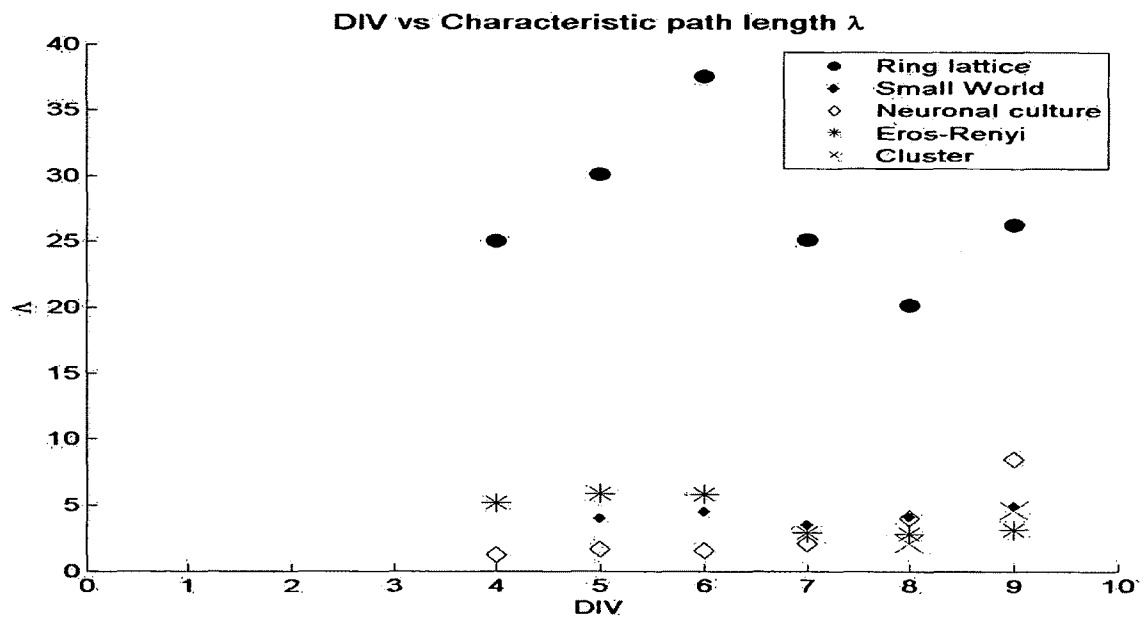


Figure 4-8: The characteristic path length of the network is compared with different network models during different days *in vitro*. Neural culture networks have a much lower value. CC of the clusters was comparable to that of random networks.

With the exception of the ring lattice model, the characteristic path lengths of all the models were closer to that of a random network. The numerical values are tabulated in Table 3.

Table 3: Characteristic Path Length Values for Different Models

DIV	$G(n, e)$		Ring Lattice	Small-world	Co-culture	Erdős-Renyi	Cluster
4	100	100	25.02	NA	NA	5.141	NA
5	230	420	30.07	4.01	NA	8.87	NA
6	151	135	37.51	4.48	1.5	5.828	NA
7	199	723	25.13	3.52	2.07	2.907	NA
8	159	557	20.13	4.13	8.511	2.801	2.1096
9	208	672	26.25	4.96	4.02	3.143	4.5

4.2.2.3 Node Connectivity:

Mature neural culture networks appear to have high clustering coefficient and low characteristic path length. These parameters suggest that information processing (i.e., the neuron-neuron interactions in the networks responsible for producing sustained synchronized oscillations in the local network) requires high local connectivity. Neural networks also many nodes with shorter lengths as shown in Figure 4-9.

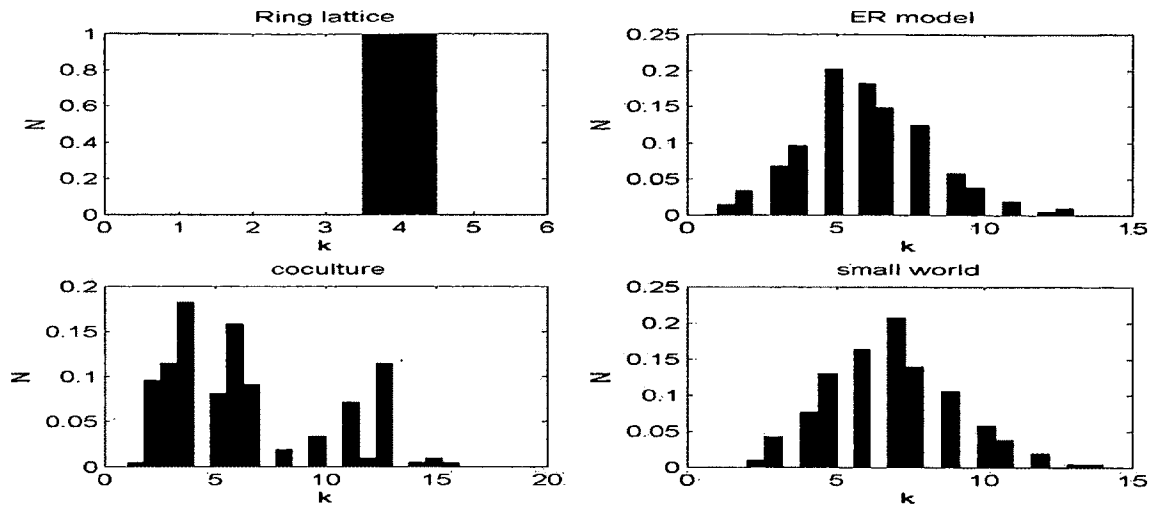


Figure 4-9: Node connectivity distributions of different networks compared with a mature neural culture.

The edge to node ratio increases around DIV 7 but begins to decrease down while the network develops. While the number of edges in the network overall decreases, the clusters also begin to become highly connected.

4.3 Functional Results (Spontaneous Activity and Spectrum)

4.3.1 Functions for Different Cell Density

Different cell densities (from 5000 neurons per dish to 500,000 neurons per dish) were plated. Our objective was to find the minimum viable density, using our culture protocol, that would (a) sustain spontaneous oscillations and synchronized behavior (b) remain healthy through the recording and imaging period, and (c) be convenient to image. Low cell densities (5,000 – 50,000 neurons per dish) did not evolve into functional networks and had a poor survivability rate. High neural densities (300,000 – 500,000) produced robust networks that exhibited strong electrical activity but led to a high density of neuritis that prevented network tracing analysis. Higher neural density networks also consume more energy, and media had to be replaced more often. Cell densities of 100

k/dish and 200 k/dish were easier to image. A density of 200 k/dish was chosen since this density was optimal for both imaging and recording purposes.

4.3.2 Emergence of Spontaneous Activity

Neural activity that arises without any external stimuli is called spontaneous activity. Spontaneous activity is observed as early as DIV 3 as shown in Figure 4-10. Initially, the spikes appear sporadic but become regular. Two types of spontaneous events were observed: spike activity (dips and rises in extracellular voltage caused by the firing of single neurons) and burst activity (activity from many neurons around the vicinity of the electrode).

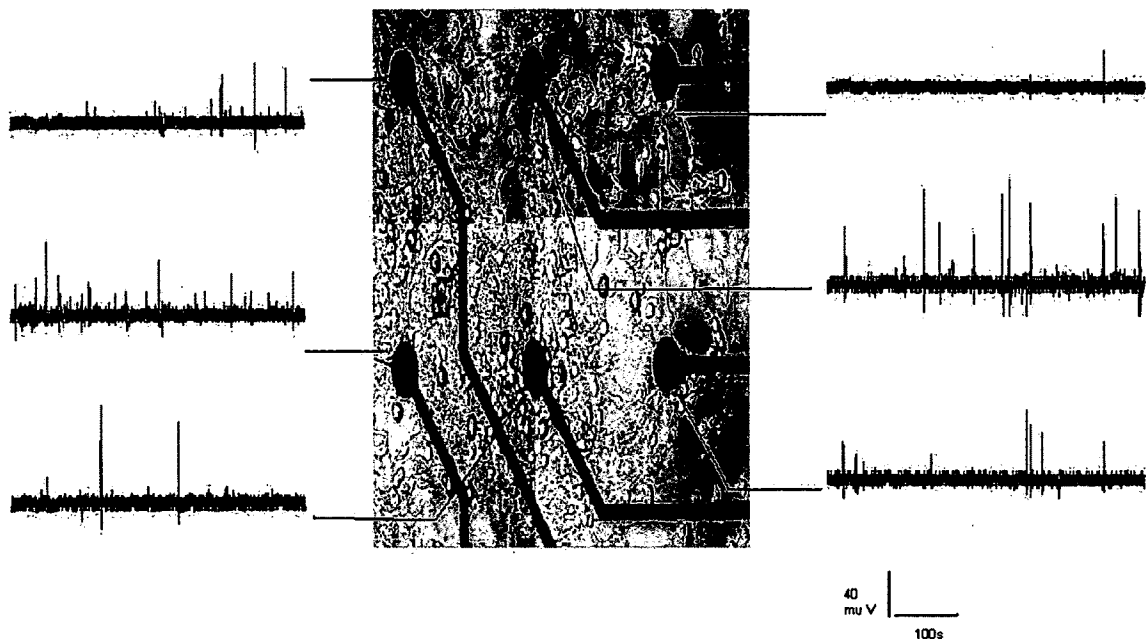


Figure 4-10: Emergence of spontaneous electrical activity after a few days of network development.

Spikes are characterized by the rise and fall times of the event, the width and amplitude. Typically, a spike represents a single action potential from a single neuron near the electrode. Since an action potential event lasts for a short time (3-5 ms), the rise and

fall time and the event width are much lower and are on the order of a few milliseconds. During the initial phase of neural development, most of the events in the network were spike events.

Burst events occur when a group of neurons near an electrode fire within a small time interval at a high frequency. It is a summation of extracellular change in voltage caused by the almost simultaneous firing of neurons. Burst events begin to occur at a later stage of network development when neurons begin to form tightly connected small clusters. Bursts typically last from a few milliseconds to seconds. They are also of higher amplitude than 'spike events' and amplitude is one of the criteria that is used to distinguish bursts from spikes. The strength of the bursts increased during the development along with intervals between bursts.

4.3.2.1 Basal Activity in Cocultures

The raster activity of spontaneous events is shown in Figure 4-11. Spikes begin to emerge about DIV 3. Thicker lines are classified as bursts. Spike activity peaks around DIV 6, but later as bursts emerge, their frequency of occurrence drops. Burst usually has fewer occurrences and the interval between bursts can be large

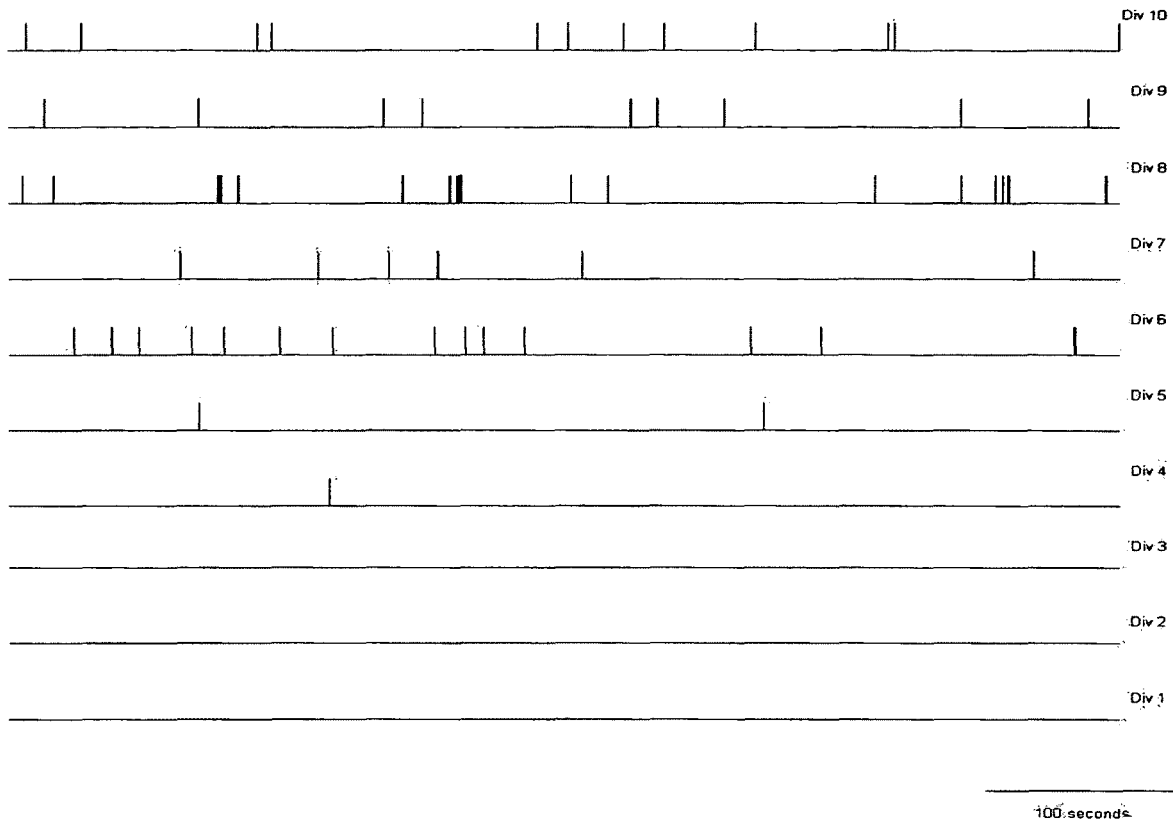


Figure 4-11: Raster activity of events at different days *in vitro*.

The event rates for both cocultures and AraC-treated plates were compared and plotted in Figure 4-12. Spike events and burst events were not discriminated and were classified together as events. Sporadic electrical activity was observed as early as DIV 4 and they gradually increased with time. Cocultures had a higher event rate compared to AraC-treated plates during the initial phases, but they were similar eventually. The reduction in spiking rate after DIV 9, as shown in Figure 4-12, is not caused by an intrinsic network property, but by deterioration of culture health and cell death.

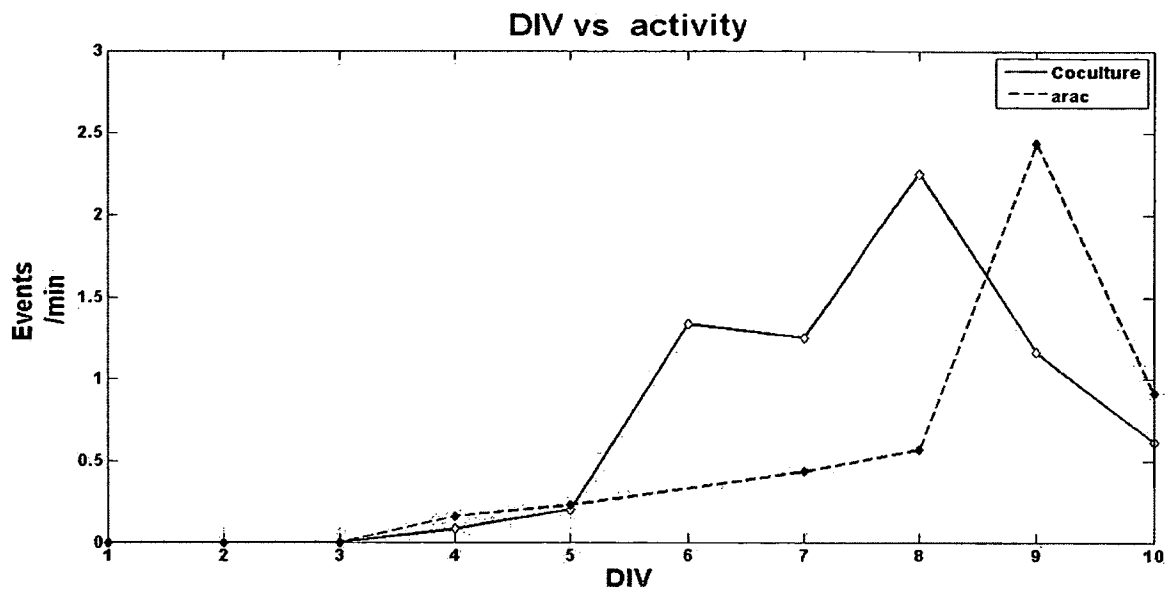


Figure 4-12: Changes in number of events for cocultures and AraC-treated plates.

Electrical recording sessions can last from thirty minutes to an hour each day. Imaging sessions of electrically active regions can take up to 15 minutes a day. Long periods of network exposure to less-than-optimal conditions deteriorate its health and results in loss of neurons and consequently a reduction in electrical activity. The risk of bacterial contamination also increases and further contributes to the deterioration of the network. Spontaneous electrical activity and network synchronization, the properties under investigation in this study, were observed by DIV 9 and the samples and data after this period were discarded and not used in our analysis.

The inter-event interval (IEI) is defined as the time elapsed between two successive events. For instance, if there are N events in a recording, there are $N - 1$ IEIs. An IEI histogram shows the distribution of IEIs. The IEI distributions for both cocultures and AraC plated dishes are shown in Figure 4-13 and Figure 4-14.

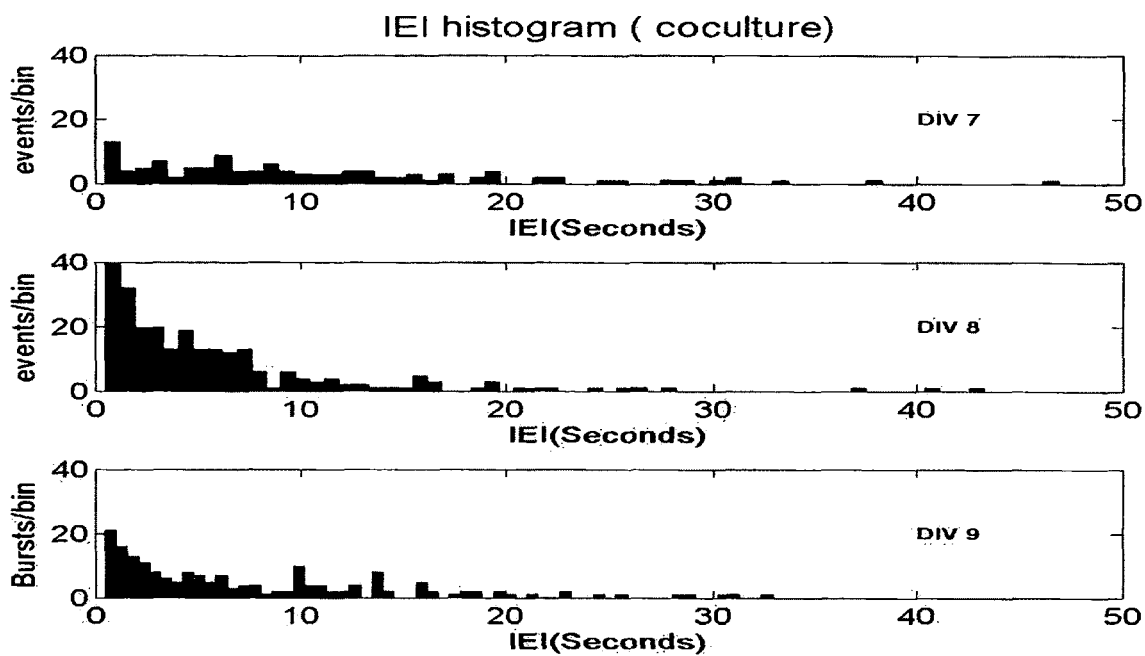


Figure 4-13: Inter-event interval (IEI) histogram during different stages for development. Event intervals are irregular during the earlier phase of development and progressively become shorter.

IEIs are distributed evenly during earlier stages of development and become shorter later. The IEI distribution of networks treated with AraC indicates that firing intervals were within a much smaller range as shown in Figure 4-14.

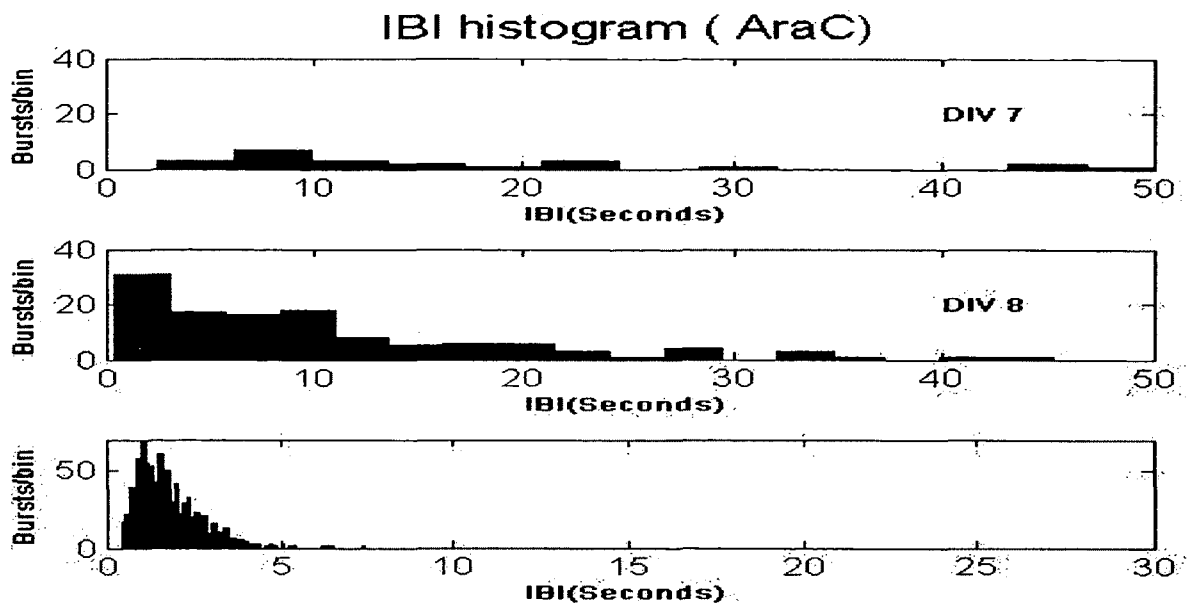


Figure 4-14: Dishes treated with AraC show similar IEI profiles to those of normal cocultures.

A first return map of IEIs for cocultures and AraC is plotted in Figure 4-15. Pairs of consecutive IEIs are plotted on this map. If the points in the map are more spread, then the network is more chaotic.

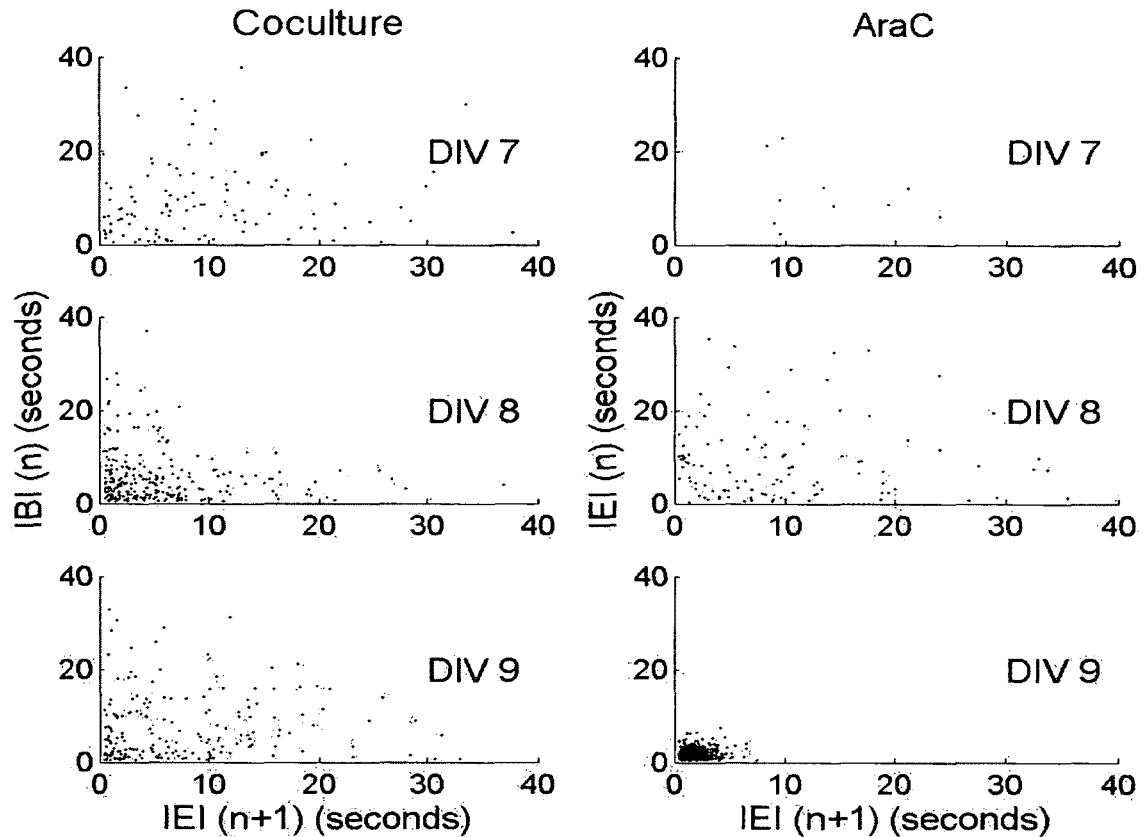


Figure 4-15: The first return map of IEI intervals of coculture and AraC plated dishes during different days *in vitro*. AraC-plated cultures tend to become more periodic (marked by a cluster of points, DIV 9) compared to cocultures.

The first return map of AraC shown in Figure 4-16 (DIV 9) shows that networks without glial cells tend to show a more tonic bursting profile compared to regular cocultures.

4.3.2.2 Basal Activity in Cancer Dishes.

Regular cocultures were treated with cancerous cells (CRL-2303) around day 4 *in vitro*. Cancer cells rapidly multiplied and spread out through the dish. The electrical activity profile of cancer induced dishes was quite different from that of normal cocultures. Firstly, the number of events was consistently lower compared to cocultures as shown in Figure 4-16.

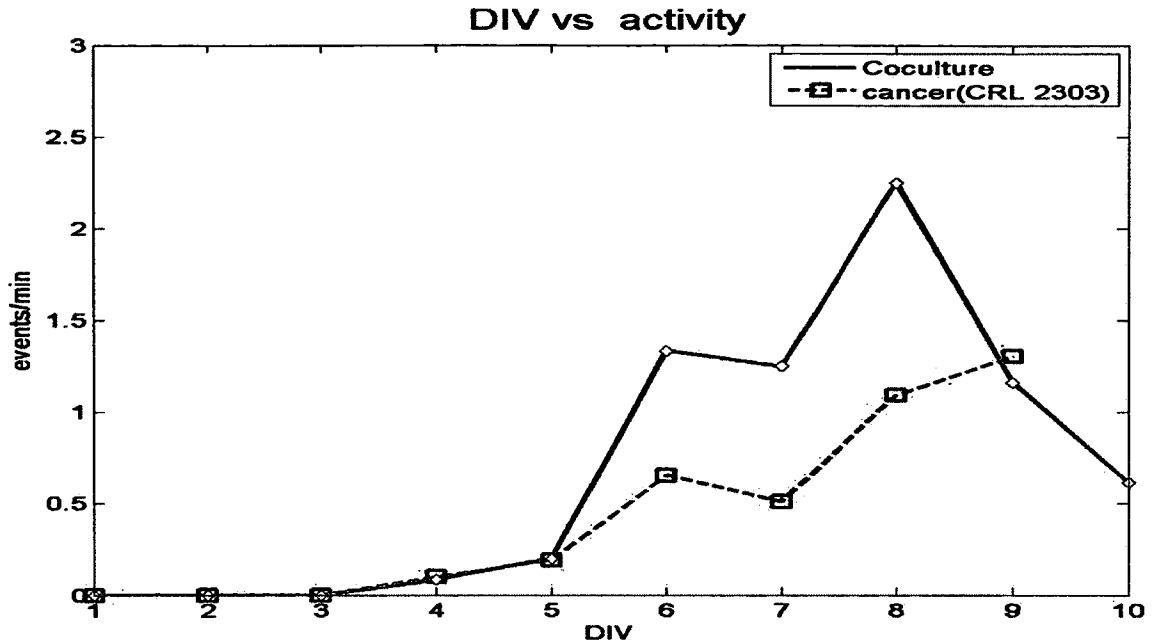


Figure 4-16: Basal event rate evolution for cocultures and CRL-2303 treated plates. Plates treated with CRL-2303 cells showed lower event rates than regular cocultures.

Secondly, the magnitude of the burst and the duration of the burst events were much longer compare to basal activity in cocultures. Bursts with these attributes are considered to be seizure-like events (SLEs). The amplitude of SLEs was up to 10 times higher for a given day *in vitro*, as shown in Figure 4-17. The SLE event lasted from a few seconds to up to a few minutes. The frequency spectrum analysis, synchronization and coherence analysis of SLE type events are presented in the following sections.

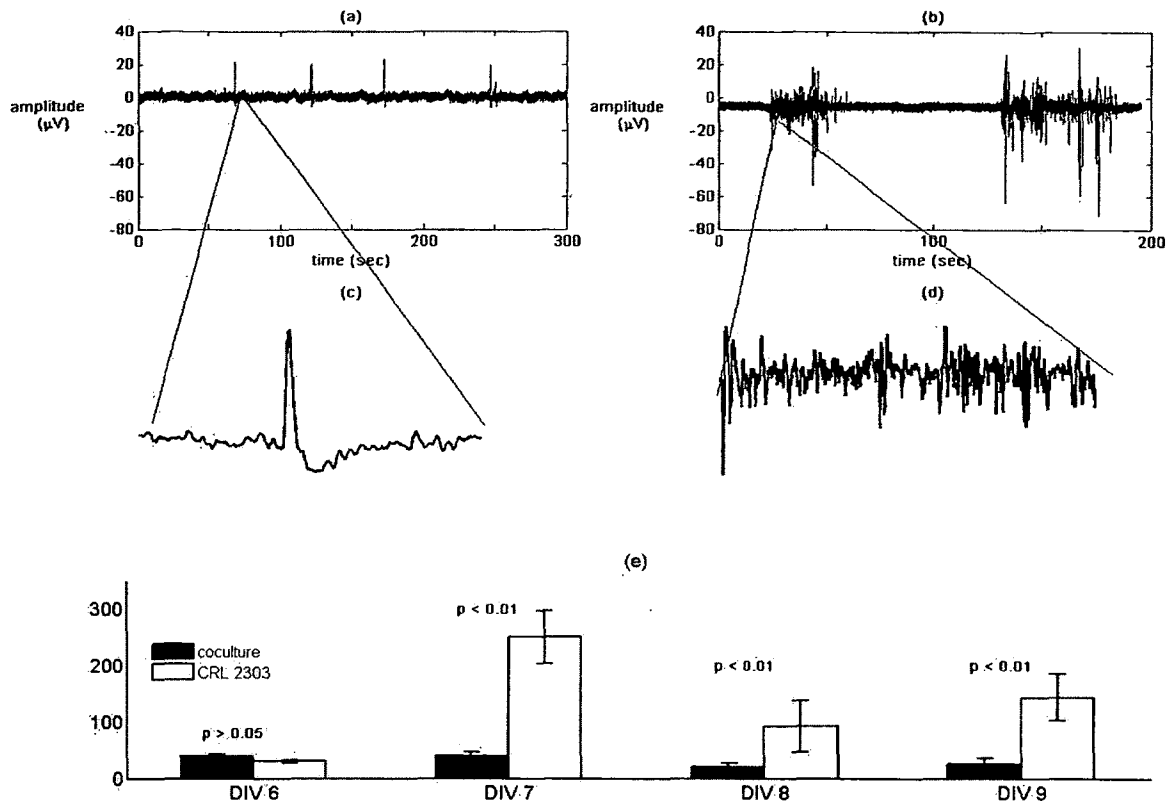


Figure 4-17: (a) A series of spikes in cocultures. (b) Cancer affected cells showed large burst events followed by long quiet periods (c) Magnified 'spike' event (d) a small section of the cancer SLE (e) CR-2303 plated networks exhibited significant higher basal burst amplitude ($p < 0.01$ for DIV 7, DIV 8 and DIV 9) compared to cocultures.

4.3.2.3 Effect of Glutamate on Basal Activity

Since cancer cells showed SLE events, it was required to check whether other typical hyper-excitable events had a similar bursting profile. For this, 500 nm of glutamate was added to regular cocultures. The basal activity (plotted blue) and the glutamate response (plotted black) is shown in Figure 4-18.

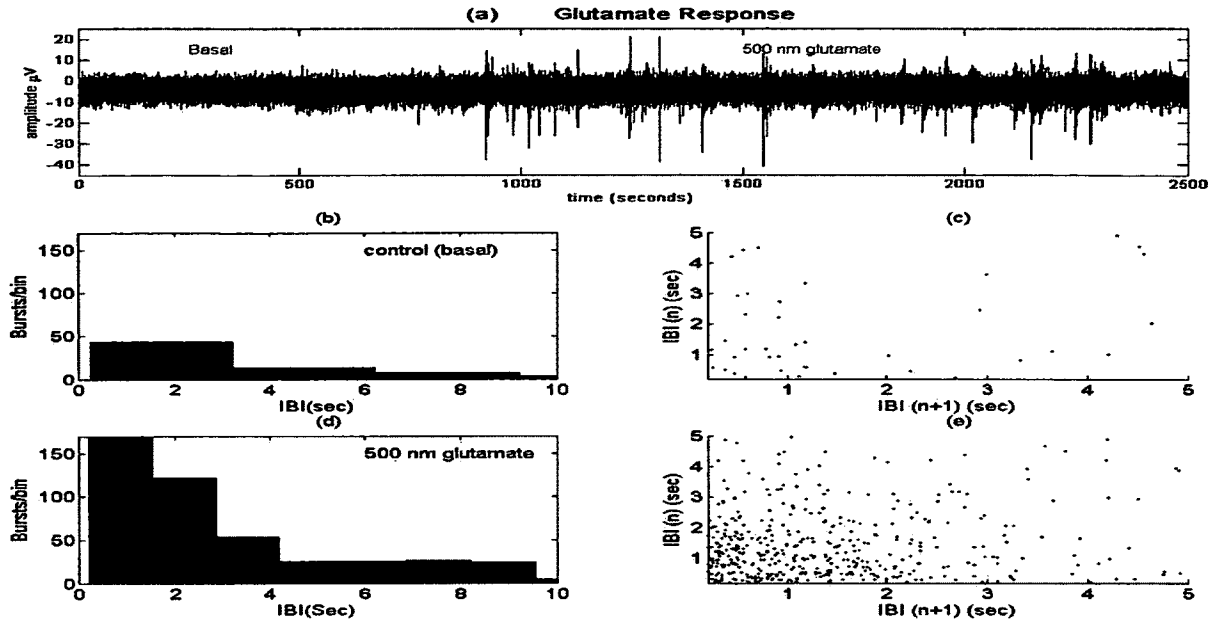


Figure 4-18: Effect of glutamate on coculture network activity. Glutamate enhances spiking activity, but the IBI profile is identical to regular cocultures.

The hyper-excitatory profile of glutamate response was characterized by increase in number of events/min with high IBI intervals and smaller burst amplitudes, quite unlike the response of CRL-2303 tumor infected activity.

4.4 Frequency Spectrum and Synchrony Analysis

In this section, frequency spectrum and synchrony analysis is presented. The previous sections provide a quantitative analysis of the events based on their size, shape and event durations. In this section, we focus on identifying the evolution of network property in terms of its frequency bands and the ability of different regions of the network to have correlated activity. The parameters for three different network types (cocultures, AraC and CRL-2303 cells are compared and contrasted).

4.4.1 Power Spectrum Analysis

After the data were filtered and down-sampled, the power spectral density (PSD) of the recording was evaluated using Welch's method. For each DIV, signals were recorded from up to fifteen channels at a time. The electrodes to record from were randomly chosen, and depending upon the activity level, the channels were re-arranged to connect with electrodes that had more activity. From the recorded channels, the channel with most activity (determined by the overall number of events) was chosen. Time periods within which the electrical activity was more pronounced were used for our analysis. During the initial stages of culture evolution, network activity was sparse. Around DIV 5 to DIV 6, a low delta level band of activity emerged as shown in Figure 4-19.

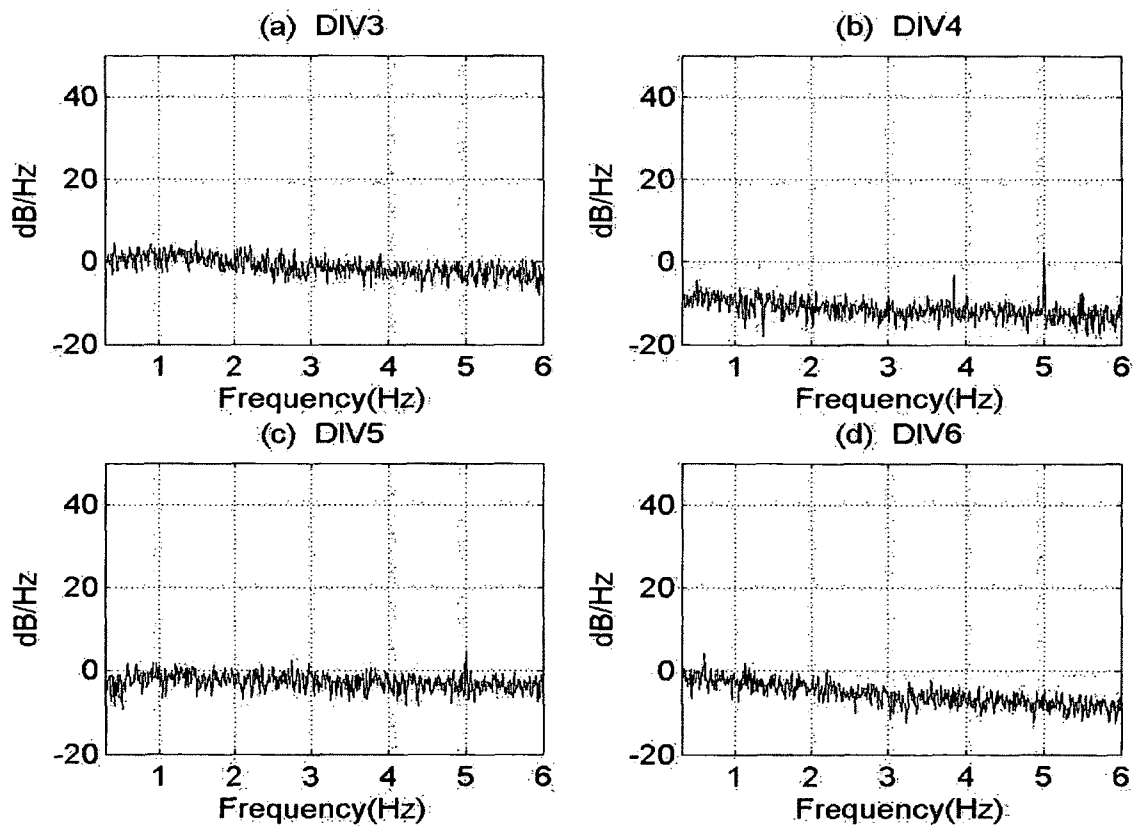


Figure 4-19: PSD of basal activity during initial stages of development.

The strength of the alpha frequency band increased as the culture matured and reached a maximum value at around DIV 8 and DIV 9 as shown in Figure 4-20. The AraC-treated network showed similar frequency profile to that of cocultures as shown in Figure 4-21. The frequency spectrum of a glutamate-treated sample is shown in Figure 4-22.

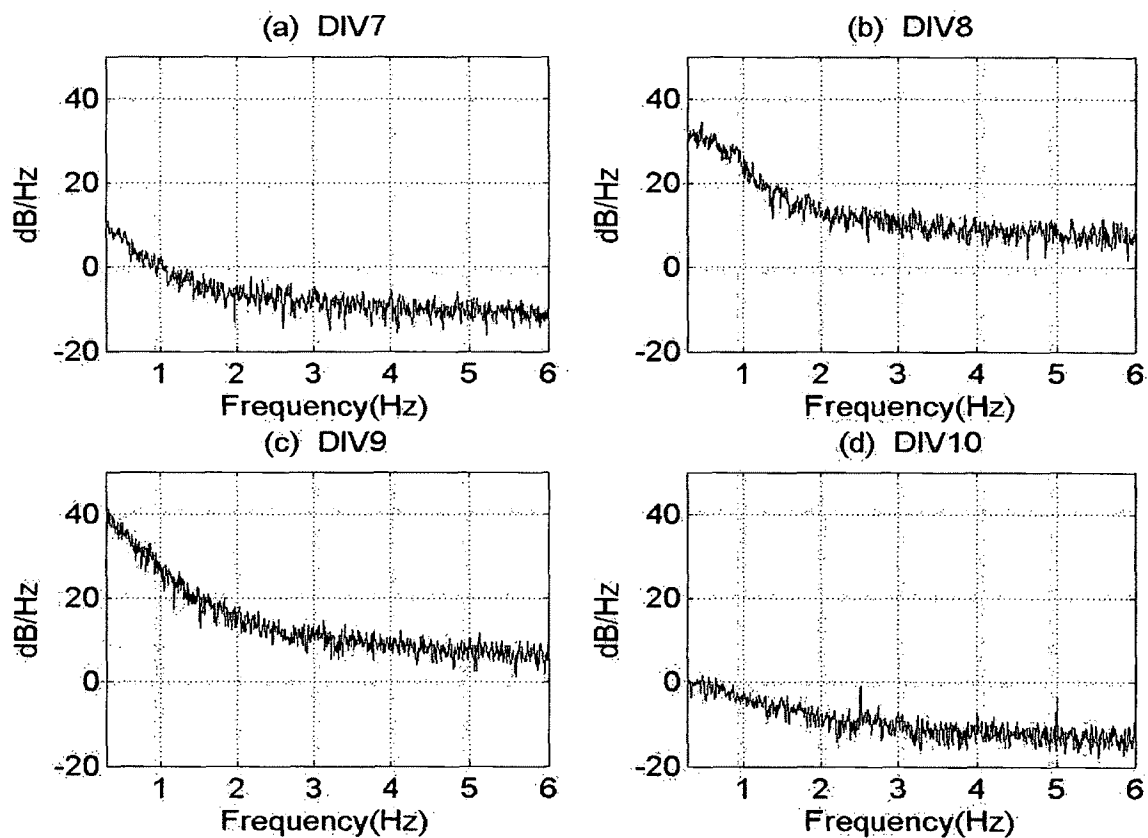


Figure 4-20: Emergence of activity in the delta band (DIV 8 and DIV 9).

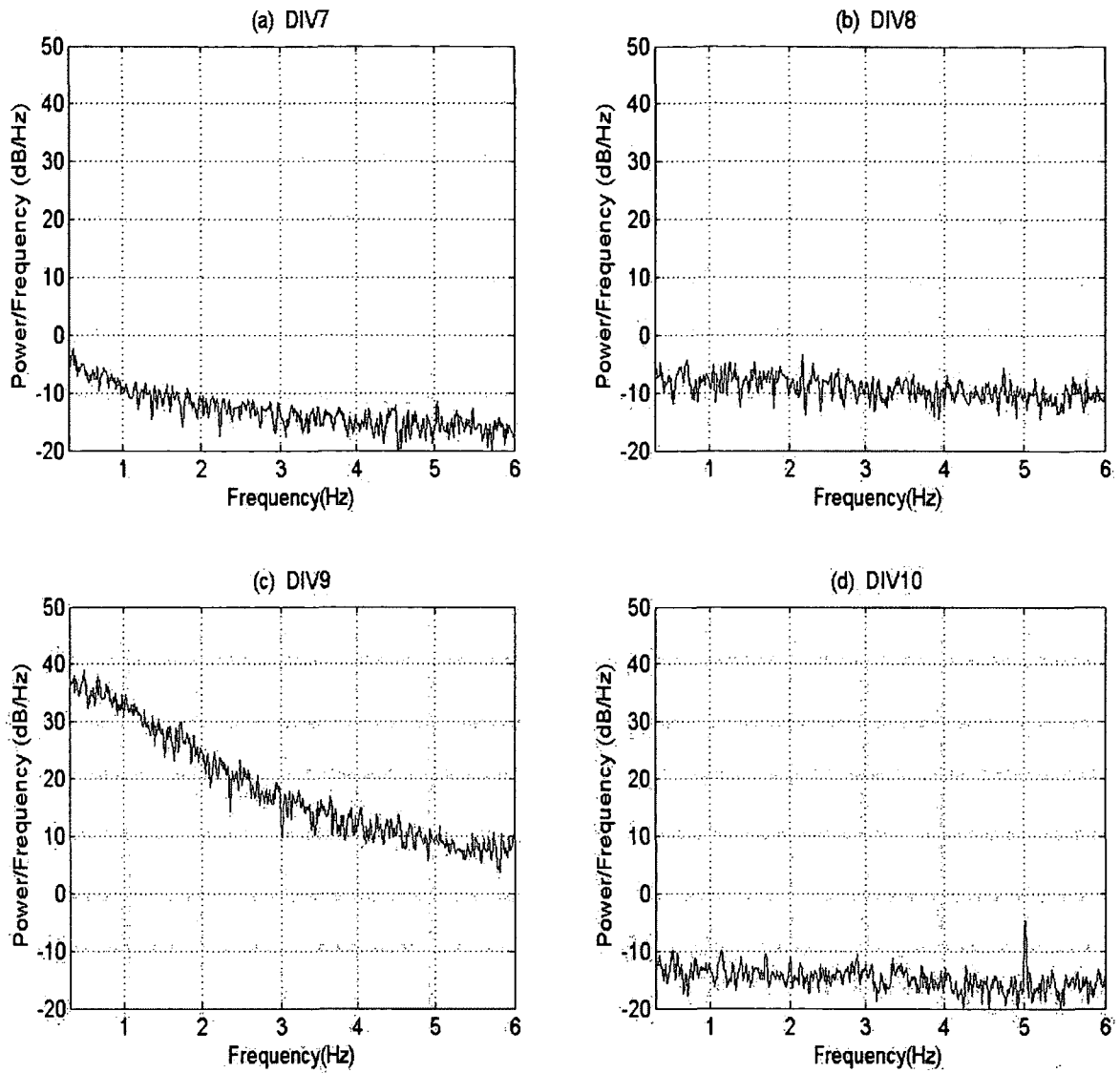


Figure 4-21: Emergence of activity for AraC-treated networks.

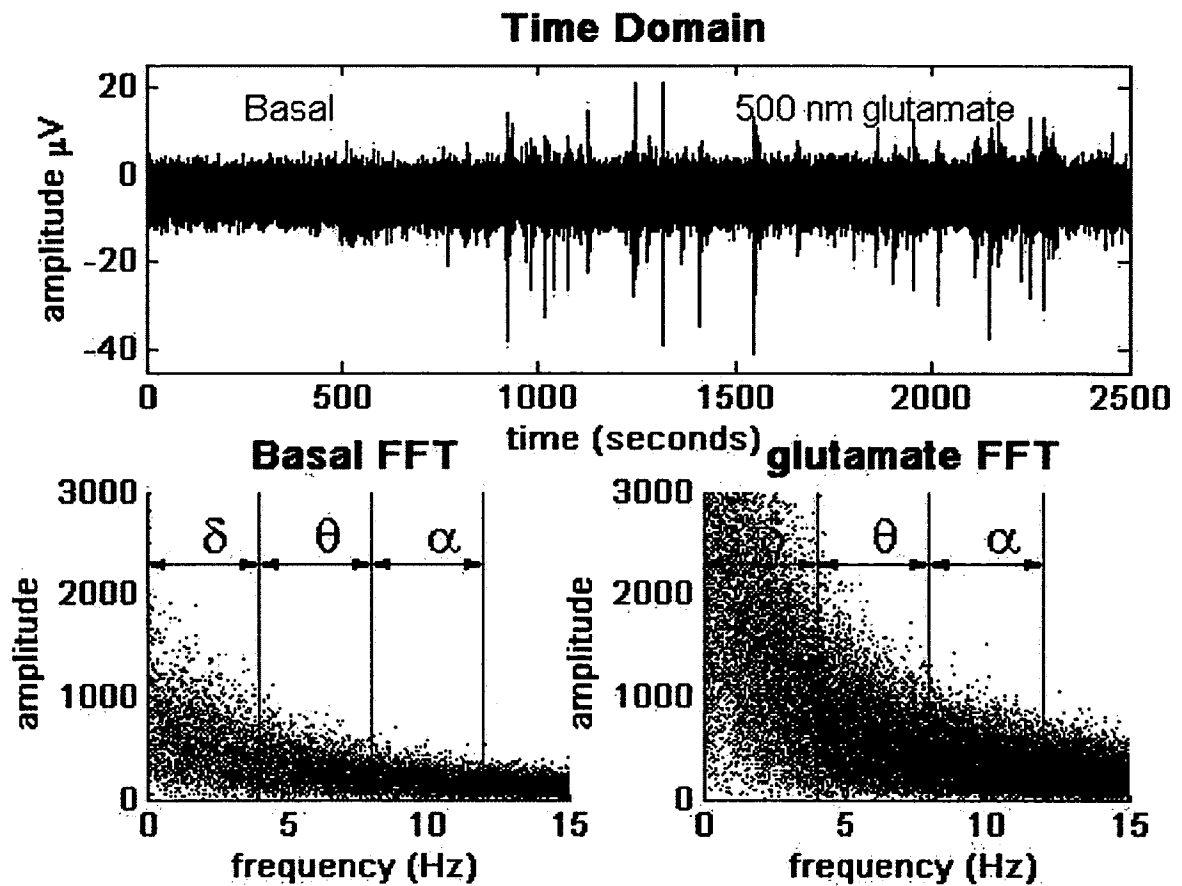


Figure 4-22: Application of glutamate results in an increase in the δ , θ , and α frequency bands. This was evaluated to compare with hyper-excitatory behavior in cancer cultures.

The application of glutamate increased frequency power in the delta, theta and alpha bands. The power spectrum profile is different compared to cancer-treated network as shown in Figure 4-23 and Figure 4-24.

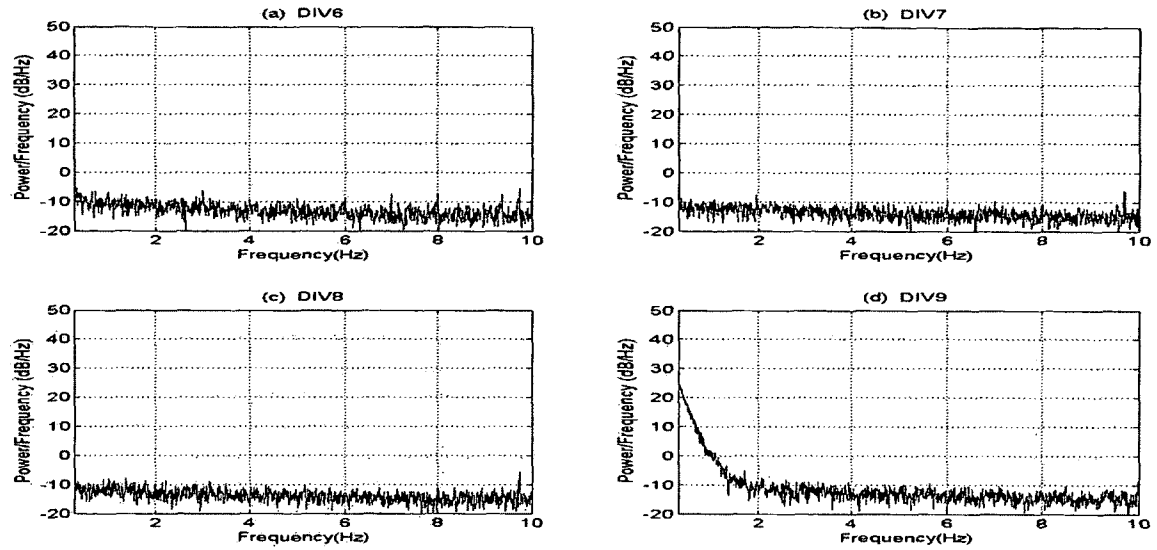


Figure 4-23: Frequency spectrum of CRL-2303-treated networks.

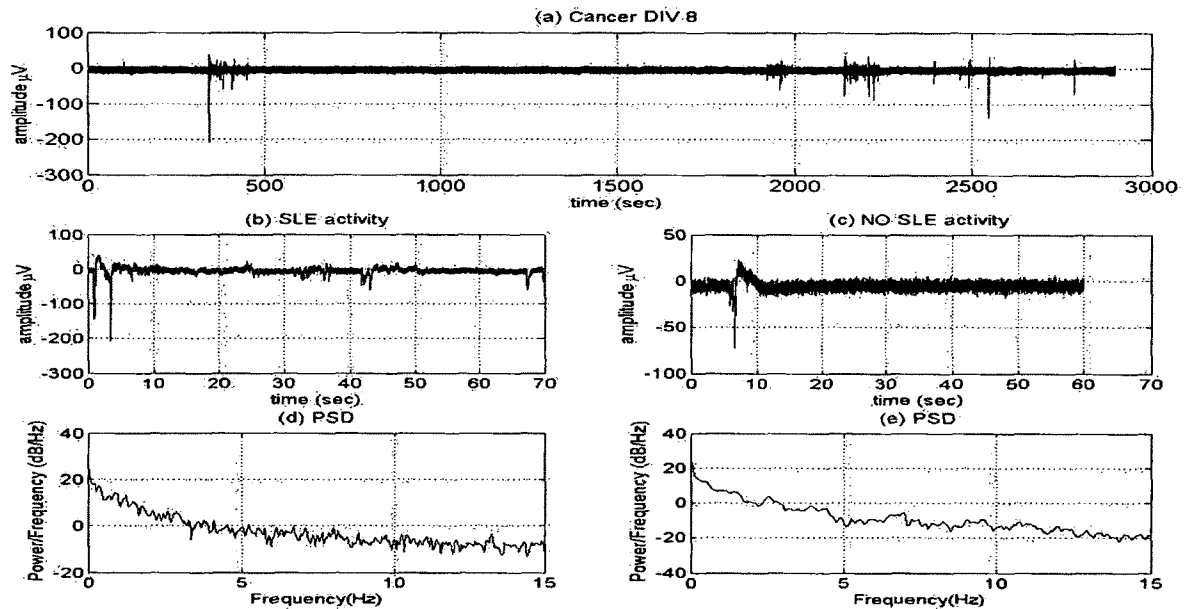


Figure 4-24: The frequency spectrum of both SLE-type events and regular events in cancer networks is shown.

4.4.2 Correlated Activity Analysis

Correlated activity for every electrode pair was calculated and shown in the map. During the earlier phase of development (up to DIV 7), CC was low, with a mild increase with time as shown in Figure 4-25. During the subsequent days (DIV 8 and DIV 9), synchronized activity among the same pairs of electrodes increased almost three times as shown in Figure 4-26.

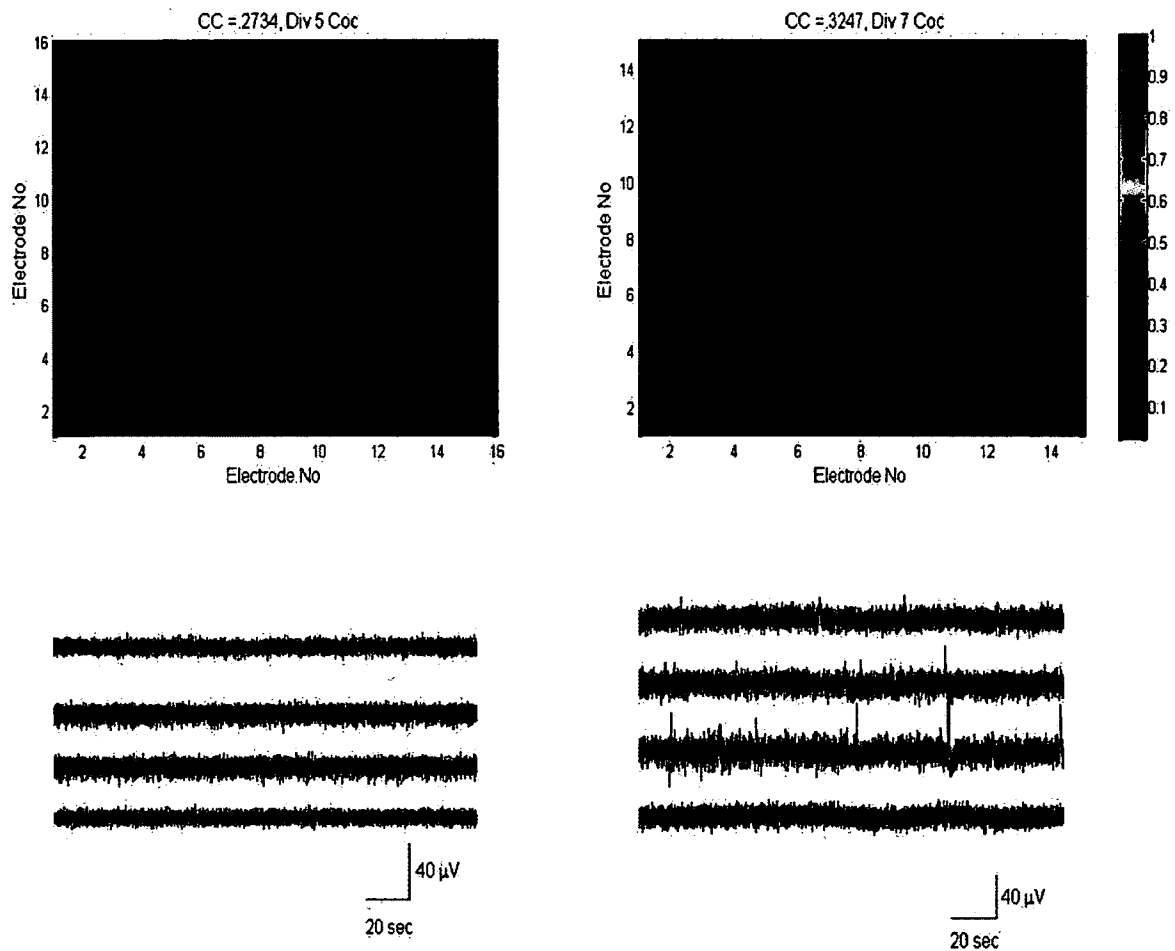


Figure 4-25: Emergence of correlated activity in electrode regions.

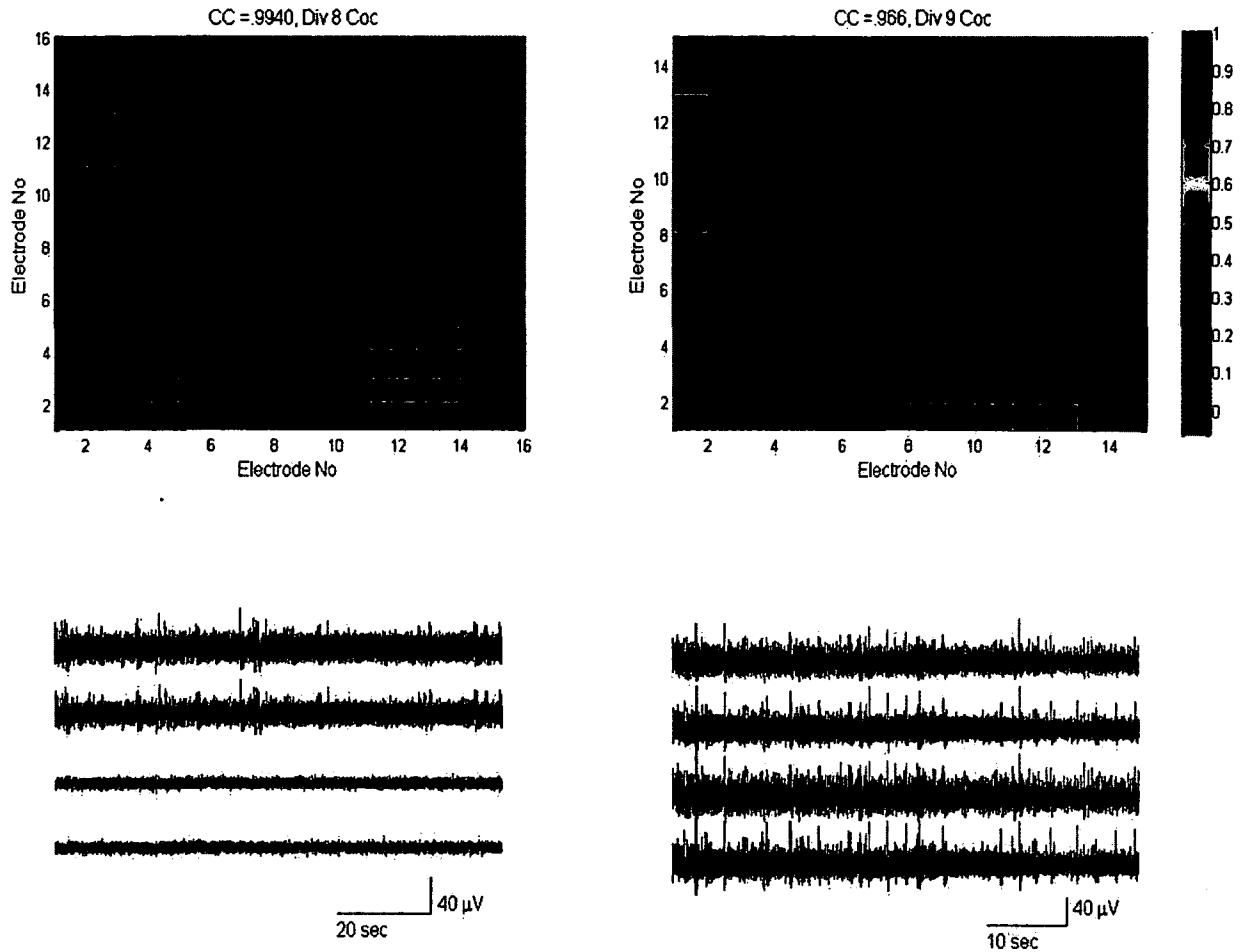


Figure 4-26: Synchronization map (DIV 8 and DIV 9)

Many global bursts were recorded (i.e., bursts that were observed in multiple electrodes). The increase in correlated activity between electrodes also coincided with the increase in the number of clusters and cluster connectivity. While many instances of global bursts occurred, strong local correlation was more prevalent. Electrical activity from four local electrodes (close to each other) is shown in Figure 4-27.

Cultures were treated with 10^{-5} M AraC around DIV 4. After AraC treatment, glial cell proliferation was limited and the culture consisted mostly of neurons. While cultures treated with ARaC showed similar bursting profile in terms of the number of

events and frequency spectrum, their degree of synchrony was only half as large as that obtained from cocultures networks.

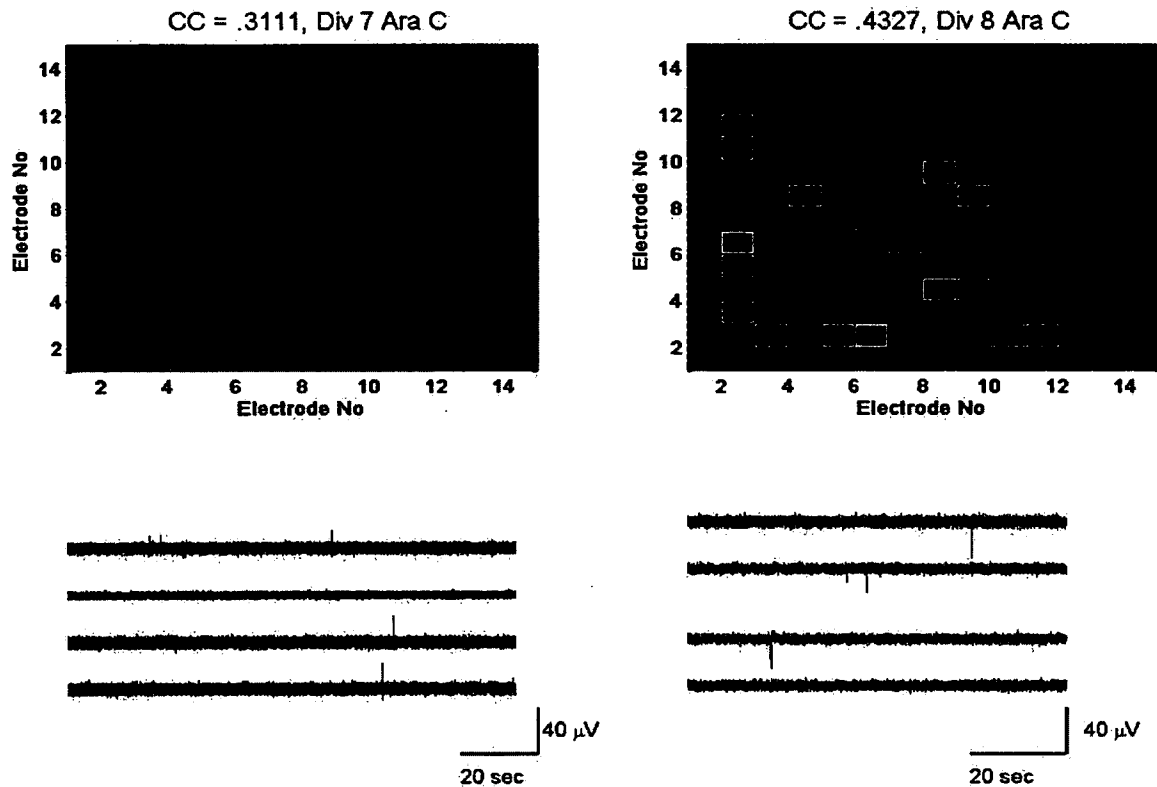


Figure 4-27: Correlation activity in cultures treated with AraC.

In another set of experiments, cocultures were infected with tumor cells and the basal activity profile are various DIV were recorded. The CRL-2303 glial cells are aggressive glioma cells and they began to rapidly proliferate through the network. In contrast to regular cocultures, tumor cultures exhibited brief synchronized hyperexcitatory events followed by longer quiescent periods as shown in Figure 4-28.

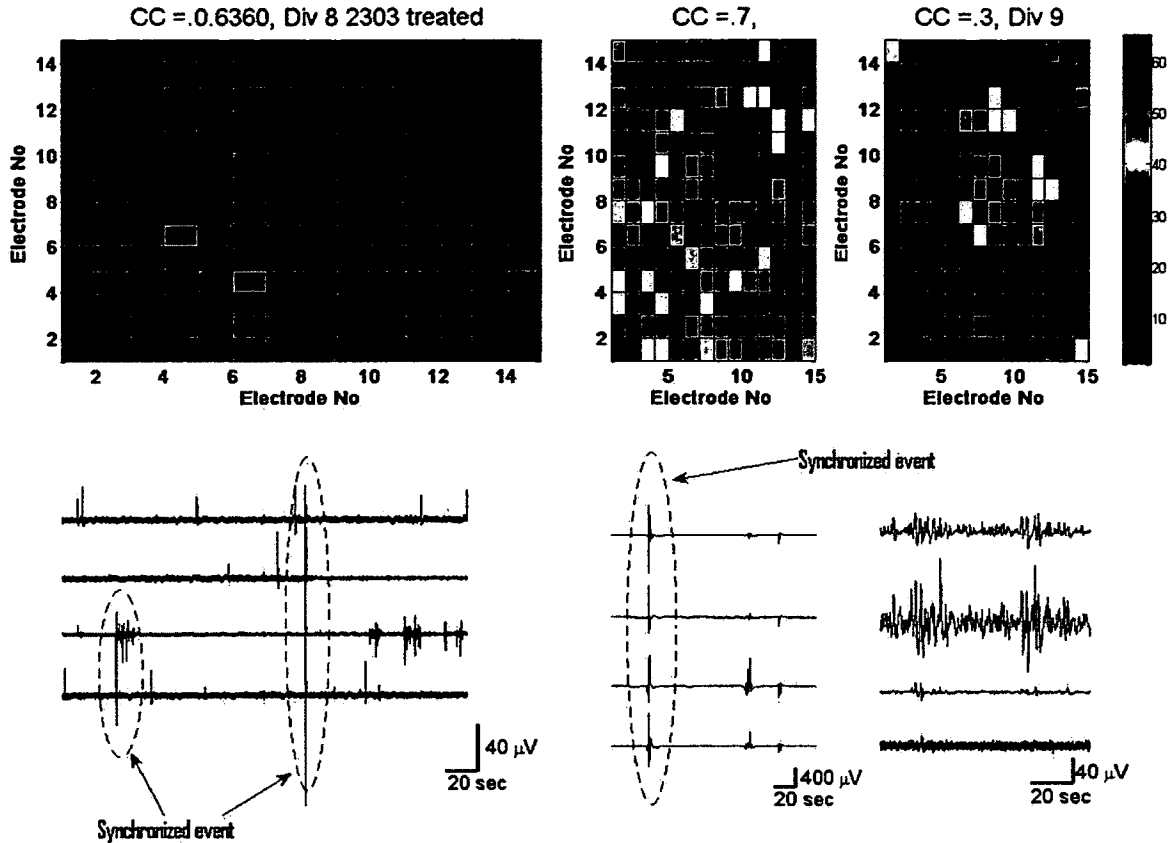


Figure 4-28: Correlated activity profile for different types of bursts in CRL-2303 plated dishes.

The electrode pair correlation coefficient map for DIV 8 is shown in Figure 4-28 (left). During the next phase of development (DIV 9), correlated activity among the same pairs of electrodes increased almost 3-times. Two different activity profiles emerged at this phase. First, the regular spiking/bursting profile occurred that was similar to that observed in cocultures and AraC-treated cultures, and a slow frequency wave-like activity, lasting for up to 50 seconds, was observed as shown in Figure 4-28 (right). The bursting activity had a higher CC than the slow wave-like activity.

The dynamics of the correlated activity for networks treated with tumor cells were compared with regular networks. The recording period was divided in smaller non-

overlapping time bins of one second and the CCs were calculated for electrodes that had maximal activity as shown in Figure 4-29.

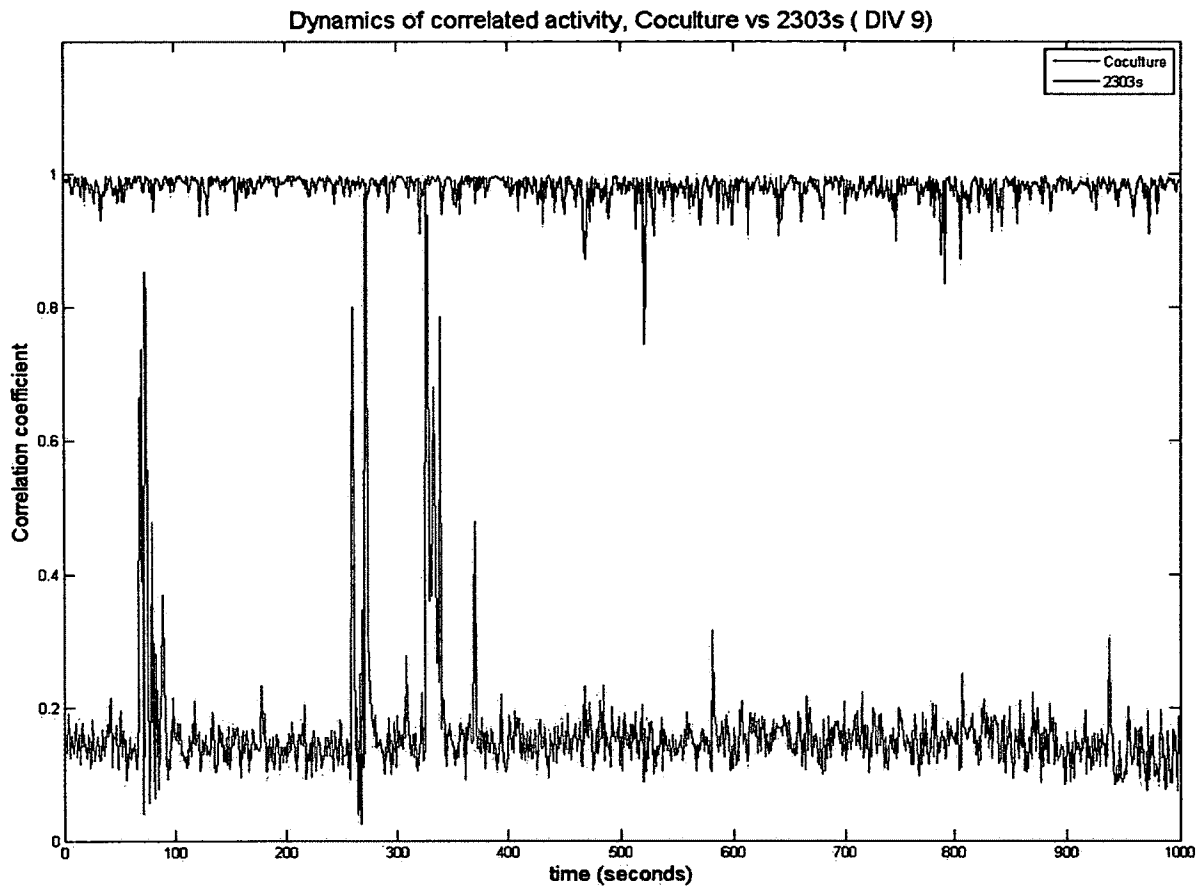


Figure 4-29: Correlation coefficient calculated for all active electrodes for same DIV in CRL-2303- plated and regular cocultures. Cocultures not only synchronized but remained in a state of synchrony for longer periods.

Coculture network activity had a high correlation coefficient throughout the period of recording compared to dishes treated with CRL-2303s. Tumor-treated networks showed only occasional bursts of synchrony and longer periods of non-correlated spiking and burst activity.

The overall correlation profile of cocultures, AraC-treated cultures and CRL-2303-treated cultures are shown in Figure 4-30. Cocultures have the highest correlated activity

compared to other(s). AraC-treated networks showed the least correlated activity. It is likely that the disruptions in glial cell activity, and consequently the disruptions in the glutamate uptake mechanisms, leads to a loss of synchronized activity that is important during the early stages of network development.

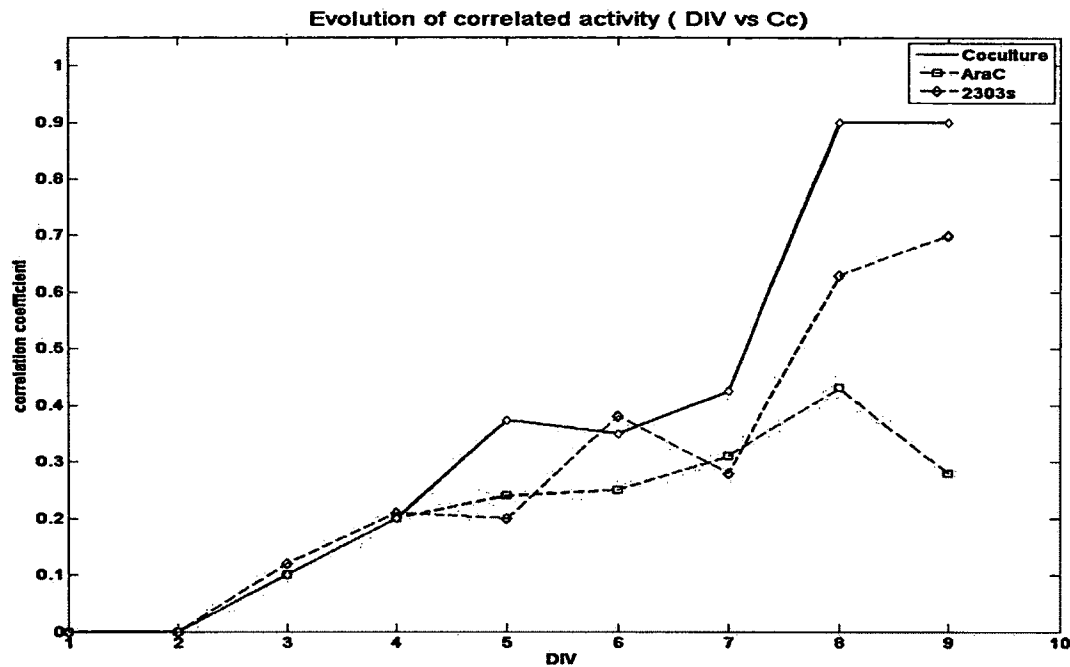


Figure 4-30: Synchrony profile for all three types. AraC-treated networks showed the least amount of synchrony. Cancerous networks showed intermediate synchrony.

4.4.3 Cross-Correlation Analysis

In this section, cross-correlation between different pairs of electrodes are presented and compared. Since AraC-treated networks exhibited the least correlated activity, they were ignored in this analysis. Only cocultures and tumor induced networks were considered for this analysis. The cross-correlation function for cocultures for different pairs of electrodes is shown in Figure 4-31 and Figure 4-32.

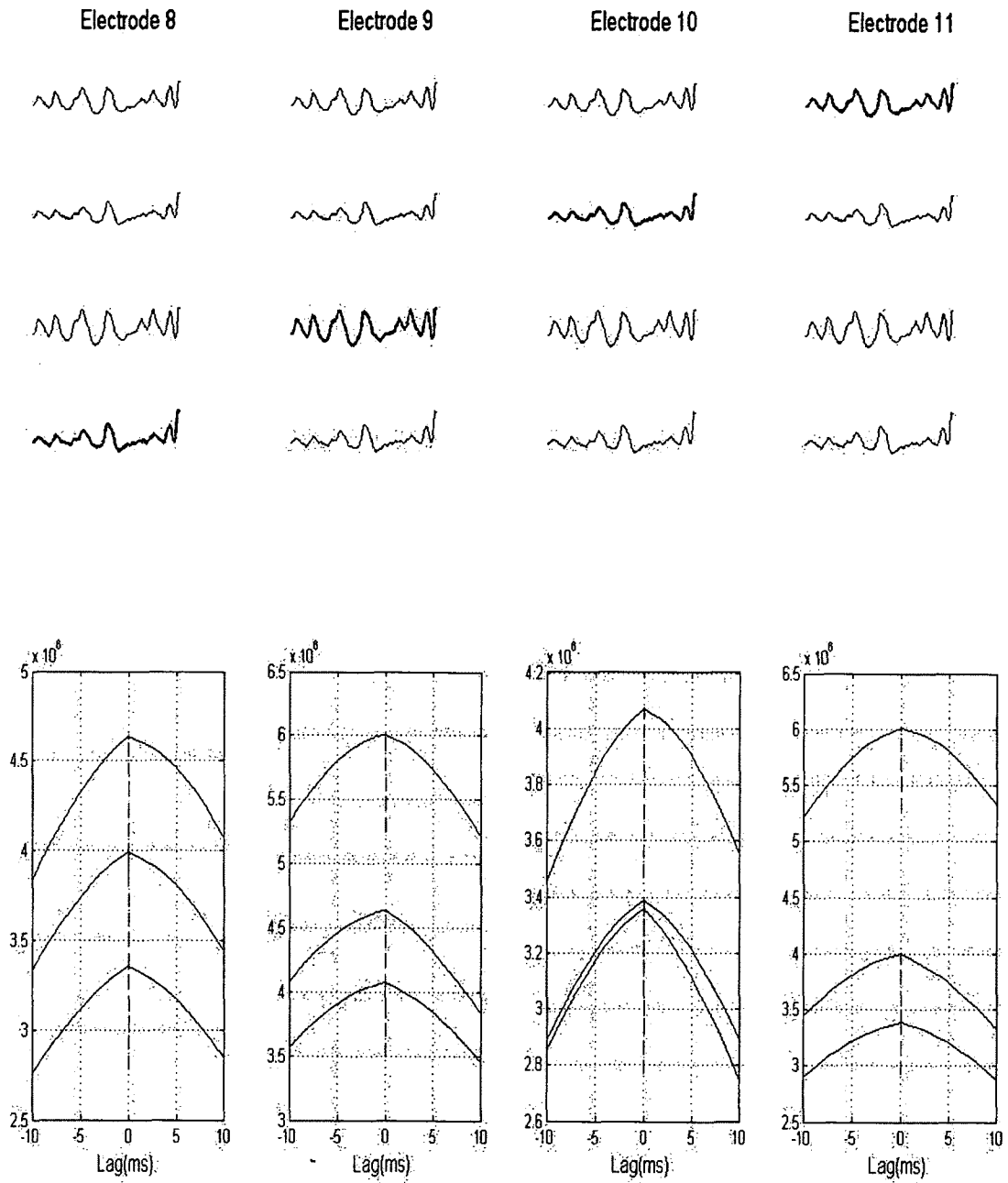


Figure 4-31: Time lags were calculated for one event (recorded in four electrodes)

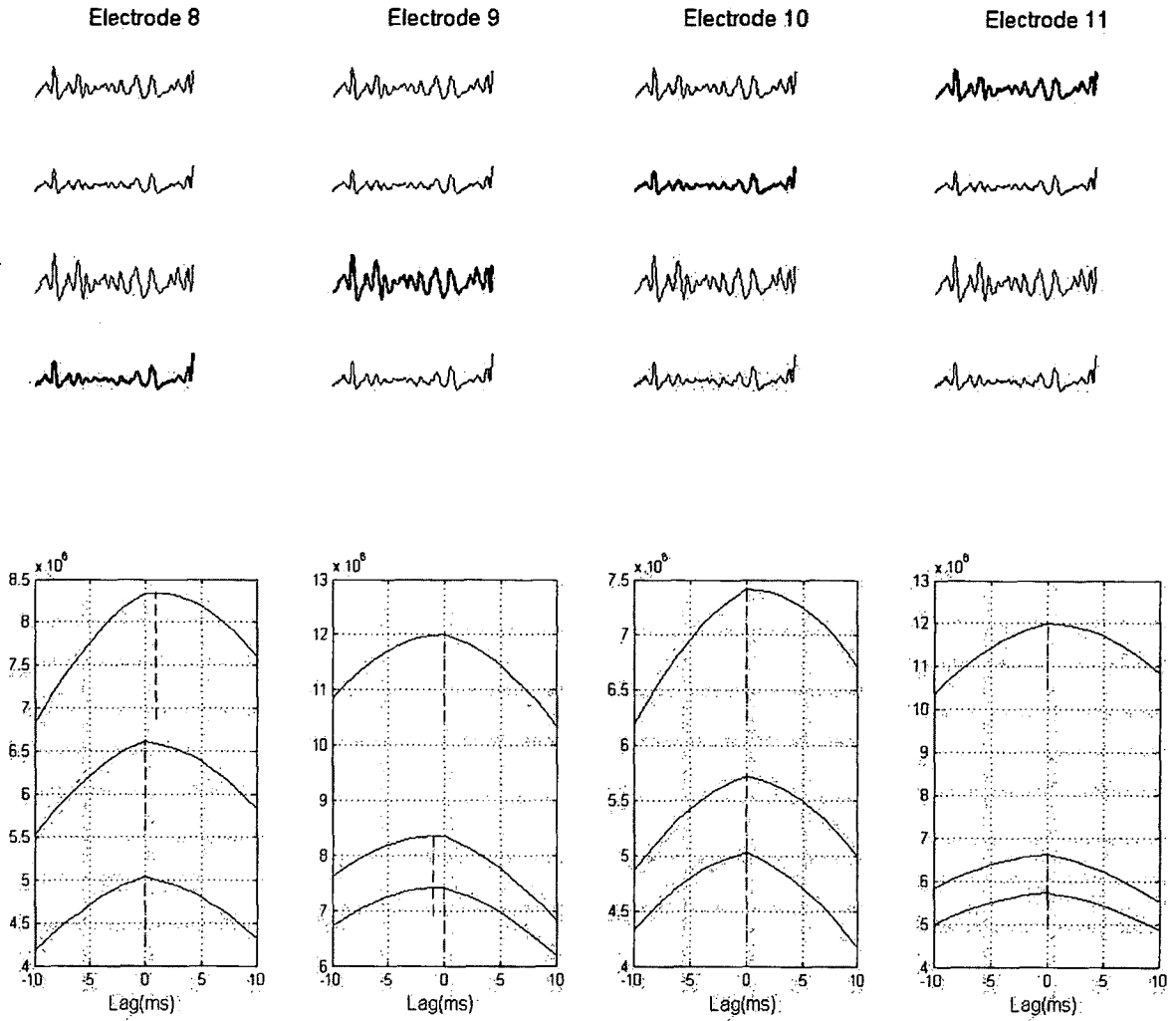


Figure 4-32: Time lags were calculated for another event across the same electrodes.

The maximum time lag between events was less than 5 ms, indicating that the spread of activity is quick. It is thus likely to be synaptically mediated because synaptic events are closer to this time scale. Time lags for different types of events were calculated. Shorter SLE events had a smaller time lag (within 20 ms) between the electrodes as shown in Figure 4-33 and Figure 4-34.

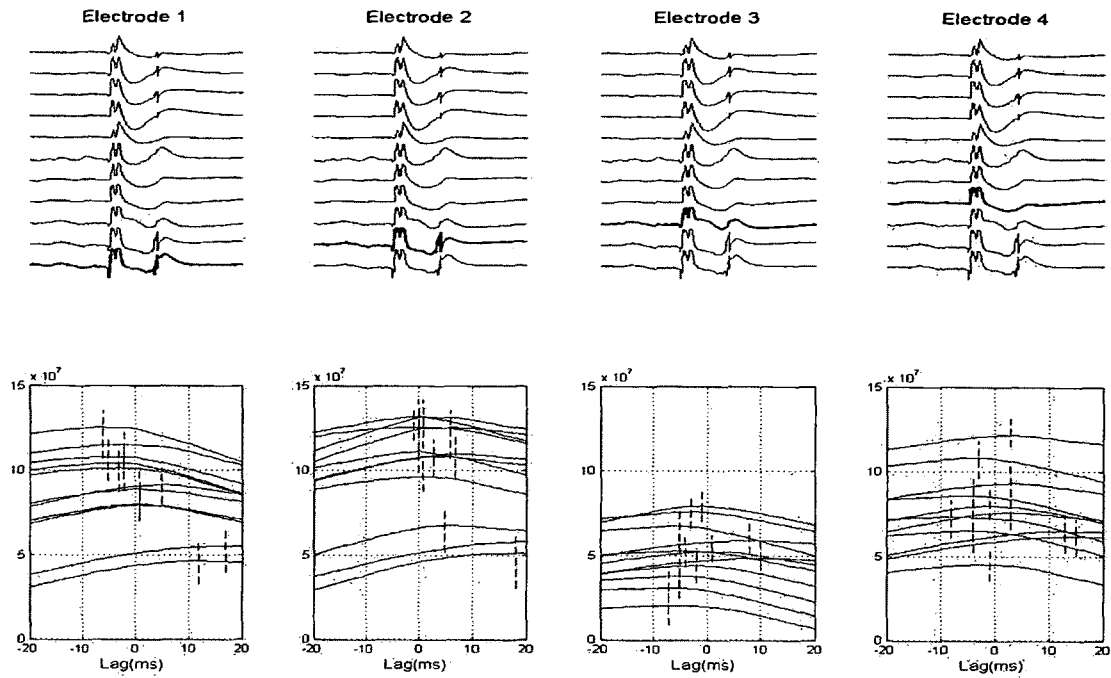


Figure 4-33: Time lags for a short SLE computed for a different pair of electrodes (E1-E4)

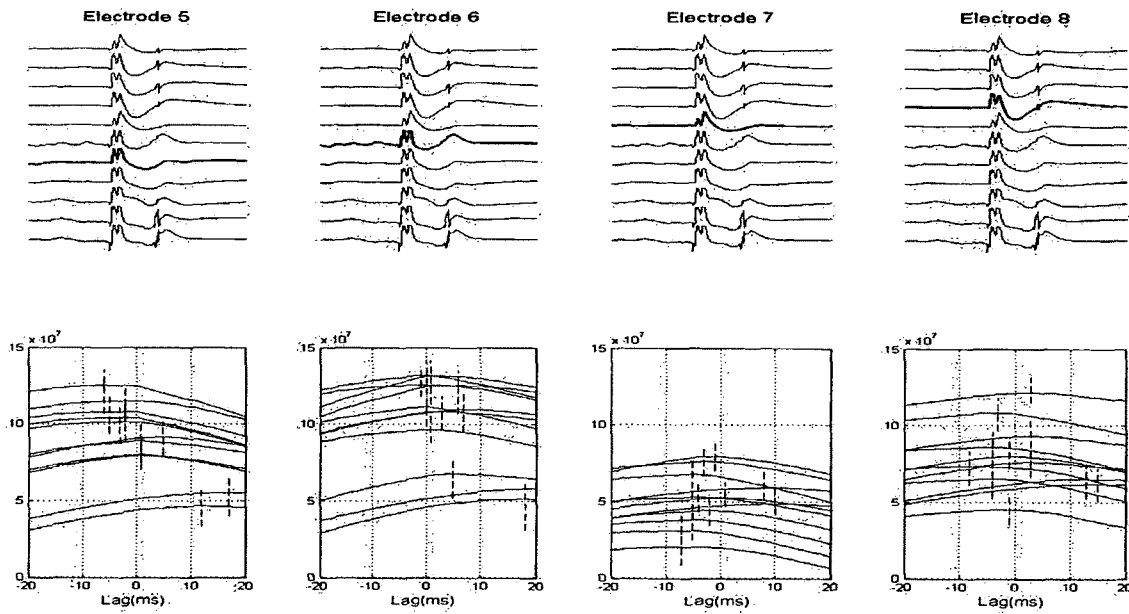


Figure 4-34: Time lags for a short SLE computed for different pair of electrodes (E5-E8)

Larger SLE events had much longer time lags (up to 400 ms) as shown in Figure 4-35, Figure 4-36, and Figure 4-37 in addition to ‘zero’ lag events.

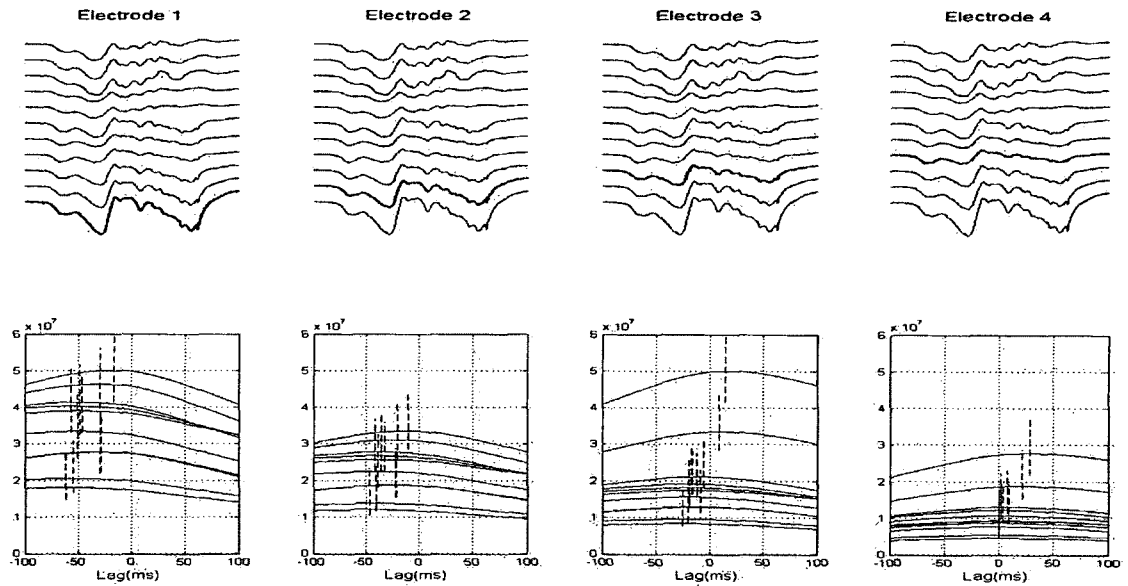


Figure 4-35: Time lags for a longer SLE computed for different pair of electrodes (E1-E4)

This combination of longer and shorter lags indicates that communications between the regions could be mediated by two separate mechanisms; a synaptic mechanism (in the order of a few milliseconds) and a slower non-synaptic wavelike mechanism. Synaptic activity is mediated by fast ion channel activity. Nonsynaptic mediation can be through a number of mechanisms including neurotransmitter diffusion. Glioma cells have been reported to secrete glutamate (Takano *et al*, 2001). Gliomas are reactive and fail to reuptake extracellular glutamate in the synapse due to the absence of glutamate transporters and hence, it is likely that excessive glutamate diffuses over from the origin of abnormal activity and stimulates distant regions.

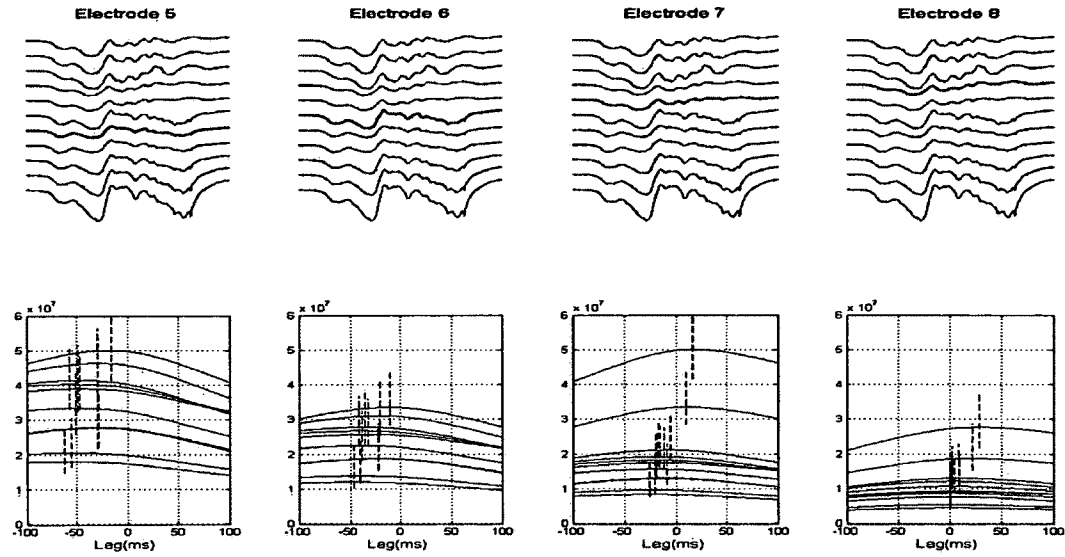


Figure 4-36: Time lags for a short SLE computed for different pair of electrodes (E5-E8)

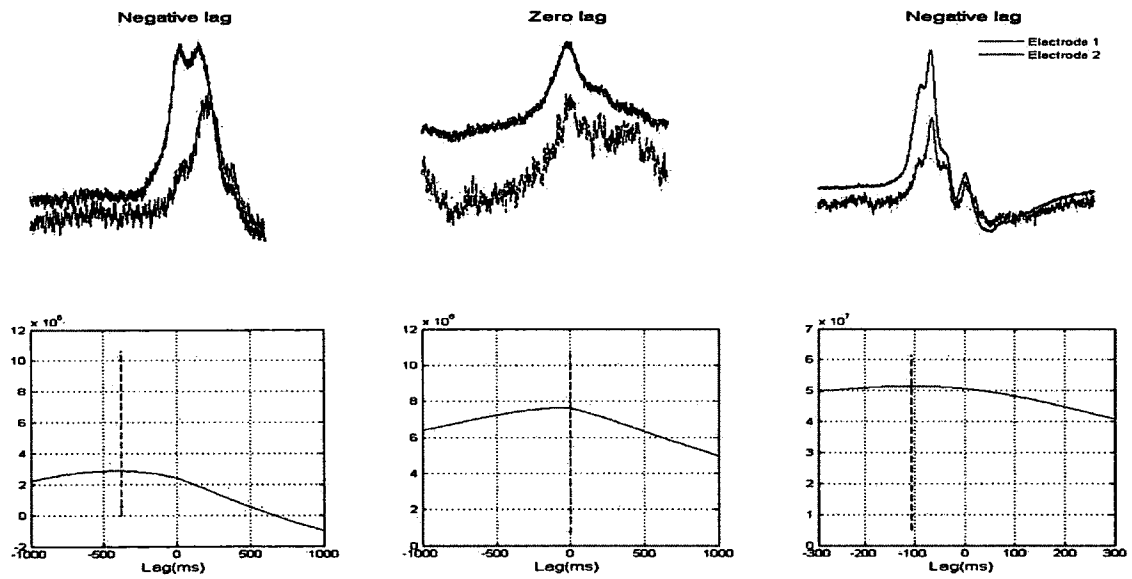


Figure 4-37: Time lags for three different time stamps in the same recording, from the same pair of electrodes. Both negative lag and zero lag were observed.

4.4.4 Coherence Analysis

4.4.4.1 CRL-2303

Coherence functions were calculated to find frequency bands overlap between pair of electrodes for both normal and dishes treated with CRL-2303. Coherence function of basal activity between pairs of electrodes in cocultures is shown in Figure 4-38.

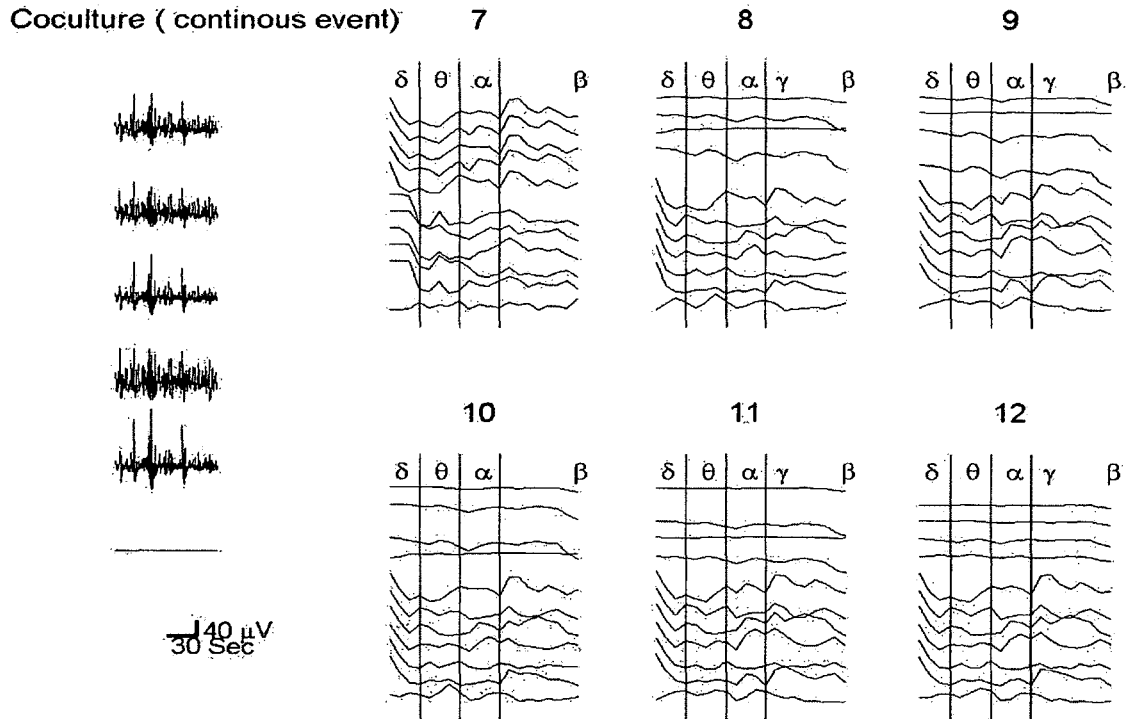


Figure 4-38: Frequency overlap in the δ range was observed with almost all pairs of electrodes

Delta range oscillations were prominent between all pairs of electrodes. While transient activity existed in other bands it was not consistent and was limited to a few electrodes.

4.4.4.2 Cancer (Large SLE)

Coherence function for two types of activity (small and large SLE were computed). Compared to regular cocultures, large SLE activity had frequency bands in

late delta and early theta stage (~4-6 Hz) as shown in Figure 4-39 and Figure 4-40. There was also a significant dip in the early beta phase across multiple electrodes.

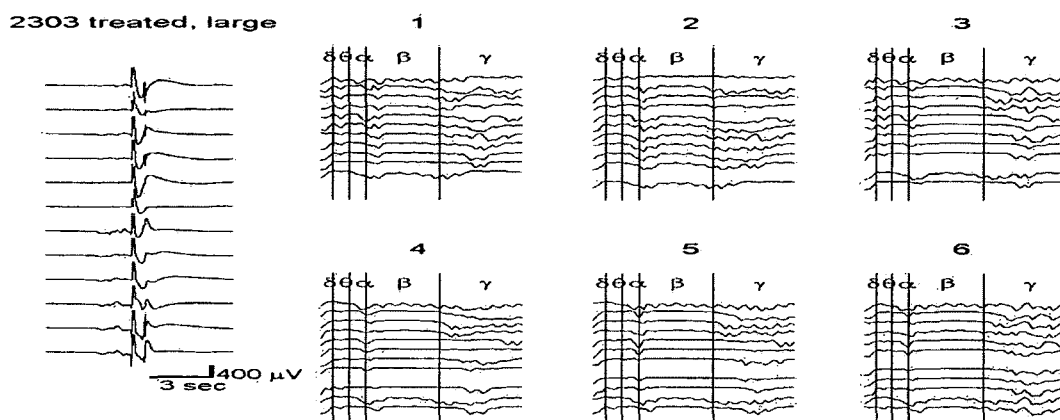


Figure 4-39: Frequency overlap in the late delta and early theta bands were observed with almost all pairs of electrodes. β -dips were also observed in large SLE events.

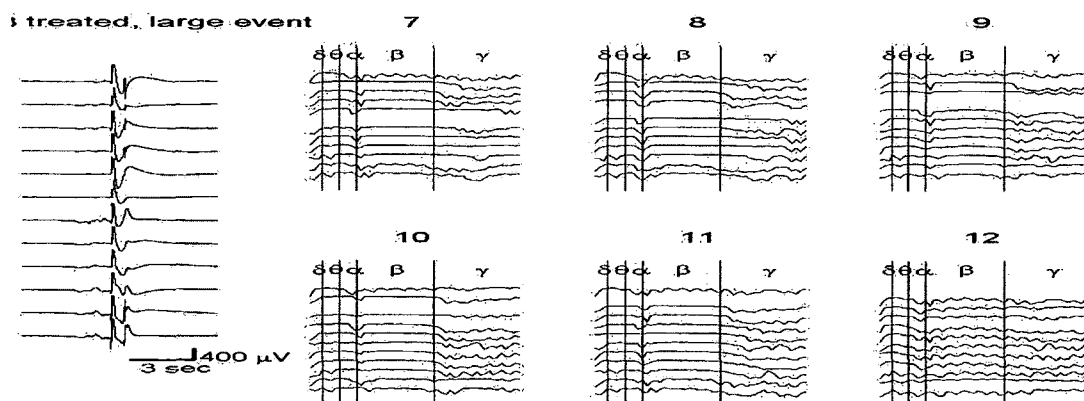


Figure 4-40: Frequency overlap in the late delta and early theta were observed with almost all pairs of electrodes. β -dips were also observed in large SLE events.

Shorter SLEs lasted for the same duration, but were much smaller in burst amplitude. The extracellular potentials, typically around 200 μ V, appeared continuous than burst like. A section of the event is shown in Figure 4-41 and Figure 4-42 . The coherence function of the frequency bands showed frequency overlap in the beta band.

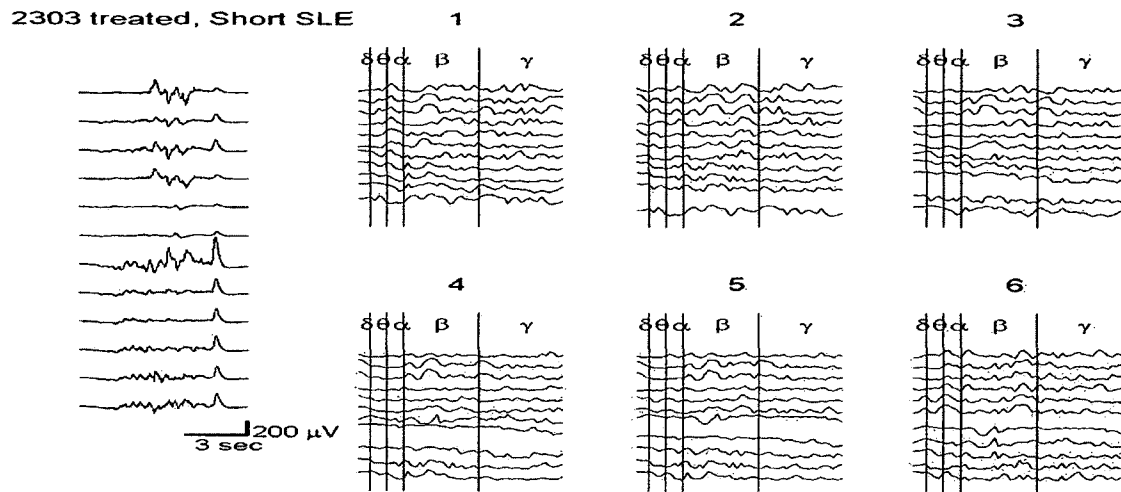


Figure 4-41: Frequency overlap in β bands were also observed in shorter SLE events (E1-E12).

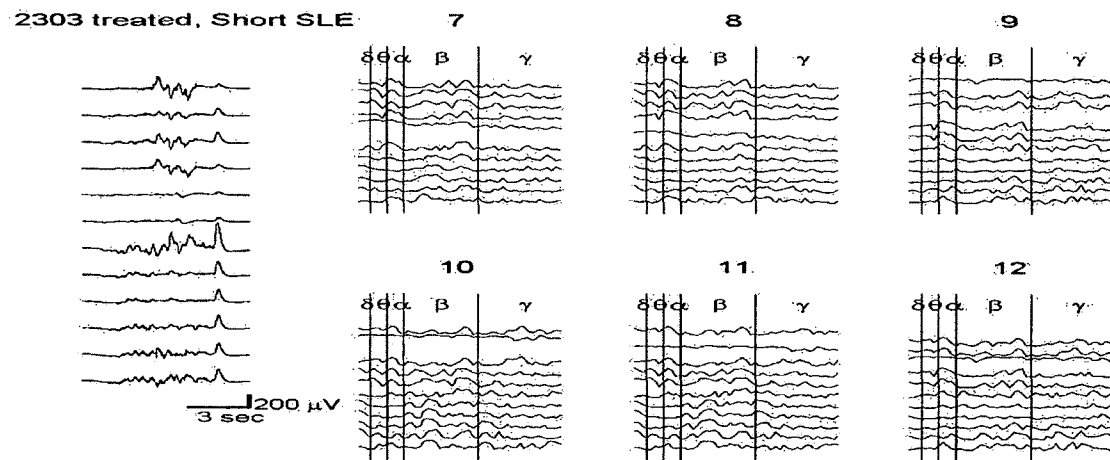


Figure 4-42: Frequency overlap in β bands in shorter SLE events (E7-E12)

CHAPTER 5

DISCUSSION

In this chapter, the results presented earlier are revisited and their implications interpreted. Six key results, labeled as *[R1]* through *[R6]* are highlighted in italics.

A network system can be defined as a system of interconnected elements. The elements are fundamental system components whose properties are usually reasonably understood. The connectivity map or wiring diagram contains the information that describes the connections and interactions among the elements. The system's behavior is a function of (a) the properties of individual elements and (b) the way in which the elements are connected. Such systems can be both man-made and natural. Natural systems include the metabolic network of *E.Coli* (Ravasz *et al*, 2002), the connectome of *Caenorhabditis elegans* nematode worm (White *et al*, 1986), and the human brain (Sporns, 2011). Man-made systems include social networks, citation networks, and computer routing networks (Watts, 2004). Naturally-inspired model networks are used to solve human problems and artificial network models are modeled to study natural and real-world networks. The multidisciplinary field of *complex systems* deals with the study and understanding of such systems. Prior to emergence of this discipline, networks were thought to be mostly either ordered structural hierarchies or random in nature. Ordered networks follow simple and well-defined connections. The crystal lattice structure of

elements and networks of computer architecture are examples of ordered networks. The network structure of these systems has clear patterns, and the direction of information flow between elements can be traced. Random networks, as the name implies, have random connectivity probabilities between the node elements. While both these models have traditionally been used to study networks, most real-world and natural works are neither structured nor completely random. While their connections follow some underlying patterns, they also incorporate randomness (Watts and Strogatz, 1998). The identification of underlying patterns in complex systems is one of the challenging problems in science.

The brain can be viewed as an intricate network of neurons and other types of cells. The resultant function (or dysfunction) of the nervous system arises from interactions in information flow between neurons. Recently, advancements in imaging techniques and new analysis tools have paved the way to the representation of brain connectivity (Bullmore and Sporns, 2009). In the current approach, the functional connectivity, which is established as a network of functionally similar brain regions, has been mapped. The structural connections between brain regions, also termed as the connectome, is much harder to obtain, mainly because current technology is limited (Sporns *et al*, 2005). An organism's simplest behavior, such as learning, locomotion, sensory processing, and synchronized activity, and an organism's more complex functions, such as pattern recognition and emotions, are emergent behaviors that arise from the interactions between system elements. Severe disruptions (injury or disease) to system elements or interactions cause dysfunctional states and neurological pathologies.

In this study, the phenomena of self-organized neural synchronization are studied. Since its discovery, synchrony behavior has been reported across several species, during different stages of development and behavior types, from locomotion to complex problem solving (Buzsáki, 2006). Disruptions in synchronous activity are also implicated in several disease states and cognitive disorders (Başar and Güntekin, 2008). Little is understood on why brain regions tend to synchronize during these states, and the role the network connectivity patterns play to support or disrupt synchronous activity.

This study was conducted to examine the degree to which the function of the network follows its form and to explore the possibility of explaining network functionality in terms of its network properties. Specifically, this work seeks relationships between the structure of small cultured neural network populations and the ability of these populations to produce spontaneous activity and synchronization. The effects of specific transitions in network properties on network behavior were investigated. The electrical behavior of networks in disease states (lack of glial cells and tumor growth) was contrasted with that of normal networks.

For our model, we used a culture of cortical cells (neurons and glial) from newborn rat brains. Dissociated cortical networks have been reported to exhibit properties similar to *in vivo* models in their ability to establish synchronized oscillations (Chiappalone *et al*, 2006). The networks were cultures on transparent MEA dishes. The microelectrode arrays enabled simultaneous recording of electrical signals from multiple sites, and the transparent property allowed tracking of network connectivity changes, through imaging, during various phases of development. The imaging data were used to trace local networks, to mathematically abstract them as graphs (via certain assumptions),

and to analyze them with graph algorithmic tools. The electrical activity data were analyzed and characterized using signal-processing techniques. The relationships between the image-based information and the microelectrode-based information were examined.

Cell cultures with neuron seeding densities that ranged from 5k – 500k per dish were tested in preliminary studies to determine the most appropriate seeding density for this study. Lower cell densities failed to self-organize and exhibit recordable electrical activity. Higher densities, while producing recordable electrical activity, consumed more resources (frequent change of media). We found that a cell density of 200k neurons per dish was optimal both for developing self-sustained oscillations and longer intervals between media change. This initial seeding was the only external cue.

5.1 Progression of Cell Culture Development

5.1.1 Initial Formation of Connections

While the placement of cells initially is random, neurite extensions were noticed as early as DIV 3. The connections were usually between neighboring neurons, and neurons appeared to be evenly distributed across the culture space. At this stage of development, the endogenous neural growth factors and signaling molecules play a role in directing the neurite extensions (Vanmali *et al*, 2003).

5.1.2 Emergence of Small Clusters and Local Activity

During the next phase in development, clusters of neurons were observed at many regions of the dish. Clusters are closely packed neurons (in physical space) that are well connected with each other. This stage is marked by migration of cells forming densely packed and sparser regions in the culture region. Clusters of different sizes (ranging from

3 to 50 neurons) were observed. This stage was also marked by the emergence of spontaneous and uncorrelated electrical activity across different regions of network as shown in Figure 4-2. Electrodes near each cluster produced stronger electrical activity. Since spontaneous electrical activity is observed only after the development of node-node interaction, and since no spike activity was recorded during the phase prior to this development, it is inferred that *at least one functional connection between two neurons must exist before spontaneous activity can emerge from those neurons [R1]*. Initially, when the clusters were smaller, individual spike activity was more prevalent, but as the cluster size increased, population bursts (the collective spontaneous activity of many neurons in a local cluster) began to emerge. Bursts and individual spikes were both detected during this stage of development. Cocultures and primary cultures (networks treated with AraC) showed a similar bursting profile during this phase as shown in Figure 4-13 and Figure 4-14 (DIV 7). The inter-event histograms shows that time intervals were uniformly distributed. With further development, the number of events increased and the bursting profile showed shorter inter-burst intervals as shown in Figure 4-13 and Figure 4-14 (DIV 8 and DIV 9). The overall event activity (events/minute) was similar ($p = 0.6$) for both groups during different stages as shown in Figure 4-12. However, primary cultures began to develop a narrower bursting profile that was more periodic as shown in Figure 4-15, while cocultures developed a much more diverse bursting profile. How does this difference in bursting profile affect network behavior? Information or the entropy content (H) of a system is proportional to the amount of disorder or variability in a system. The variability of a neural system (individual neurons or clusters) can be quantified by the distribution of event intervals. If the distribution was more irregular,

then H is larger and vice versa. Pacemaker cells, for instance, can be said to have low entropy because they normally oscillate around a fixed frequency, whereas cortical structures responsible for information processing show a more diverse operating range. Normal human brain activity can be termed as chaotic and has high entropy (Faure and Korn, 2001). *The results indicate that a reduction in the number of glial cells causes a decline in basal information content of a neural network [R2].*

5.1.3 Inter-Cluster Connectivity Development

During the final stage of development (DIV 8 and DIV 9), cluster formation was almost complete. Most of the nodes (neurons) were linked with other nodes. Neurite proliferation stabilized compared to earlier phases. The clusters were also connected to each other through direct links or other hubs of clusters. The emergence of spanning tree (i.e., the existence of a trace from one node to any other node in a group of clusters) is likely during this stage. Development of global activity was observed during this stage. Global activity is defined as simultaneous events in different regions in the network, as recorded at multiple electrodes. Global burst play a role in modifying synapses (Pike *et al*, 1999), modulate inter neuron communication via resonance (Izhikevich *et al*, 2003) and indicate network activity state (Morefield *et al*, 2000). Development of synaptic pathways connecting distant regions may play a role in transferring burst activity from one region to another making it global. The observed global events may be causal or non-causal. In almost all our recordings during this phase (n=11), functionally active cells produced at least one globally synchronized event. The presence of at least one link is an indicator that the clusters are connected within the vicinities of the electrodes which record them. An abstract representation of such a network is shown in Figure 5-1 (left).

The cluster connectivity of the network is low and there exists a minimum number of links connecting any two nodes in the network. However, the robustness of the network is poor and no duplicate links exist between edges on the network. Such networks do sustain synchronized behavior, but because they lack robustness, they will most likely fail to synchronize with minimal external disturbances. During the final stage of development, cluster connectivity increased, producing stronger synchrony (correlation coefficient ≈ 0.9) across multiple electrodes. Abstraction of a network transition is shown in Figure 5-1 (right).

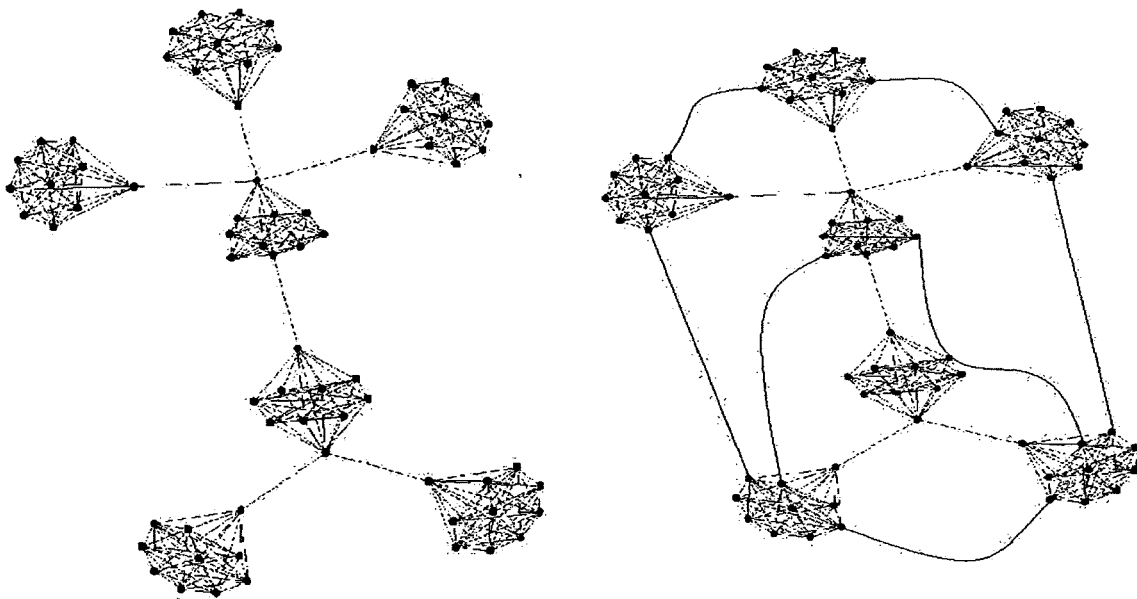


Figure 5-1: Abstract representation of network transition of the same network in consecutive days. While the network is completely connected, small increments in cluster connectivity could result in significant changes in network functionality.

The connectivity between clusters improves without many changes to the connectivity of nodes within each cluster. During this robust state and during the

connected state, the overall clustering coefficients (of the nodes) were not different (0.64 and 0.69).

However, a critical transition in the network led to 6-fold increase in the clustering coefficient values of the clusters (0.0542 to 0.3163 from DIV 8 to DIV 9). Clustering coefficients and path lengths were compared between neural cultures and the different graph models (ring lattice models, Erdős-Renyi random network and small-world model). Values for neural cultures were most similar to those for small-world networks. The transitions in cluster parameters were not caused by an increase in the number of neurites, but by the reorganization of both existing neuritis and smaller clusters to form links with other nodes. The ability of the cultures to transition without increasing the number of neurites implies that *when all other factors being the same, a network that has multiple neural pathways between any two nodes can synchronize more robustly than a network that has fewer pathways [R3]*.

5.2 Disruption of Synchrony in Primary Cultures

The role of glial cells in information processing of brain is poorly understood. At least a 1:1 neuron-to-glial ratio exists in the brain (Azevedo *et al*, 2009). Glial cells provide scaffolding for the brain, but they also regulate and clear neurotransmitters near the synapse and release neurotransmitters. Disruptions in neuron-glia interactions are implicated in abnormal brain states such as epilepsy (Dudek, 2002). In this study, we investigate the effect of diminishing glial concentration on the network's ability to synchronize. The addition of AraC to cocultures had an anti-mitotic effect and stopped proliferation of glial cells in the S-phase by damaging their DNA. AraC was usually added on DIV3. The effects of lack-of-glia on the spontaneous event activity were

examined. No difference was found between the number of events recorded from AraC-treated and untreated cocultures. However, among the three types of networks we studied (cocultures, CRL-2303-infected cultures, and primary cultures), primary cultures showed the least amount of synchronous behavior as shown in Figure 4-30. The average correlation coefficients for recordings samples in DIV 9 (n =3) and DIV 8 (n =2) were three-fold less than those for cocultures and half as large as those for CRL-2303 treated dishes for same DIVs. They were significantly lower for dishes treated with AraC (Student's T test, $p < 0.05$). Why does lack of glial cells disrupt synchrony? A possible reason is that glial cells release glutamate via a Ca^{2+} -dependent mechanism (Araque *et al*, 2000). They target extra synaptic NMDAr receptors in neighboring neurons and generate slow transient currents in them (Angulo *et al*, 2004). Glutamate released from glia affects multiple neurons; it has been reported that neurons separated by a distance ($< 100 \mu\text{m}$) showed synchronized transient currents (within a 100 ms time lag), and that glial cells affect both of these neurons with great precision. A single glial cell (or a cluster) spontaneously releases glutamate, thus affecting the synchrony of the entire network (Angulo *et al*, 2004). The data in our study corroborates this result. Therefore, *decrease in number of glial cells disrupts the ability of neurons to synchronize [R4]*.

5.3 Seizure-like Events (SLEs) in CRL-2303 treated Dishes

Aberrant electrical activity, particularly seizure, is one of the earliest symptoms accompanying brain tumors. Most glioma patients experience some type of seizures during the course of the disease. Elevated peritumoral and astrocytic glutamate concentrations, potassium homeostasis, astrogliosis, and tumor related changes in the blood-brain barrier have all been implicated in epileptic activity in the brain

(Buckingham and Robel, 2013). The implantation of C6 glioma cells in rat cortex resulted in spontaneous epileptiform activity consisting of sharp spikes and slow waves, as monitored by EEG, without significant changes in animal behavior (Köhling *et al*, 2006). Similar aberrations in brain electrical profile have been reported in animal and human studies (Lynam *et al*, 2007). Since tumor cells are reactive, they lose their ability to efficiently uptake glutamate, resulting in elevated levels of extracellular glutamate concentrations that can cause Alzheimer's, Parkinson's and seizure (Wang and Qin, 2010). Extracellular concentration of glutamate near tumor regions was significantly higher than that in healthy areas (Roslin *et al*, 2003). These elevated concentration levels persist throughout the period of tumor growth (Behrens *et al*, 2000). Because glioma cells lack GLT-1 and GLAST transporters, they are unable to remove glutamate. They also release cytotoxic levels of glutamate into the extracellular space due to the expression of cystine-glutamate exchanger; system xc (Ye and Sontheimer, 1999). Further, high extracellular glutamate concentrations may further contribute in the spread of the tumor (Takano *et al*, 2001).

In this study, healthy cocultures were infected with CRL-2303 cells around DIV 4, and electrical activity was monitored during different stages of coculture development. Approximately 10,000 cells were added to the culture. CRL-2303s are aggressive cell lines that can proliferate rapidly. Event rates, bursting profile (burst amplitude and frequency), spectral content, and synchrony were analyzed and contrasted with results from disease-free cocultures. While the event rate was lower in CRL-2303 treated dishes than in cocultures, as shown in Figure 4-16, the spectral power of active channels from CRL-2303 treated dishes, as shown in Figure 4-23, was similar to that obtained from

cocultures, as shown in Figure 4-20, in that it was primarily contained in the δ band (< 4 Hz). However, as the tumors progressed, they led to bursting profiles unlike bursts in cocultures and primaries. The burst amplitudes were larger and the durations were longer. To verify whether the bursts were distinguishable from other hyper-excitatory conditions, cocultures were stimulated with glutamate (500 μ m), and their bursting profiles and frequency spectra were analyzed as shown in Figure 4-22. Glutamate-stimulated networks showed an increase in bursting activity, spike activity, and δ , θ and α frequency band power. In CRL-2303 treated cells, fewer bursts occurred, and much of the activity was in the δ band. Burst activities of cancer-treated dishes differed from hyper-excitability bursting (caused by glutamate), and they were categorized as SLEs as shown in Figure 4-17. Normal astrocytes play an important role in preventing increase of extracellular glutamate concentration, the disruption of which could result in pathological brain states (Wang and Qin, 2010). Astrocytes also play a role in K^+ buffering in extracellular medium (Walz, 2000). Astrocytes, connected by gap junctions, act as a K^+ buffer by redistributing excessive K^+ from one region to another (Steinhäuser and Seifert, 2012). Astrocyte dysfunction has been implicated in epilepsy (Seifert *et al*, 2010). Therefore, the abnormal hyperactivity of cocultures is caused by either the inability of reactive astrocytes to remove glutamate via glutamate transporters or the inability of astrocytes to buffer potassium from the extracellular medium. *Cocultures treated with CRL-2303 generated SLEs when tumor cells proliferated [R5].*

Short-duration and long-duration SLEs were found. Both events were global and were observed in multiple regions of the recording site. SLEs of short burst time had higher amplitudes and higher correlation coefficients than long-duration SLEs in the

same recordings as shown in Figure 4-28 (right). Compared to cocultures networks, they remained less synchronized, as shown in Figure 4-29, over time. Cross-correlation function between any two signals is a function of time. It is a measure of the time separation between the signals. Cross-correlation lag between a given channel and all other channels ranged from near zero to a few ms (0 ± 5 ms) as shown in Figure 4-31 and Figure 4-32. This time lag is small, probably because synchrony in cocultures may be mediated by glial glutamate release received by many neurons within a short period of time. For large SLE events (characterized by higher amplitude and shorter burst duration time), time lags were 0 ± 10 ms as shown in Figure 4-33 and Figure 4-34. For the second type of SLEs (longer burst durations and smaller amplitudes), the time lags were much longer (0 ± 50 ms). For other isolated very slow propagating events as shown in Figure 4-37 (left), lags were as long as 400 ms. A few spike events exhibited no lag, similar to those observed in cocultures. Since the order of time lag is 10-100s of milliseconds, it is likely that these synchrony events could originate in one location (or multiple locations) and propagate in a wave-like motion rather than being simultaneously generated. *The spread of synchronized activity in CRL-2303 is mediated nonsynaptically [R6].*

While the spectral power of recordings from CRL-2303 treated cultures was mostly in the δ band, the bursts themselves were composed of smaller ripples of higher frequency. To find the overlap of frequencies across different electrodes, coherence functions were analyzed for both types of SLE events and compared to those of disease-free cocultures. In the coherence spectrum of cocultures, during resting (basal) state, frequency overlaps in the alpha range was observed as shown in Figure 4-39 and Figure 4-40. The coherence of large SLEs with smaller burst duration showed dips in late α and

early β band of the frequency spectrum. For shorter SLEs of longer duration, a peak within a narrow spectrum in the β band is observed. Aberrations in EEG electrical activity have been used to deduce brain tumor growth. Study of the electrical activity at the local network level may help improve detection techniques.

CHAPTER 6

FUTURE WORK

Extending the number of electrodes and recording channels would vastly improve the resolution of the electrical signals recorded from the network. At any time, we were only able to use about 15 channels. Also, not all of the recordings from these channels could be used because some channels tended to be noisier and to deteriorate much faster with repeated use. The number of recordable channels can be increased if dishes with more recordable channels are used, although that modification would considerably increase the cost of the setup. During a typical recording day, a dish is removed from the incubator and imaged (different portions of the grid) at a high resolution. It is then taken to a recording chamber and recorded from for up to an hour. Since prolonged time spent outside the incubator greatly decreased the viability of the networks, cultures could not be maintained for more than a few days after recordings began. Also, evaporation of the media during the recording sessions necessitated constant replacement of new media, with consequent changes in the molarity of the media.

Identifying neuron-neuron connections was also a challenge in this approach. Higher magnification of images from recording regions improved identification but decreased the area of the networks that could be imaged at a time. Taking multiple

images and merging them would require too much time. Selective staining of synapses (or neuritis) might allow neuritis to be more easily identified. It would also be useful to pattern the network in small cluster islands with links between them.

Based on the culture network data that we have collected, a culture model can be developed that is a slight variant of the small world model. Once we establish the number of clusters in the network and the size of individual clusters in the network (in terms of the number of nodes in each cluster), we could then assign two probabilities that would govern the connectivity of the network. One would be the probability of edge occurrence between neurons within clusters (p). We have assumed that nodes within small clusters were completely connected (since it was difficult to quantify the high neuritis density connections between them). Realistically, this assumption may not be valid. Cluster connectivity can also be varied (and perhaps even strengthened or weakened) by assigning either an independent probability or a preferential probability model (P). Changes in network properties such as characteristic path lengths and cluster coefficients can then be related to these probabilities. The probabilities for both culture models and other disease states could be estimated. If imaging techniques existed that could map smaller regions of the brain at the network level, this model could distinguish between normal and abnormal states.

Large scale computer simulations of neural networks are increasing in popularity. They serve as models to study neurophysiological phenomena (at the network level), and they are used to solve more general problems in computer science. However, most of the connectivity information for the models is derived from anatomical studies that are statistical in nature. Mapping networks in culture (assuming the network properties are

scale-free) could provide useful information that will help computational neuroscientists to build relevant models.

In a typical neural network, the nodes (neurons) come in different shapes and sizes, and hence a weight could be assigned to each node. Also, depending upon the placement in the network, some neurons could be functionally more important than others. Synapses are directional and could be excitatory or inhibitory. Synapse also has strengths associated with them (mainly depending upon the presynaptic neurotransmitter concentration levels). Any connection in this type of network would be weighted (variable weights, if we were to include network training), directional, and signed ('+' or '-') while node weight could be reasonably assumed. Determining synaptic weight and direction would be a greater challenge, but if addressed, could tremendously improve results.

Improvement in the size of the network, spatial resolution of imaging and recording, and time resolution would result in data that would also require newer algorithms and network properties that have to be developed. Improvements in signal processing algorithms (spike sorting algorithms especially) would increase the resolution of data to the spike level.

CHAPTER 7

CONCLUSION

In vitro neural networks exhibited similar properties such as spontaneous oscillations and synchrony during the development phase. Critical transitions in network architecture increased spontaneous activity and synchronization. Networks treated with AraC exhibited spontaneous oscillations but poor synchrony. CRL-2303 treated cells showed SLEs who's bursting profile were larger, infrequent and had a wavelike spread.

BIBLIOGRAPHY

- Angulo, Cecilia M, Kozlov A, Charpak S, and Audinat E. Glutamate Released from Glial Cells Synchronizes Neuronal Activity in the Hippocampus. *The Journal of Neuroscience* 24 (31):6920–6927, 2004.
- Araque A, Li N, Doyle RT, and Haydon PG. SNARE Protein-dependent Glutamate Release from Astrocytes. *The Journal of Neuroscience*. 20 (2):666-73, 2000.
- Azevedo, Frederico AC, Ludmila RB, Carvalho, Grinberg L, Farfel JM, Renata EL Ferretti, Renata EP, Filho WJ, Lent R, and Herculano-Houzel S. Equal Numbers of Neuronal and Nonneuronal Cells Make the Human Brain an Isometrically Scaled-up Primate Brain. *The Journal of Comparative Neurology* 513 (5):532–541, 2009.
- Bak, Lasse K, Schousboe A, and Waagepetersen HS. The glutamate/GABA-glutamine Cycle: Aspects of Transport, Neurotransmitter Homeostasis and Ammonia Transfer. *Journal of Neurochemistry* 98 (3):641–653, 2006.
- Başar, Erol, and Güntekin B. A Review of Brain Oscillations in Cognitive Disorders and the Role of Neurotransmitters. *Brain Research* 1235 (15):172–193, 2008.
- Batagelj V and Mrvar A. Pajek - Analysis and Visualization of Large Networks. *Graph Drawing Software* 2265:77–103, 2003.
- Behrens PF, Langemann H, Strohschein R, Draeger J, and Henning J. Extracellular Glutamate and Other Metabolites in and Around RG2 Rat Glioma: An Intracerebral Microdialysis Study. *Journal of Neuro-Oncology* 47 (1):11–22, 2000.
- Benda, Lightbody PJ, Sato G, Levine L, and Sweet W. Differentiated Rat Glial Cell Strain in Tissue Culture. *Science*. 161 (3839):370–371, 1968.
- Bohland, Jason W and Minai A. Efficient Associative Memory Using Small-world Architecture. *Neurocomputing* 38–40(0):489–496, 2001.

- Bromfield, Edward B, Cavazos JE, and Joseph I Sirven. *An Introduction to Epilepsy*. West Hartford (CT): American Epilepsy Society, 2006.
- Buckingham, Susan C, Susan L, Campbell, Haas BR, Montana V, Robel S, Ogunrinu T, and Sontheimer H. Glutamate Release by Primary Brain Tumors Induces Epileptic Activity. *Nature Medicine* 17 (10): 1269–1274, 2001.
- Buckingham, Susan C and Robel S. Glutamate and Tumor-associated Epilepsy: Glial Cell Dysfunction in the Peritumoral Environment. *Neurochemistry International*. (in preparation)
- Bullmore, Ed, Sporns O. Complex Brain Networks: Graph Theoretical Analysis of Structural and Functional Systems. *Nature Reviews Neuroscience* 10 (3): 186–198, 2009.
- Buzsáki, G. *Rhythms of the Brain*. Oxford University Press US, 2006.
- Buzsáki G. Theta Oscillations in the Hippocampus. *Neuron* 33 (3):325–340, 2002.
- Cabral, Joana, Hugues E, Sporns O, and Deco G. Role of Local Network Oscillations in Resting-state Functional Connectivity. *NeuroImage* 57 (1):130–139, 2011.
- Chiappalone, Michela, Bove M, Vato A, Tedesco M, and Martinoia S. Dissociated Cortical Networks Show Spontaneously Correlated Activity Patterns During *in Vitro* Development. *Brain Research* 1093 (1): 41–53, 2006.
- Danbolt NC. Glutamate Uptake. *Progress in Neurobiology* 65 (1): 1–105, 2001.
- Day, Keith B, Eisenman L, and Hogan RE. Neurochemistry of Epilepsy. In *Oxford Textbook of Epilepsy and Epileptic Seizures*, ed. Oxford University Press, 27–37, 2012.
- Dement, William and Kleitman N. Cyclic Variations in EEG During Sleep and Their Relation to Eye Movements, Body Motility, and Dreaming. *Electroencephalography and Clinical Neurophysiology* 9 (4):673–690, 1957.
- Dudek F, Edward. Role of Glial Cells in Seizures and Epilepsy: Intracellular Calcium Oscillations Sn Spatial Buffering. *Epilepsy Currents* 2(4):137–139, 2002.
- Engel AK and Singer W. Temporal Binding and the Neural Correlates of Sensory Awareness. *Trends in Cognitive Sciences* 5 (1): 16–25, 2001.
- Erdős P and Rényi A. On the Evolution of Random Graphs. *Publication of mathematical institute of Hungarian academy of sciences*, 5:17–61, 1960.

- Faure P and Korn H. Is There Chaos in the Brain? I. Concepts of Nonlinear Dynamics and Methods of Investigation. *Comptes Rendus De l'Académie Des Sciences. Série III, Sciences De La Vie* 324 (9): 773–793, 2001.
- Fell, Juergen and Axmacher N. The Role of Phase Synchronization in Memory Processes. *Nature Reviews. Neuroscience* 12 (2): 105–118, 2001.
- Fisher, Robert S, Boas W, Blume W, Elger C, Genton P, Lee P and Engel J. Epileptic Seizures and Epilepsy: Definitions Proposed by the International League Against Epilepsy (ILAE) and the International Bureau for Epilepsy (IBE). *Epilepsia* 46 (4):470–472, 2005.
- Fonnum and Frode. Glutamate: A Neurotransmitter in Mammalian Brain. *Journal of Neurochemistry* 42 (1): 1–11, 1984.
- Grobben, Bert, De Deyn PP, and Slegers H. Rat C6 Glioma as Experimental Model System for the Study of Glioblastoma Growth and Invasion. *Cell and Tissue Research* 310 (3): 257–270, 2002.
- Gross GW, Rieske E, Kreutzberg GW and Meyer A. A New Fixed-array Multi-microelectrode System Designed for Long-term Monitoring of Extracellular Single Unit Neuronal Activity in Vitro. *Neuroscience Letters* 6 (2–3):101–105, 1977.
- Habets AM, Dongen AMV, Van Huizen F and Corner MA. Spontaneous Neuronal Firing Patterns in Fetal Rat Cortical Networks During Development *in vitro*: a Quantitative Analysis. *Experimental Brain Research* 69 (1): 43–52, 1987.
- Haig AR, Gordon E, De Pascalis V, Meares RA, Bahramali H and Harris A. Gamma Activity in Schizophrenia: Evidence of Impaired Network Binding? *Clinical Neurophysiology* 111(8):1461–1468, 2000.
- Holliday, J, and N C Spitzer. Spontaneous Calcium Influx and Its Roles in Differentiation of Spinal Neurons in Culture.”*Developmental Biology* 141 (1): 13–23, 1990.
- Hooper SL. Central Pattern Generators. *Current Biology* 10(5):R176, 2000.
- Izhikevich EM, Desai NS, Walcott EC and Hoppensteadt FC. Bursts as a unit of neural information: selective communication via resonance. *Trends in neurosciences* 26 (3):161–167, 2003.
- Kiehn O and Butt SJB. Physiological, Anatomical and Genetic Identification of CPG Neurons in the Developing Mammalian Spinal Cord. *Progress in Neurobiology* 70 (4): 347–361, 2003.

- Köhling R, Senner V, Paulus W and Speckmann EJ. Epileptiform Activity Preferentially Arises Outside Tumor Invasion Zone in Glioma Xenotransplants. *Neurobiology of Disease* 22 (1):64–75, 2006.
- Kramer MA and Cash SS. Epilepsy as a Disorder of Cortical Network Organization. *The Neuroscientist* 18 (4):360–372, 2012.
- Kwok HF, Jurica P, Raffone A and Leeuwen CV. Robust Emergence of Small-world Structure in Networks of Spiking Neurons. *Cognitive Neurodynamics* 1(1): 39–51, 2007.
- Lenz D, Krauel K, Schadow J, Baving L, Duzel E and Herrmann CS. Enhanced Gamma-band Activity in ADHD Patients Lacks Correlation with Memory Performance Found in Healthy Children. *Brain Research* 1235: 117–132, 2008.
- Levinson AJ, Young LT, Fitzgerald PB and Daskalakis ZJ. Cortical Inhibitory Dysfunction in Bipolar Disorder: a Study Using Transcranial Magnetic Stimulation. *Journal of Clinical Psychopharmacology* 27 (5): 493–497, 2007.
- Liu H, Dean C, Arthur CP, Dong M and Chapman ER. Autapses and Networks of Hippocampal Neurons Exhibit Distinct Synaptic Transmission Phenotypes in the Absence of Synaptotagmin I. *Journal of Neuroscience*. 29 (23): 7395–7403, 2009.
- Lynam LM, Lyons MK, Drazkowski JF, Sirven JI, Noe KH, Zimmerman RS and Wilkens JA. Frequency of Seizures in Patients with Newly Diagnosed Brain Tumors: A Retrospective Review. *Clinical Neurology and Neurosurgery* 109 (7): 634–638, 2007.
- Marom S and Shahaf G. Development, Learning and Memory in Large Random Networks of Cortical Neurons: Lessons Beyond Anatomy. *Quarterly Reviews of Biophysics* 35(1):63–87, 2002.
- McDonald, JW and Johnston MV. Physiological and Pathophysiological Roles of Excitatory Amino Acids During Central Nervous System Development. *Brain Research. Brain Research Reviews* 15(1):41–70, 1990.
- McDonnell MD and Abbott D. What Is Stochastic Resonance? Definitions, Misconceptions, Debates, and Its Relevance to Biology. *PLoS Comput Biol* 5 (5), 2009.
- Morefield SI, Keefer EW, Chapman KD and Gross GW. Drug evaluations using neuronal networks cultured on microelectrode arrays. *Biosensors & bioelectronics* 15 (7-8): 383–396, 2000.

- Nunez J. Primary Culture of Hippocampal Neurons from P0 Newborn Rats. *Journal of Visualized Experiments* (19): 895, 2008.
- O’Keefe J and Dostrovsky J. The Hippocampus as a Spatial Map: Preliminary Evidence from Unit Activity in the Freely-moving Rat. *Brain Research* 34:171–175, 1971.
- Penn AA and Shatz CJ. Brain Waves and Brain Wiring: The Role of Endogenous and Sensory-Driven Neural Activity in Development. *Pediatric Research* 45 (4, Part 1 of 2):447–458, 1999.
- Pike FG, Meredith RM, Olding AW and Paulsen O. Rapid report: postsynaptic bursting is essential for ‘Hebbian’ induction of associative long-term potentiation at excitatory synapses in rat hippocampus. *The Journal of physiology* 518 (Pt 2): 571–576, 1999.
- Pine J. Recording Action Potentials from Cultured Neurons with Extracellular Microcircuit Electrodes. *Journal of Neuroscience Methods* 2 (1):19–31, 1980.
- Potter SM, Wagenaar DA, Madhavan R and DeMarse TB. Long-term Bidirectional Neuron Interfaces for Robotic Control, and in Vitro Learning Studies. In *Proceedings of the 25th Annual International Conference of the IEEE Engineering in Medicine and Biology Society* 4:3690 – 3693, 2003.
- Ravasz E, Somera AL, Mongru DA, Oltvai ZN, and Barabási AL. Hierarchical Organization of Modularity in Metabolic Networks. *Science* 297 (5586):1551–1555, 2002.
- Rothstein JD, Martin L, Levey AI, Dykes-Hoberg M, Jin L, Wu D, Nash N and Kuncel RW. Localization of Neuronal and Glial Glutamate Transporters.” *Neuron* 13 (3): 713–725, 1994.
- Rudnick SA, Cadman EC, Capizzi RL, Skeel RT, Bertino JR and McIntosh S. High Dose Cytosine Arabinoside (HDARAC) in Refractory Acute Leukemia. *Cancer* 44 (4): 1189–1193, 1979.
- Sanz-Arigita EJ, Schoonheim MM, Damoiseaux JS, Rombouts SA, Erik Maris E, Barkhof F, Scheltens P and Stam CJ. Loss of ‘Small-World’ Networks in Alzheimer’s Disease: Graph Analysis of fMRI Resting-State Functional Connectivity.” *PLoS ONE* 5 (11), 2010.
- Segev R, Benveniste M, Shapira Y and Ben-Jacob E. Formation of Electrically Active Clusterized Neural Networks. *Physical Review Letters* 90 (16):168101, 2003.
- Seifert, Gerald, Giorgio Carmignoto, and Christian Steinhäuser. Astrocyte Dysfunction in Epilepsy. *Brain Research Reviews* 63 (1–2):212–221, 2010.

- Singer W . Synchronization of Cortical Activity and Its Putative Role in Information Processing and Learning. *Annual Review of Physiology* 55(1):349–374, 1993.
- Spencer KM., Nestor PG, Margaret AN, Salisbury DF, Shenton ME and McCarley RW. Abnormal Neural Synchrony in Schizophrenia. *The Journal of Neuroscience* 23 (19): 7407–7411, 2003.
- Spitzer NC. Spontaneous Activity: Functions of Calcium Transients in Neuronal Differentiation. *Perspectives on Developmental Neurobiology* 2 (4): 379–386, 1995.
- Sporns O. Graph Theory Methods for the Analysis of Neural Connectivity Patterns. *Neuroscience Databases* 171–185, 2003.
- Sporns O, Chialvo DR, Kaiser M and Hilgetag CC. Organization, Development and Function of Complex Brain Networks. *Trends in Cognitive Sciences* 8 (9): 418–425, 2004.
- Sporns O, Tononi G and Kötter R. The Human Connectome: A Structural Description of the Human Brain. *PLoS Comput Biol* 1(4):e42, 2005.
- Srinivas KV, Jain R, Saurav S and Sikdar SK. Small-world Network Topology of Hippocampal Neuronal Network Is Lost, in an in Vitro Glutamate Injury Model of Epilepsy. *European Journal of Neuroscience* 25 (11): 3276–3286, 2007.
- Steinhäuser C, Carmignoto G and Seifert G. Astrocyte Dysfunction in Epilepsy. *Brain Research Review* 63(1-2):212-221, 2010.
- Svensson M and Aldskogius H. Infusion of Cytosine-arabioside into the Cerebrospinal Fluid of the Rat Brain Inhibits the Microglial Cell Proliferation After Hypoglossal Nerve Injury. *Glia* 7(4): 286–298, 1993.
- Takano T, Lin JH, Arcuino G, Gao Q, Yang J and Nedergaard M. Glutamate Release Promotes Growth of Malignant Gliomas. *Nature Medicine* 7 (9): 1010–1015, 2001.
- Thomas CA Jr, Springer PA, Loeb GE, Berwald-Netter Y and Okun LM. A Miniature Microelectrode Array to Monitor the Bioelectric Activity of Cultured Cells. *Experimental Cell Research* 74 (1): 61–66, 1972.
- Tovée MJ, Rolls ET, Treves A and Bellis RP. Information Encoding and the Responses of Single Neurons in the Primate Temporal Visual Cortex. *Journal of Neurophysiology* 70 (2): 640–654, 1993.

- Uhlhaas PJ, Roux F, Rodriguez E, Rotarska-Jagiela A and Singer W. Neural Synchrony and the Development of Cortical Networks. *Trends in Cognitive Sciences* 14 (2): 72–80, 2010.
- Uhlhaas PJ and Singer W. Neural Synchrony in Brain Disorders: Relevance for Cognitive Dysfunctions and Pathophysiology. *Neuron* 52 (1): 155–168, 2006.
- Vanmali BH, Romanova EV, Messner MC, Singh M, Maruniak J, Sweedler J and Kirk MD. Endogenous Neurotrophic Factors Enhance Neurite Growth by Bag Cell Neurons of Aplysia. *Journal of Neurobiology* 56 (1): 78–93, 2003.
- Varshney LR, Chen BL, Paniagua E, Hall DH and Chklovskii DB. Structural Properties of the Caenorhabditis Elegans Neuronal Network. *PLoS Comput Biol* 7(2):1, 2011.
- Walz W. Role of Astrocytes in the Clearance of Excess Extracellular Potassium. *Neurochemistry International* 36 (4-5):291–300, 2000.
- Wang Y and Qin ZH. Molecular and Cellular Mechanisms of Excitotoxic Neuronal Death. *Apoptosis* 15 (11):1382–1402, 2010.
- Watts DJ. The ‘New’ Science of Networks. *Annual Review of Sociology* 30: 243–270, 2004.
- Watts DJ and Strogatz SH. Collective Dynamics of ‘small-world’ Networks. *Nature* 393 (6684): 440–442, 1998.
- Weiss SR, Eidsath A, Li XL, Heynen T and Post RM. Quenching Revisited: Low Level Direct Current Inhibits Amygdala-kindled Seizures. *Experimental Neurology* 154 (1): 185–192, 1998.
- White JG, Southgate E, Thomson JN and Brenner S. The Structure of the Nervous System of the Nematode Caenorhabditis Elegans. *Philosophical Transactions of the Royal Society of London. B, Biological Sciences* 314 (1165):1–340, 1986.
- Ye ZC and Sontheimer H. Glioma Cells Release Excitotoxic Concentrations of Glutamate. *Cancer Research* 59 (17):4383–4391, 1999.
- Yener GG, Güntekin B, Oniz A and Başar E. Increased Frontal Phase-locking of Event-related Theta Oscillations in Alzheimer Patients Treated with Cholinesterase Inhibitors. *International Journal of Psychophysiology* 64 (1): 46–52, 2007.

Yordanova J, Banaschewski T, Kolev V, Woerner W and Rothenberger A. Abnormal Early Stages of Task Stimulus Processing in Children with Attention-deficit Hyperactivity Disorder--evidence from Event-related Gamma Oscillations. *Clinical Neurophysiology* 112 (6): 1096–1108, 2001.

Yu S, Huang D, Singer W and Nikolić D. A Small World of Neuronal Synchrony. *Cerebral Cortex* 18(12):2891–2901, 2008.